International journal of Geosciences

Vol. 1, No. 1, May 2010

www. scirp. org/journal/ijg

Scientific Research

Journal Editorial Board

http://www.scirp.org/journal/ijg/

International Journal of Geosciences, **2010, 1-50**
Published Online May 2010 in SciRes (http://www.SciRP.org/journal/ijg/)

TABLE OF CONTENTS

The Bayamo Earthquake (Cuba) of the 18 October 1551

M. O. Cotilla-Rodríguez, D. Córdoba-Barba……1

Sedimentation Processes at the Navigation Channel of the Liquefied Natural Gas (LNG) Port, Nile Delta, Egypt

E. A. E. M. Deabes……14

Surface Rupture and Hazard of Wenchuan Ms 8.0 Earthquake, Sichuan, China

Y. Li, R. Q. Huang, L. Yan, A. L. Densmore, R. J. Zhou……21

The Analysis of Accelerograms for the Earthquake Resistant Design of Structures

V. Corchete……32

The Co-planarity and Symmetry Principle of Earthquake Occurrence

Z. Yin……38

Effects of Polypropylene Fibers on the Shear Strength of Sandy Soil

M. F. Attom, A. K. Al-Tamimi……44

International Journal of Geosciences

Journal Information

SUBSCRIPTIONS

The international Journal of Geosciences (Online at Scientific Research Publishing, www.SciRP.org) is published quarterly by Scientific Research Publishing, Inc., USA.

Subscription rates:

Print: $50 per copy.

To subscribe, please contact Journals Subscriptions Department, E-mail: sub@scirp.org

SERVICES

Advertisements

Advertisement Sales Department, E-mail: service@scirp.org

Reprints (minimum quantity 100 copies)

Reprints Co-ordinator, Scientific Research Publishing, Inc., USA.

E-mail: sub@scirp.org

COPYRIGHT

PRODUCTION INFORMATION

For manuscripts that have been accepted for publication, please contact:

E-mail: ijg@scirp.org

International Journal of Geosciences, **2010, 1-13**
doi:10.4236/ijg.2010.11001 Published Online May 2010 (http://www.SciRP.org/journal/ijg)

The Bayamo Earthquake (Cuba) of the 18 October 1551

Mario O. Cotilla-Rodríguez, Diego Córdoba-Barba
Departamento de Física de la Tierra y Astrofísica 1, *Facultad de CC Físicas, Universidad Complutense de Madrid, Ciudad Universitaria, Madrid, Spain*
E-mail: *macot@fis.ucm.es*, *dcordoba@fis.ucm.es*
Received February 23, 2010; *revised March* 21, 2010; *accepted April* 20, 2010

Abstract

Using contemporary and original documents from the Archivo General de Indias it has been possible to complete the data for the 18 October 1551 earthquake in Cuba. The seism took place at midday, approximately. It had foreshocks and aftershocks. In Bayamo, 7 inhabitants were injured, and the town was severely affected. Maximum seismic intensity was IX degrees on the MSK scale, and the area of perceptibility is estimated at 40,000 km^2. Liquefaction processes and soil type in Bayamo contributed to the damage. This locality is in the Eastern region of the island, and continues to suffer the most and the strongest seismic events. The epicenter was in the southern marine area of the western segment of Oriente trough (19.6 N 77.8 W, h = 15 km, Ms = 6.6), where there is a crossing of faults, and neotectonics and focal mechanisms are affected by transtension, although the Bartlett-Cayman region's tendency to left-lateral strike-slip movement is maintained, in the Caribbean and North American plate boundary zone.

Keywords: Bayamo, Cuba, Earthquake, Historical Seismicity

1. Introduction

In previous papers we have shown that relatively large and destructive earthquakes have occurred frequently in the past along the Oriente fault system [1,2]. We have also shown that American contemporary documents must be studied with care, in their historical and cultural context, in order to avoid overrating when evaluating intensity [3]. In this paper, we will discuss an historic Cuban earthquake, which occurred in the year 1551. The information for this seismic event comes from contemporary sources, such as unpublished consular correspondence, official documents and damage claims, as well as from the observations of travelers who passed through the epicentral region during and after the earthquake. An extensive literature search for documents relative to this earthquake was carried out in libraries and archives of Belgium, Cuba, Dominican Republic, England, France, Jamaica, Mexico, Spain, and United States of America.

Cuba's written history is fairly extensive. It began in 1492 with the diaries of the first Spanish explorers [4,5]. The Spanish colonizers and priests established Catholic churches throughout the island, in all the villages founded from 1512 onwards. Many of these documents are available in the Archivo General de Indias (AI), Spain. Consultation at the AI enabled access to the original sources of information, for the first time, revealing that information on many XVIth century earthquakes has been compiled. Cotilla [3] and Cotilla and Córdoba [2] have already shown the usefulness of the AI, in the studies of four earthquakes in Santiago de Cuba.

In 1687, Cuban newspapers were published for the first time, initially issued in Santiago de Cuba and La Habana [5,6]. They mentioned perceptible earthquakes, continued to spread across the Eastern Cuban region as the population increased. Descriptions of the Cuban earthquakes were catalogued by Poey [7-9], and were later interpreted in terms of shaking intensity, and later, earthquake epicenters and magnitude [10-12]. Cotilla and Udías [5] classify the earthquake information quality of the works by Andrés Poey y Aguirre, concluding that the information given for the event of 1551 in Bayamo is unsatisfactory.

The aim of this paper is to detail what is known about the 1551 Cuban earthquake (Bayamo) including its sequences, the location of the epicentral areas, assessment of magnitude, and its effects both on the ground and on man-made structures. A further aim is to provide a critical review of the information available and to resolve some ambiguities appearing in previous works. Attempts are made to associate these events with local tectonics or to evaluate the associated seismic hazard.

2. Short Notes on Tectonics and Seismicity

The relative motion between the North American and Caribbean plates is decisive for the area's tectonic regime on a regional scale [13-20] (**Figures 1(a)**, **1(b)**). Cuba is a megablock (or microplate) located in the southern part of the North American plate (**Figure 2**) [21-23]. The active plate boundary is situated along the southeast coast where the main seismic activity follows the eastern segment of Bartlett-Cayman fault zone (Oriente fault) [14,24,25]. In this segment, faulting is mostly sinistral strike-slip (**Figure 1(d)**) [1,14].

The general pattern of seismicity in the Caribbean region is shown in **Figure 1(b)**. Large earthquakes occur along the plate boundary near Hispaniola, Jamaica and Puerto Rico [12,26], but no event since the XVIIIth century has reached a magnitude of 7.0 [1,5]. **Table 1** presents the most significant earthquakes in Southeastern Cuba [2-4]. Low magnitude seismicity (Ms < 4) occurs throughout the Western region of the island and particularly around Santiago de Cuba [14]. The seismicity determined with the Eastern Cuban network appears in **Figure 1(c)**. These low-energy events have been registered by 3 or more stations in the period 1979-1994 [1]. It shows two important earthquake clusters, namely, in Cabo Cruz and Pilón-Baconao. The second cluster is the largest and it corresponds to most important seismogenetic segment of Oriente fault [22] where the strongest earthquakes are observed there. The cluster of Cabo Cruz has an important epicentral error and the accuracy in azimuth is about 15-30%. Using the mentioned Cuban seismic data, Cotilla [1] presented the **Figures 1(e)** and **1(f)** where appear the predominant depth range of earthquake occurrence.

The Cotilla *et al.* [22] results suggest that Cuba is a seismotectonic province, composed of four units (Western, Central-Eastern, Eastern, and Southeastern). **Figure 2** shows the location of the two main units and their limits, and the three crust types (wide transitional, fine transitional and oceanic) [27] in the region. According to Makarov [28], the neotectonic structure of Eastern Cuba (**Figures 3(a)**, **3(b)**) includes extremely diverse areas, differing in layout, morphology and historical development. Development began in the Late Eocene, on a mixed basement and, in general, on crusts of various thicknesses and types, ranging from sub continental to sub oceanic, as

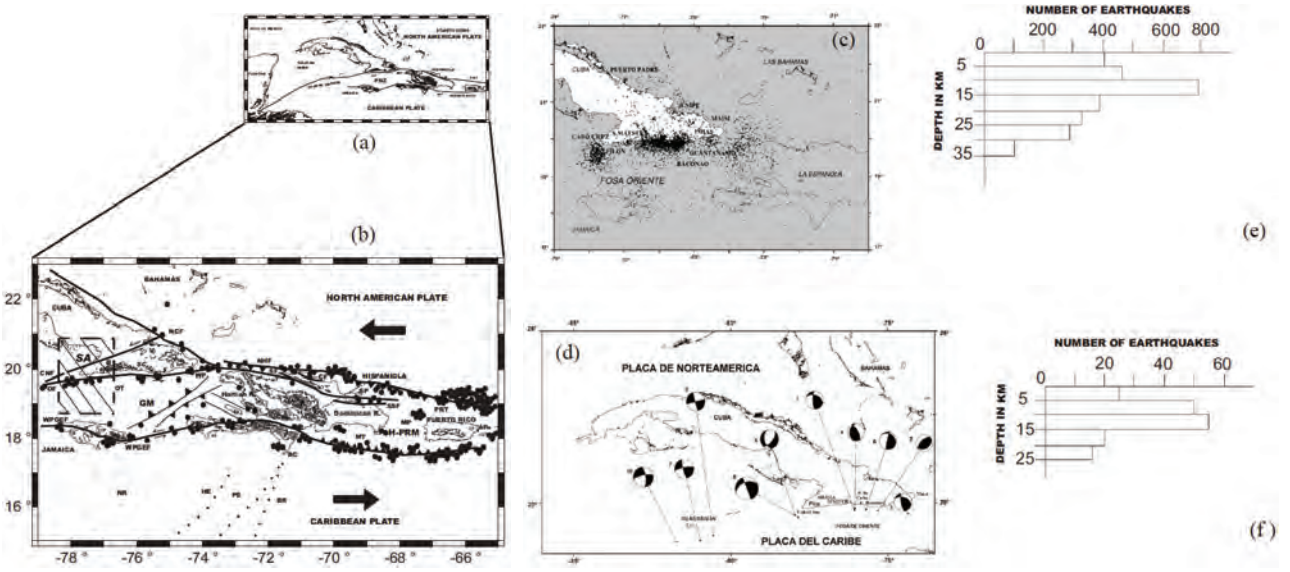

Figure 1. a) Simplified tectonic map of the Caribbean. General view (Heavy black lines-main fault systems: MT = Muertos trough, OT = Oriente trough; PBZ = Plate Boundary Zone; PRT = Puerto Rico trench, WP = Winward Passage)**; b) Main structures in the Caribbean [Eastern Cuba–Puerto Rico].** (Heavy black arrows= sense of plate movements; black circles= epicentres [1]; black lines = the main faults: CF = Camú, CNF = Cauto-Nipe, NCF = Nortecubana, NHF = North Haitian, OF = Oriente, SF = Septentrional, SSF = South Samaná, WPGEF = Walton-Platain Garden-Enriquillo; the drawing of the points outlines the structures BR = Beata Ridge and HE = Hess Escarpment; passages: AP = Anegada, MP = Mona, WP = Windward; islands: Cuba, Hispaniola, Jamaica, Puerto Rico; microplates: GM = Gonave, HPRM = Hispaniola-Puerto Rico; troughs: MT = Muertos, OT = Oriente, PRT = Puerto Rico; other structures: NR = Nicaragua Rise, PE = Pedro Escarpment; open rectangle (SA) = study area)**; c) Eastern Cuba seismicity determined with a National network in 1979-1994 [1]; d) Selection of ten focal mechanism solutions in Oriente fault zone.** (1: 13.11.1978 [Ms = 5.1], 2: 01.09.1985 [Ms = 5.1], 3: 12.02.1989 [Ms = 5.2], 4: 22.05.1990 [Ms = 5.1], 5: 26.08.1990 [Ms = 5.9], 6: 04.09.1990 [Ms = 5.2], 7: 26.08.1991 [Ms = 5.2], 8: 25.05.1992 [Ms = 6.9], 9: 27.06.1992 [Ms = 5.3], 10: 27.06.1995 [Ms = 5.6]) [1]**; e) Frequency distribution of hypocentres of Southeastern Cuba in 1979-1994; f) Frequency distribution of hypocentres in Cabo Cruz in 1979-1994.**

Table 1. The most significant earthquakes in southeastern Cuba.

Date/ Locality	Coordinates/ Depth (km)	Magnitude/ Intensity (MSK)	Fatalities/ Injured
11.06.1766/S.Cuba	19.9N,-76.1W/25	6.8/IX	34/700
20.08.1852/S. Cuba	19.75N,-75.32W/30	6.4/VIII	2/200
03.02.1932/S. Cuba	19.75N,-75.58W/35-40	6.75/VIII	14/300

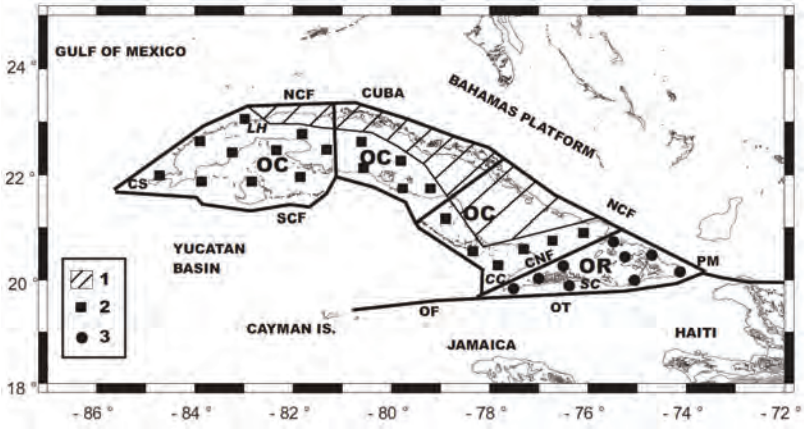

Figure 2. Cuban megablock according with Cotilla *et al.* [22]. (Heavy black line = faults: CNF = Cauto-Nipe, NCF = Nortecubana, OF = Oriente, SCF = Surcubana; Neotectonic Unit: OC = Western, OR = Eastern; crust type: 1 = post-orogenic complex, 2 = orogenic complex, 3 = volcanic arc complex; localities: CC = Cabo Cruz, CS = Cabo de San Antonio, LH = La Habana, PM = Punta de Maisí, SC = Santiago de Cuba).

established by Prol *et al.* [27]. The evolution of this structure was associated with, and considerably influenced by, deep-water troughs such as the Yucatan basin in the southwest, the Old Bahamas Channel in the northeast, and the Oriente trough in the south (**Figure 1(a)**).

Sierra Maestra Range (h = 1,974 m) (**Figures 3(a)**, **3(b)**) has a simple structure [21,29]. Overall, it is an asymmetric swell, derived from an anticlinorium which was formed in the concluding phase of sheet folding in the Late Eocene. Its southern limb is cut off by a series of stepped faults from a deep-water trench (the Oriente trough) and is shifted eastward (**Figure 3(b)**). The relief in this area has a range of up to 10 km, with an average slope dip of up to 16º. On the northern limb the relief varies by about 2 km and the slope, by 3º-5º. Some geomorphologic characteristics [30] indicate that the northern limb is also deformed, and sub latitudinal uplift zones successively decreasing in size from south to north can be identified within it.

The largest newly generated neotectonic element in the structure of Eastern Cuba is the Cauto-Nipe synclinorium system. It developed in association with the Sierra Maestra Range, but is not a piedmont downward in the strict sense of the term [21,30]. According to Mann and Burke [25], the Cauto area constitutes a pull-apart basin, and the city of Bayamo is located within it (**Figures 3(a)**, **4(a)**). The zone where it is located is characterized by significant layers of sediments form the Cauto-Nipe basin [21,30,31] (**Figure 4(b)**), something which evidently favors the amplification of the ground oscillations.

Cabo Cruz, in the eastern end of Southeastern Cuba (**Figures 3(a), 3(b)**), was discovered and named by Cristóbal Colón on 3 May 1494, during his second journey. It is a coastal bar with marine terraces of up to 190 m in altitude and approximately 120 km^2 (**Figure 3(c)**) [29]. It is some 30 km from Niquero (**Figure 3(d)**). This latter location and its surroundings, constitutes a region of plains neighboring the Gulf of Guacanayabo, into which the rivers of the northwest Sierra Maestra flow. The Cabo Cruz submarine area was studied tectonically by Calais and Mercier de Lèpinay [24], who concluded that it is a narrow E-W trending depression, bordered to the north and south by equal numbers of Oriente fault segments. These comprise a set of horst-grabens inside a discontinuous trace of the Oriente fault system.

3. Some General Cuban Data

Cuba was discovered in 1492 by Cristóbal Colón; however it was not until 1512 that the Spanish became established there. To understand the importance of the earthquake under discussion and the information contained in contemporary documents, the historical and demographic situation of Cuba, and in particular of Bayamo, must be

taken into account. **Table 2** shows the different cities and towns founded in Cuba by Don Diego Velázquez de Cuellar, all of them endowed with a church [6]. By the year 1544, more than forty churches and five hospitals existed on the island-Bayamo (in 1518), Santiago de Cuba (in 1520), La Habana (in 1521), Puerto Príncipe (in 1523), and Sancti Spíritus (in 1523)-. All of them had barbers, medical assistants, or itinerant quacks, but no doctors [32]. Population data appear in **Table 3** [6]. All these structures have enabled an evaluation to be made of the damage produced by the earthquake, and consequently, an estimation of seismic intensity.

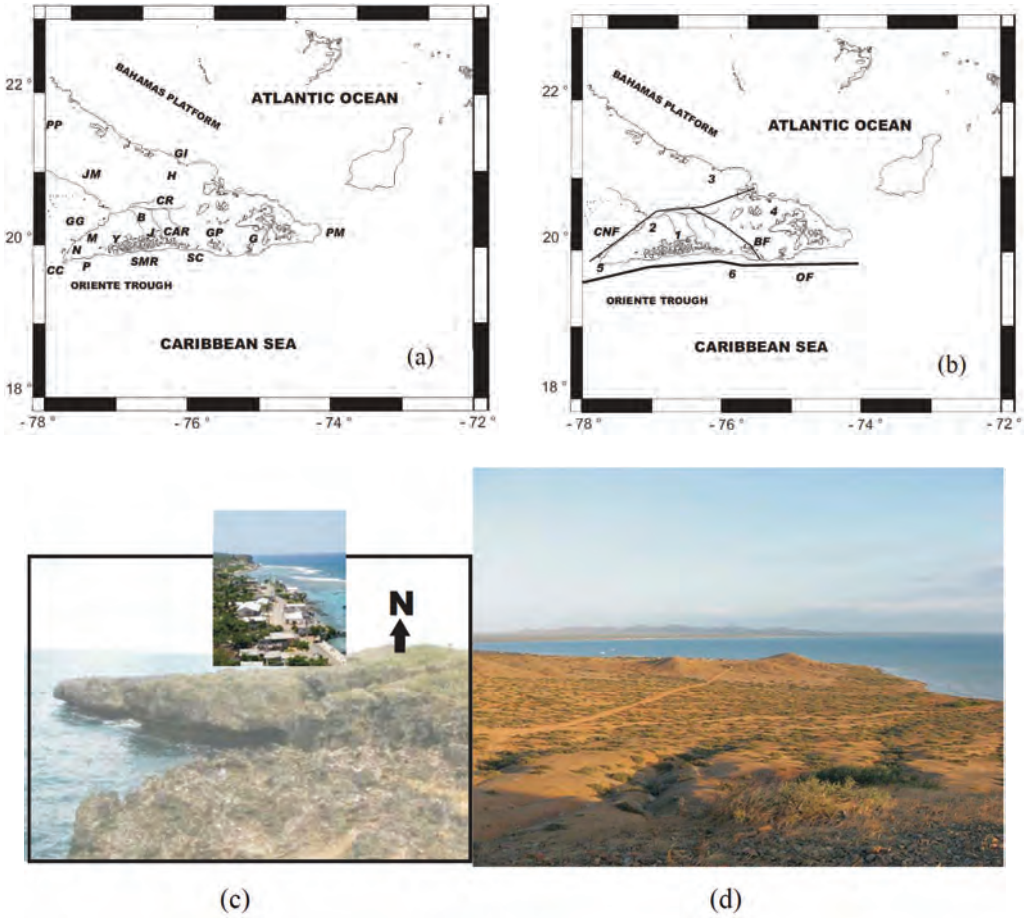

Figure 3. a) Eastern Cuba. Localities (B = Bayamo, CC = Cabo Cruz, CR = Cauto river, CAR = Cautillo river, G = Guantánamo, GG = Guacanayabo Gulf, GI = Gibara, GP = Gran Piedra Mountains, H = Holguín, J = Jiguaní, JM = Jobabo Mines, M = Manzanillo, N = Niquero, P = Pilón, PM = Punta de Maisí, SC = Santiago de Cuba, SMR = Sierra Maestra Range, Y = Yara)**; b) Main structures of Eastern Cuba.** (1 = Sierra Maestra Range, 2 = Cauto basin, 3 = Holguín Heights, 4 = Nipe-Cristal-Sagua-Baracoa Mountains, 5 = Cabo Cruz basin, 6 = Santiago de Cuba deformed belt; faults: BF = Baconao, CNF = Cauto-Nipe, OF = Oriente)**; c) Photo of Cabo Cruz area and the Jaimanitas Formation in the marine terraces (karst); d) Relief and red soil type in Níquero area.**

Table 2. Data of the population census.

Year	Data
1527	Only Spaniards: Baracoa = 12, Puerto Príncipe = 20, Sancti Spíritus = 26, Santiago de Cuba = 20, Trinidad = 12, Bayamo, La Habana and in other localities = 300 (Total = 390)
1556	3,000 Spaniards on the island: Santiago de Cuba = 450, La Habana = 360, Bayamo = 300, Sancti. Spíritus = 200, Puerto Príncipe = 200, Trinidad = 150, Baracoa = 120, Tunas = 100, Cienfuegos = 60, Remedios = 60, Guantánamo = 50, Holguín = 50, Matanzas = 50, San Cristóbal = 30, Consolación del Norte = 30, and in other localities = 790

Table 3. First villages and its dates of foundation.

Date	First denomination	Actually	Date	First denomination	Actually
03.10.1512	Nuestra Señora de la Asunción de Baracoa	Baracoa	19.01.1514	Sancti Spíritus	Sancti Spíritus
05.11.1513	San Salvador de Bayamo	Bayamo	31.01.1514	Santa María de Puerto Príncipe	Camagüey
04.12.1513	San Juan de los Remedios	Remedios	06.07.1515	Santiago de Cuba	Santiago de Cuba
04.01.1514	Trinidad	Trinidad	16.09.1519	San Cristóbal de La Habana	La Habana

The Governor of Cuba initially lived in Bayamo city. Later, in 1517, the residence was moved to Santiago de Cuba (**Figures 1(b)**, **2**, **3(a)**), and finally, from 1550 onwards, the Governor-then Don Gonzalo Pérez de Ángulo (1548-1553)-established his residence on a permanent basis in La Habana (**Figure 2**), given the importance of this port as a point of control for all ships and fleets on their way to the metropolis or to the mainland. However, by 1600 Cuba was under the jurisdiction of Santo Domingo (Hispaniola) (**Figures 1(a)**, **1(b)**, **1(c)**) by a Real Order of the Spanish King Carlos I (1516-1556). On the 8 October 1607, the Spanish King-Felipe II (1598-1621)-divided the island of Cuba into two Governmental administrations, namely, Santiago de Cuba and La Habana (the second one subordinate to the first up until 1628). These administrative elements have subsequently enabled a literature search on historic earthquakes to be carried out successfully.

4. The 1551 Earthquake

4.1. Initial Data

Various authors have referred to the 1551 earthquake in Bayamo, including Álvarez *et al.* [10,11], Bacardí [33], Cotilla [4,6,14], Cotilla and Udías [5], de la Pezuela [34,35], Grases [36], Herrera [37], Montelieu [38], Poey [7-9], Salteraín y Legarra [39], Somohano [40], and Tomblin and Robson [41], but Poey [8] was the first to write about it, "*Tremblement de terre à Bayamo"*. Shortly after, he reaffirmed his previous work about "1551 *earthquake Cuba (Bayamo)*" [7]. However, he did not provide data concerning the time, the day, or the month. Later authors refer only to the information provided by Poey, without contributing anything new with regard to this matter.

The earthquake occurred 59 years after the discovery of Cuba, and 39 years after the founding of the Bayamo city (1512). At that time (1551), the economic and social development of Bayamo had been equal to, or slightly inferior to, that of La Habana and Santiago de Cuba (site of the island Government), because up to 1517, when Santiago de Cuba was named the capital, it had been the capital city of Cuba. As a capital city, it had a coat of arms, and the official residences of both the Governor and of the Bishop of the Diocese, among others, were located there. In 1616, the Cauto River (the most important in Cuba) was navigable as far as the Cautillo River (**Figure 3(a)**). This enabled the movement of goods, principally between Bayamo and Santiago de Cuba. However, its course was modified by a hurricane, bringing a definitive halt to the economic activity, and resulting in the impoverishment of the region. The fluvial course of the Cauto River has subsequently been modified at least twice by tropical cyclones, in 1964 and 2007.

Bayamo and its surroundings formed a center of smuggling activities in Eastern Cuba. In fact this was the main source of discontent among the authorities of the metropolis, and contributed to the war in the XIXth century. The town received resources and goods that were then re-distributed throughout the Eastern District (Holguín, Gibara, Mayarí, Minas de Jobabo, Puerto Príncipe, etc.) (**Figures 3(a)**, **3(b)**). Although the area was frequently attacked by pirates and corsairs, the wealth of financial resources available favored significant development of both the town and the surrounding area (Yara, Niquero, Manzanillo, Jiguaní, etc.) (**Figures 3(a)**, **3(b)**, **4(a)**). In addition to the town of the same name, the jurisdiction of Bayamo included the nearby localities mentioned above, the farms in the area, and those coastal sites that were also inhabited, principally by soldiers, miners, farmers and fishermen. Cuba's first public school and first cemetery were in Bayamo. The first church in Bayamo was originally built (in 1514) in the style of a thatched hut ("bohío") typical to the region, being replaced shortly after by a stone construction built with blocks of limestone (in 1522), in order to welcome the scores of faithful devotees of San Salvador. This was destroyed during the earthquake of 1551, and reconstructed in 1613; however, it was in ruins again following the seism of October 1624 [7-9]. Although Poey mentions "*Tremblement à Bayamo" in his work*, but the authors have not located any other document which confirms this. The event of 1624 will be commented later on.

In La Ilustración Española y Americana [42] the following report appears: "*In November* 1518, *the famous Spanish conqueror Diego Velázquez laid the first foundations of Bayamo*" (this detail is incorrect; it was on the 5 November 1513), "*and at first, the task of colonization was taken very seriously*. *However this undertaking was soon to be paralyzed by emigration to Mexico and other*

parts of the American continent, leaving Bayamo with scarcely 100 *inhabitants*" (erroneous, there were ~200 inhabitants) "*when an earthquake destroyed both housing and the first church*" (imprecise; neither the day nor month of the earthquake in which the earthquake took place are mentioned, and the report only indicates that the first church was destroyed).

Population census data for Bayamo, given in **Table 2**, for the years 1527 and 1556, mention ~200 and 300 Spaniards, respectively (an increase of ~100 people in 29 years, a significant number for the time). This increase can be accounted for by the economic status of the town (church, Government House, Archiepiscopal House, etc., all of them built with limestone blocks), the fertile lands, the favorable position for fishing in the Gulf of Guacanayabo (**Figures 3(a)**, **4(a)**), the navigability of the Cauto River at that time, smuggling, etc.

4.2. New Data

In the present study, new documentation has been uncovered in the AI. Among the contemporary documents there are some sketches and maps of Cuba and Bayamo. We following types should be mentioned: 1) a topographic map of Bayamo and its surroundings (SANTO DOMINGO 582-AI denomination-) from the year 1548 (**Figure 4(a)**); 2) a map of Cuba (SANTO DOMINGO 574-AI denomination-) from the year 1600; and, 3) a sketch of Middle Eastern Cuba (SANTO DOMINGO 608-AI denomination-) from the year 1640 (**Figure 5(a)**). A joint assessment of these documents make it possible to: 1) estimate the level of territorial occupation and the spatial distribution of Spanish towns on the island in its eastern part; 2) establish the names of population centers at that time; and, 3) determine the true position of the main towns and villages. Thus it has been possible to establish that the town of Bayamo, founded by Velásquez, was located very near to the coast on the Gulf of Guacanayabo, south of the Cauto River, on the eastern bank of the Bayamo River (which flows into the Cauto River (**Figures 3(a)**, **4(a)**, **5(a)**). In other words, it was located on the same site it occupies today, and not, as some authors have suggested, on the site of the town of Yara (where Spaniards fought a fierce battle in 1513 against the natives led by their chief Hatüey, who was eventually burnt alive). In addition, the map of Bayamo clearly shows the existence of the church and the Governor's House, as well as their respective dimensions.

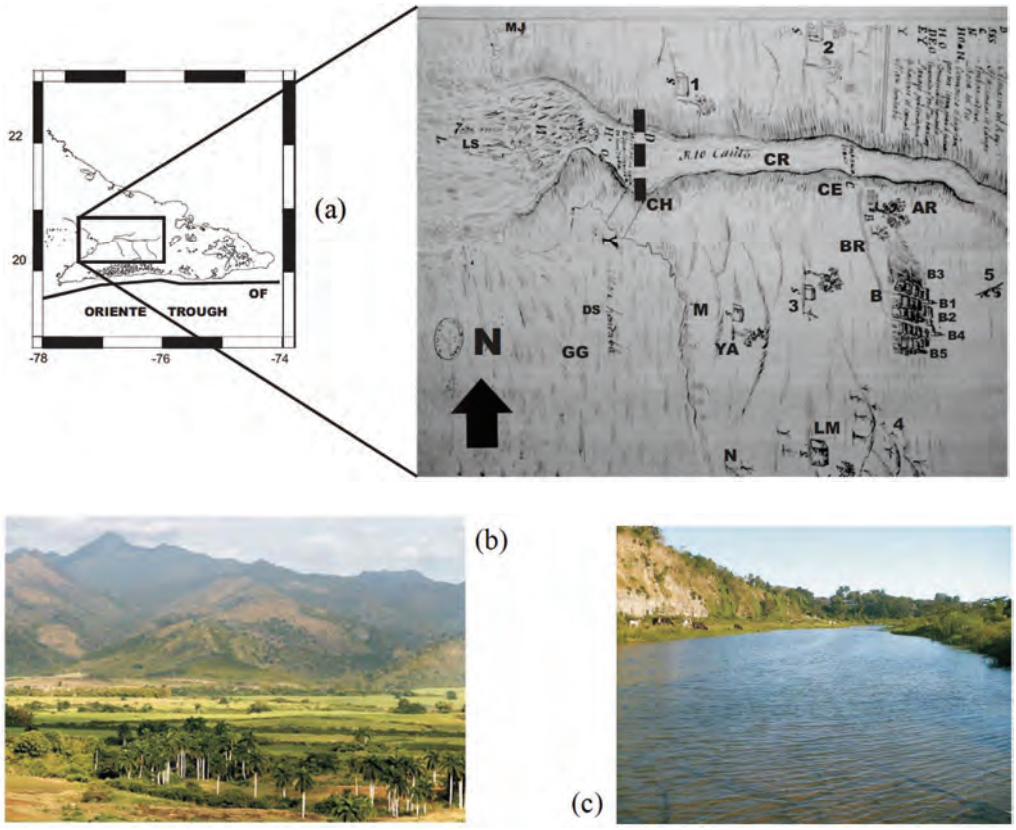

Figure 4. a) Topographic scheme of Bayamo [SANTO DOMINGO 582 of 1548 (-AI denomination-)]. (AR = Almacén del Rey, B = Bayamo, B1 = Cathedral, B2 = Hospital, B3 = Government House, B4 = Cuartel, B5 = Archiepiscopal House, BR = Bayamo river, CE = Cauto Embarcadero, CH = Iron Chain, CR = Cauto river, DS = Deep sea, GG = Guacanayabo Gulf, LM = La Merced, LS = Low sea, M = Manzanillo, MJ = Jobabo mines, N = Niquero, YA = Yara, farms = 1, 2, 3, 4, 5)**; b) Panoramic view of the northern Sierra Maestra Range from Bayamo; c) Segment of Cauto River near Bayamo.**

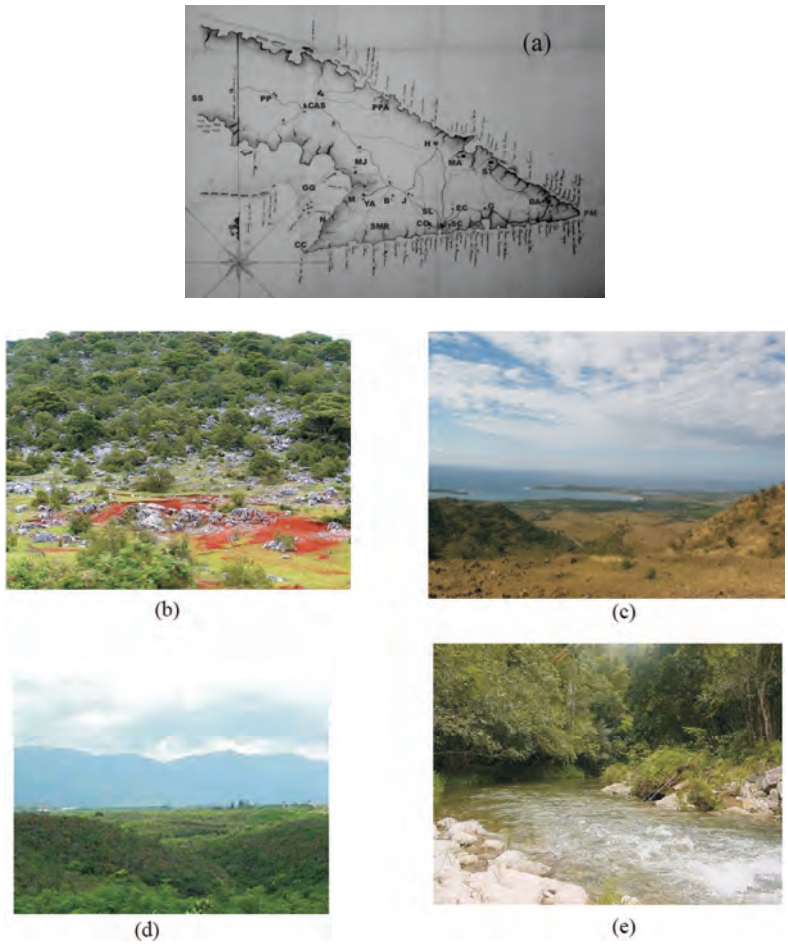

Figure 5. a) Map of the Eastern Cuba [SANTO DOMINGO 608 of 1640 (-AI denomination-)]. See **Figure 3(a)**. (B= Bayamo, BA = Baracoa, BC= Baconao, CAS= Cascorro, CC= Cabo Cruz, CO = El Cobre, G= Guantánamo, GG= Guacanayabo Gulf, H= Holguín, J= Jiguaní, M= Manzanillo, MA= Mayarí, MJ= Jobabo mines, N= Niquero, PP= Puerto Príncipe= Camagüey, PPA= Puerto Padre, SC= Santiago de Cuba, SL= San Luis, SMR= Sierra Maestra Range, SS= Sancti Spiritus, ST= Sagua de Tánamo, Y= Yara); **b) Photo of the relief and rock types in San Luis area; c) View of Manzanillo and Guacanayabo Gulf areas; d) View from Las Mercedes to northern of Sierra Maestra Range; e) Photo of a mountain river in Jiguaní.**

The map of 1548 (SANTO DOMINGO 582) (**Figure 4(a)**) shows, among other things: 1) the dimension of the Cauto River and its navigability upstream, including beyond the town of Bayamo; 2) the town of Bayamo, together with the Cathedral, the Governor's House, and the residential neighborhoods; 3) the river port (today Cauto Embarcadero); 4) the King's Storehouse; and, 5) five farms; etc. This geographic position for Bayamo is supported by the fact that the town would thus have had direct access to the sea (the Gulf of Guacanayabo) close to the mouth of the Cauto River, making navigation inland feasible even as far as Jiguaní (**Figures 3(a)**, **5(a)**), and from there the journey to Santiago de Cuba by road was relatively flat and straightforward, continuing as far as San Luis (**Figures 5(a)**, **5(b)**).

It should be mentioned that between the XVIth and XIXth centuries, at least 10 maps that include the island of Cuba have been edited [43], and the scientific works of the following authors can be cited: 1) Juan de la Cosa (in 1500); 2) Abraham Ortelieus (in 1580); 3) Heyronymi Benzoni (in 1594); 4) Guiljelmus Blaen (in 1638); 5) N. Sanson d'Abbuille (in 1656); 6) Pieter Vander A. A. (in 1728); and 7) Esteban Pichardo (in 1855). In general the cartography of these maps improves with successive editions. However, the map of 1728 has serious errors still, for example: 1) placing Bayamo city in Holguín area (**Figures 3(a)**, **5(a)**); 2) denominating the Cauto River as the Zaza River (which is in the Central region of the island). Even at that time, Guantánamo (**Figures 3(a)**, **5(a)**) was being called Puerto Grande. In the year 1638, the Cauto River was designated on the map as the Bahamas River, and on the same map, the town of Manzanillo (**Figures 3(a)**, **4(a)**, **5(a)**, **5(c)**) appears for the first time. With regard to the cartographic deficiencies in the maps of Cuba, Pichardo [44] commented: "*many earlier and current maps have been compiled by people who have not so much as stepped on*

Cuban territory…" Such comment explains all deficiencies in the mentioned Cuban maps.

The three maps located by the authors in the AI were drawn up in 1548-1640 and it can be seen that the contents are similar to those of maps 2-4 mentioned above. However, the geographic position of Cuban localities given in the materials located in the AI is considerably more accurate than that given in map number 7 (by Pichardo). We are of the opinion that this is due to the fact that they were the work of specialists who were familiar with the territory that they represented, and are therefore reliable. In addition four contemporary hand-written documents relating to the earthquake of 1551 have been located in the AI. A summary of these materials follows:

(Document 1.-) GOVERNMENT PAPERS: 1492-1858. SANTO DOMINGO, JUDICIAL DISTRICTS: 1511, 1512-1858 [-AI denomination-]. (Correspondence of Don Juan de Hiniestrosa, Governor of the village of San Salvador de Bayamo, with Don Gonzalo Pérez de Ángulo, Governor of Cuba)

San Salvador de Bayamo, 28 Octubre 1551

His Excellency, Don Gonzalo Pérez de Ángulo

General Governor of Cuba

It is my duty to inform your Excellency of the events which took place on the 18^{th} (according to the date in the wording of the document, October 1551) *in San Salvador de Bayamo. Close to midday* (11-12 o'clock), *work was interrupted by a dreadful shake* (the main earthquake). *Many have been injured, and the town has suffered serious damage*… (There were no deaths)… *The principal and most severe damage was sustained by the solid and regal barracks, which collapsed, with one person being injured. The Parochial Church which adjoins the barracks, and the hospital* (**Figure 4(a)**), *were completely destroyed*… *all the farms* (according to the 1548 map, there were farms to the south and north of the Cauto River, in the area around Bayamo) *suffered severe damage as a result of the violence of the movements of the earth*… (Destruction)… *in the town, on the* 18^{th} *day at midday, terror struck in the hearts of the men and women laboring in the fields. Beasts fled, sixteen houses in the village collapsed, and another three, although still standing, have huge cracks in their walls*… *two wounded were found*… *the Embarcadero* (on the south bank of the River Cauto, today called Cauto Embarcadero, **Figure 4(a)**) *was destroyed, causing damage to four ships and injuring two people*… *the Church, built of solid stone, has been completely destroyed, the central pillars hang by a miracle*… *the barracks collapsed, and one person was injured*… *the stables fell*… *the prison and the hospital are in ruins*… *the well in the Square has collapsed*… *five houses on the riverside* (Bayamo) *were overturned and sank into the mud* (liquefaction)… *muddy, stinking water flowed from the banks of the river*… *beasts sprawled on the ground*… *The King's Storehouse* (on the southern bank of the Cauto River and to the east of the Embarcadero, **Figure 4(a)**) *has been destroyed. All the merchandise and goods were lost*… *three canons and the defensive line of heavy iron chain* (an army obstacle in the Cauto River which impeded the entry of enemy ships) *have sunk into the mud*… (liquefaction)… *the land is fertile and flat, and the hills only rise in the distance, to the south as an enormous mass, the Gran Sierra* (nowadays known as the Sierra Maestra Range [**Figures 1(c)**, **3(a)**, **3(b)**, **4(b)**, **5(a)**])… *the oldest inhabitants here say that the plain here is different to that of Cuba* (at that time, Santiago de Cuba was frequently referred to as Cuba, and vice versa), *always jerking and shaking*… *the danger was not felt in Cuba*… (Santiago de Cuba seismicity was perfectly well known, but in Bayamo any report)… *the night was pitiful and cold...people kept vigil and there were sudden shocks* (aftershocks)… *a procession carried a statue of the Saintly and Divine Patron Saint* (San Salvador) *in their arms*… *the sub-lieutenant Fernando Rodríguez de Castro returned from patrolling the hills to the south* (Sierra Maestra Range) *and from the coastal posts of Cabo Cruz, Niquero and La Costa* (today Manzanillo) (**Figures 3(a)**, **3(c)**, **5(a)**, **5(c)**), *with the garrison detachment. He reports that at midday on the* 18^{th} *October, they noted the ground moving beneath their feet, and heard noises like thunder emanating from beneath the ground*… *the noises came from the south* (Cabo Cruz), *and huge, solid rocks could be seen strewn across the road to La Merced* (in the mountainous part of the Sierra Maestra range, on the northern side, today Las Mercedes) (**Figures 4(a)**, **5(d)**)… *the beasts of burden refused to advance*… *the cracks in the road were* 12 *varas* (~9 m) *wide* (1 Castillian vara = 0.8359 m)… *two soldiers fell in their saddles to the ground*… *in Yara, all the houses, around twenty or more, were in ruins*… *the timbers and pillars scattered*… (This town is on a low alluvial plain well irrigated by fluvial currents from the Sierra Maestra. Therefore, it is highly probable that liquefaction occurred)… *the sub-lieutenant ordered two soldiers to return at a gallop to the coastal posts* (Cabo Cruz and Níquero [**Figures 3(a)**, **3(d)**, **4(a)**, **5(d)**]) *in order to acquaint themselves of the situation there, whilst the rest marched to La Costa* (Manzanillo)… *they informed him that Cabo Cruz was in ruins*… *two canons were overturned*… *but that there had been no injuries*… *the posts at Níquero and La Costa* (Manzanillo)… *lost everything, and a soldier received a heavy blow when he fell*… *all canons were overturned*… *Jiguaní* ([**Figures 3(a)**, **5(a)**, **5(e)**] town on the western bank of the Cautillo River) *was fiercely and brutally shaken, and the houses ruined, the church and the heavy wood barracks destroyed*… (the above-mentioned towns appear in **Figure 3(a)**)

… *on the night of the* 16^{th} *and the morning of the* 17^{th}, *short, strong earth tremors had been noticed* (foreshocks)… *the ground collapsed and moved like an angry sea*… *never before has such an event been heard of*

here…

(Document 2.-) CUBA 2007 [-AI denomination-]
San Salvador de Bayamo, 19 December 1551
His Excellency, Don Gonzalo Pérez de Ángulo
General Governor of Cuba

…with regard to the inspection of the barracks in this town of San Salvador de Bayamo, the captain Don Bartolomé Quesada de Castro was very surprised and saddened to see the serious damage caused to the town and the destruction of the barracks. He reports that in Sancti Spiritus and Jobabo Mines (**Figures 3(a)**, **4(a)**, **5(a)**) *a strong earth tremor was felt at mid-morning* (12 hours) *on the* 18^{th} *day* (October) *in the barracks. And in the neighboring town of Santa María de Puerto Príncipe* (now Camagüey, [**Figures 3(a)**, **5(a)**]), *the Garrison officer in command assured him that three strong earth tremors had been felt on the* 18^{th} *and* 19^{th} *at dinner time and at night*… (The authors can confirm the occurrence on 18 October of an earthquake and of some aftershocks. In addition, information on perceptibility was gathered in Sancti Spíritus and Camagüey but any subterranean noise was perceptible [**Figure 5(a)**]).

(Document 3.-) CUBA 2027 [-AI denomination-]
San Salvador de Bayamo, 20 December 1551
His Excellency, Don Gonzalo Pérez de Ángulo
General Governor of Cuba

… I can report with pride of the Crown's loyal troops, who have undertaken the repair of the coastal posts… [Cabo Cruz, Niquero and Manzanillo]

(Document 4.-) CUBA 2070 [-AI denomination-]
San Salvador de Bayamo, 14 February 1552
His Excellency, Don Gonzalo Pérez de Ángulo
General Governor of Cuba

…the town's barracks have been rebuilt with timber, and one part serves as a jail. The troops are in good humor, and the terror is fading…

4.3. Earthquake Parameters and Intensity Values Identify the Headings

Using these data (Documents 1-4) the authors have established that the town of San Salvador of Bayamo was located on the present site of Bayamo and not at Yara (**Figures 3(a)**, **4(a)**, **5(a)**) and since the foundation of the town in 1513, earthquakes had never previously been reported. In addition, it can be stated that: 1) the exact date of the occurrence of this earthquake was the 18 October 1551; 2) the approximate time of the seismic event was around midday (11-12 hours); 3) there were at least two foreshocks, on the 16 and 17 October; 4) there were three aftershocks on the 18 October; 5) subterranean noises originating from the south-southwest, Cabo Cruz, were heard up to Bayamo city; 6) there were only seven persons injured, but no deaths; 7) there was panic among the population of Bayamo and alarm and nervousness among the beasts of burden in everywhere; 8) the army post at Cabo Cruz was destroyed and the two heavy cannons overturned, severe subterranean noises [I = 9 degrees, MSK]; 9) the greatest damage to the ground (cracks and large block rocks) was in the surrounding area of the Sierra Maestra Range (La Merced) and soldiers were shaken in their saddles and two fell to the ground together with the saddles [I = 9-8 degrees, MSK]; 10) other two army posts in Niquero and Manzanillo were heavy damaged and all cannons overturned [I = 9-8 degrees, MSK]; 11) the church in Bayamo (built of solid limestone blocks) was totally destroyed, along with the residential neighborhood, the hospital, the jail, the storehouse, and the dock [I = 8 degrees, MSK]; 12) the town at Cauto Embarcadero and four ships were totally destroyed (liquefaction) [I = 8 degrees, MSK]; 13) 21 houses were destroyed and 3 were severely damaged in Bayamo [I = 8 degrees, MSK]; 14) the farms (outside of Bayamo on the southern and northern banks of the Cauto River, but near to the town) were destroyed [I = 8-7 degrees, MSK]; 15) over 20 robust houses (heavy woods) were destroyed in Yara (probably due to liquefaction) [I = 8-7 degrees, MSK]; 16) there were several houses destroyed in Jiguaní [I = 6 degrees, MSK]; 17) Puerto Príncipe village (Camagüey) was very strong shacked [I = 5 degrees, MSK]; 18) in Sancti Spíritus the earthquake was perceptible [I = 3 degrees, MSK].

We must comment that the intensity values of 8 and 9-8 degrees (MSK scale) in Bayamo, Cauto Embarcadero, and Niquero (and it can be assumed also in the King's Storehouse) is explained by the liquefaction phenomena and site effects. That means there are unconsolidated soils in a large fluvial basin (Cauto-Nipe). This is not the case of Cabo Cruz area.

Using these references, it is possible to construct an isoseismal scheme (**Figure 6(a)**), and to estimate a perceptibility area of 40,000 km^2. Then taking the area of greatest value as the central point and as the starting point for a line extending offshore to the south, the approximate epicentral location can be estimated as 19.6 N -77.8 W, which is situated on the knot of faults previously mentioned (**Figure 2**). In addition, this location has a cluster of low magnitude earthquakes with a predominant depth of 15 km (**Figures 1(e)**, **1(f)**) [1,14]. But there were also strong earthquakes in the surrounding area in October 1624 and on the 03.08.1926 [12]; more recently, other five strong earthquakes have been registered [19.02.1976 (Pilón, M = 5.7), 12.02.1989 (M = 5.1), 26.08.1990 (M = 5.1), 25.05.1992 (M = 6.9), and 04.02.2007 (M = 6.2), h~15 km] [6]. These earthquakes, except the one in Pilón (**Figure 6(b)**), are delimited by crossing active faults (Oriente and Cauto-Nipe) in the marine area. This is to the NE of the Cabo Cruz basin (in the marine area).

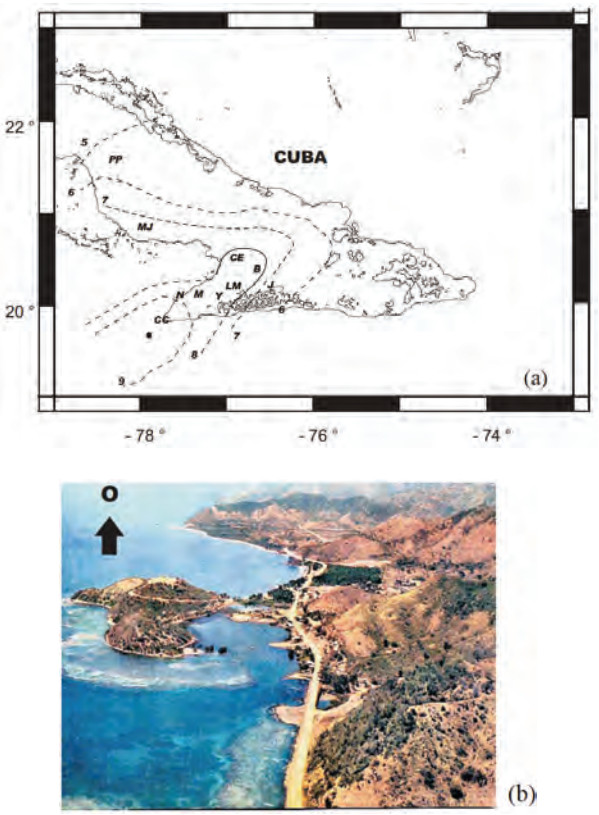

Figure 6. a) Epicentre and isoseismals scheme of the 18 October 1551. (B= Bayamo [I = 8], CC= Cabo Cruz [I = 9], CE = Cauto Embarcadero [I = 9-8], J = Jiguaní [I = 6], LM = Las Mercedes [I = 9-8], M= Manzanillo [I = 8-7], MJ = Jobabo Mines [I = 7], N= Niquero [I = 8], PP = Puerto Príncipe = Camagüey [I = 5], Y = Yara [I = 8-7]; Intensity values [MSK scale] = 6); b**) Photo of Pilón area from the eastern side of the Sierra Maestra Range.**

The maximum intensity value of 1551 earthquake was found in Cabo Cruz, falling off 9-6 degrees (MSK scale) mainly toward the NE (Bayamo). That strike coincides with the direction of the Cauto-Nipe fault [45]. Meanwhile, a study of the latest strong earthquakes which have occurred in the same region (for example, on the 25 May 1992, in Cabo Cruz [46]) shows that the intensity, although decreasing towards the NE (Bayamo), did not exceed 7-5 degrees (MSK scale) [1,47]. Furthermore, the seism of 1992 was noticeable in Sancti Spíritus, just as it was in 1551 [46]. Therefore, we consider the focal region to be in Cabo Cruz area.

The epicenter of the 1551 earthquake has been proposed previously by other authors: 1) Morales y Pedroso [48]; 2) Álvarez *et al.* [11]; 3) Chuy [47]; and 4) Álvarez *et al.* [10]. The locations they identified differ from our proposal and this difference will be discussed. In the first place, these four works have been based exclusively on the seismic event reported by Poey [7-9]. Such data did not include information concerning the month, the day, or the time, of the event, or information on the places where perceptibility was reported. It was simply known that a church in Bayamo had been affected. For this reason, in Cotilla and Udías [5] considered that these identifications were inadequate for being used in seismic hazard situation.

Morales y Pedroso [48] presented an interesting hypothesis of the occurrence of strong earthquakes in Southeastern Cuba. However, we do not share their view, and argue that the 1551 earthquake data fails to support it. For the above author, the epicenter was in the southern marine area of the Sierra Maestra Range, but on the meridian that passes through Bayamo, almost equidistant between Santiago de Cuba and Cabo Cruz. This epicenter location is approximately the same as that for the earthquake of 16 February 1976 in Pilón [12]; however, this last event only produced intensities of 5 degrees (MSK scale) in Bayamo. The other works are more recent. Álvarez *et al.* [11] presented the following data for the earthquake of 1551: 20.40 N-76.60 W, h = 15 km, M = 5.8, I_{max} = 8 degrees (MSK scale). Álvarez *et al.* [11] reported different data for the seism: 19.75 N-75.32 W, h = 30 km, Ms = 7.3, I_{max} = 8 degrees (MSK scale). With respect to these works, that the following should be observed: 1) the data is not consistent; 2) there are no discussions about such changes. An ample discussion regarding similar problems can be found in Cotilla's work [1,14], among other issues. Thus, we also reject these hypotheses.

In order to estimate the magnitude, we started with the experience and results of Cotilla [14], whereby based on the maximum intensity of 9 degrees (MSK scale) at Cabo Cruz, using the Sponheuer [49] relation (Ms = 0.66 I_o + 1.7 log h – 1.4), while assuming a depth of 15 km [14], we obtain a value of 6.6. Álvarez *et al.* [12] and Cotilla [14] determined that the seismogenetic deep of the Oriente fault is of 15-20 km. **Figures 1(e)** and **1(f)** show the main values of hypocentres. Another expression relating magnitude and intensity was used (Ms = 1 + 2/3 I_o [See: Karnik [50]]). This relation gives a magnitude value of 7.0. Also, using Shebalins' relation [51] [I_0 = bM – slog h + c; $I_0 - I_i$ = slog $(\Delta_C{}^2 + h^2)^{1/2}$] we obtained M = 6.7 and h = 17 km. This last value (h) is very similar to our estimation. Consequently, it is our belief that the 18 October 1551 earthquake reached a magnitude rank of 6.6-7.0, and most probably value was 6.6. The fact that there were no deaths and only seven wounded in this earthquake can be explained as being the result of two main factors: 1) foreshocks (alerting the population to the danger); 2) time of the event, at midday (11-12 hours), when the inhabitants were working in the fields.

Finally, we shall briefly refer to the aforementioned October 1624 earthquake in Bayamo. This earthquake

happened 73 years after the event of 1551 and 8 years after closing the Cauto River to the navigation as a consequence of the damages by a strong tropical hurricane. Regardless of the scarce amount of data contributed by Poey, it is possible to assert the following concerning the earthquake: 1) the important intensity value of the seismic event; 2) the repetition of large earthquakes in the Cauto zone; 3) Bayamo's cost-reducing decrease and in consequence the low interest of the authorities, once the migration had started toward Santiago de Cuba and La Habana, and the Governor Residence had changed to La Habana. Likewise, it can be assumed that: 1) the damages at the Cathedral of Bayamo were due to the combination of two adverse factors, soil type and soil conditions; 2) the earthquake focus was located in the same region at 1551.

5. Conclusions

Eastern Cuba suffered a strong earthquake at midday on the 18 October 1551. It has been possible to confirm this data based on a collection of unpublished documents and others in the Archivo General de Indias, thus improving knowledge on the seismicity of this territory. An analysis of historical sources has shown that documents need to be judged very critically, establishing which ones provide first hand information and which more generalized literary accounts are. In addition, awareness of the socioeconomic situation, demographic conditions, building characteristics, etc. is necessary in order to reach a correct damage assessment. Failure to take these considerations into account can lead to significant errors in intensity estimations with the consequent effect on seismic risk assessment.

From the foregoing it appears that the 1551 earthquake was of a greater magnitude than believed until now. Maximum damage was experienced along the Cauto-Nipe fault. There is conclusive field evidence to show that this earthquake was associated with surface faulting. As a result of the shocks, some areas surrounding Bayamo, as well as others at some distance away were intensely damaged. From the description of the effects of the earthquake, it is clear that liquefaction of the ground had a significant effect on damage and on the intensities assigned to the Bayamo area.

According to the information found in the documents, the damage caused by this earthquake may be summarized as follows (locality = Intensity, MSK scale): Cabo Cruz = 9, Sierra Maestra (Las Mercedes) = 9-8, Bayamo = 8, Cauto Embarcadero = 8, Niquero = 8, Yara = 8-7, Manzanillo = 8-7, Jobabo Mines = 7, Jiguaní = 6, Puerto Príncipe = 5, and Sancti Spíritus = 3. The earthquake reached a magnitude of 6.6 and the epicenter was situated at 19.6 N-77.8 W.

6. Acknowledgements

The authors wish to thank the Archivo General de Indias for providing important information and data. The effort and help by the responsible of the reading rooms and the specialists of the AI were decisive to culminate this work. Observations and suggestions made by Agustín Udías and Armando Cisternas allowed us to improve the manuscript. This work has been partially funded by the REN2003-08520-C02-02, REN2002-12494E/RIES and CGL2005-25012-E. Access to facilities and information technology resources was made available to the authors by the Departamento de Física de la Tierra y Astrofísica 1, Facultad de Ciencias Físicas, Universidad Complutense de Madrid.

7. References

[1] M. O. Cotilla, "An Overview on the Seismicity of Cuba," *Journal of Seismology*, Vol. 2, No. 4, 1998, pp. 323-335.

[2] M. Cotilla and D. Córdoba, "Notes on the Three Earthquakes in Santiago de Cuba (14.10.1880, 18.09.1826, 07.07. 1842)," *Russian Geology and Geophysics*, Vol. 51, No. 2, 2010, pp. 228-236.

[3] M. O. Cotilla, "The Santiago de Cuba Earthquake of 11th June 1766: Some new insights," *Geofísica Internacional*, Vol. 42, No. 4, 2003, pp. 589-602.

[4] M. O. Cotilla, "Cuban Seismology," *Revista Historia de América*, Vol. 140, 2010.

[5] M. Cotilla and A. Udías, "La Ciencia Sismológica en Cuba (II). Algunos Terremotos Históricos," *Revista de Historia de América*, in Spanish, Vol. 125, 1999, pp. 45-90.

[6] M. O. Cotilla, "Un recorridoPor La Sismología de Cuba," Editorial Complutense, in Spanish, Madrid, 2007.

[7] A. Poey, "Catalogue Chronologique des Tremblements de Terre Ressentis Dans Les Indes Occidentales de 1530 à 1857. Accompagnè d' une revue bibliographique contenant tous les travaux relatifs aux tremblements de terre des Antilles," *Annuarie de la Societé Mété-orologique de France*, in French, Vol. 5, 1857, pp. 75-227.

[8] A. Poey, "Tableau Chronologique des Tremblements de Terre Resentís a l' ile de Cuba de 1551 à 1855," *Annales des Voyages*, in French, Vol. 11, 1855, p. 301.

[9] A. Poey, "Supplément au Tableau Chronologique des Tremb-Lements de Terre Resentís à l' ile de Cuba de 1530 à 1855," *Annales des Voyages*, in French, Vol. 4, 1855A, p. 286.

[10] L. Álvarez, T. Chuy, J. Garcia, B. Moreno, H. Álvarez, M. Blanco, O. Expósito, O. González and A. I. Fernández, "An Earthquake Catalogue of Cuba and Neighbouring Areas," Internal Report IC/ IR/99/1, The Abdus Salam International Centre for Theoretical Physics, Miramare, Trieste, 1999.

[11] L. Álvarez, R. S. Mijailova and T. Chuy, "Catálogo de Los Terremotos Fuertes de la Región 16°/24°N y

-78°/-86°O, Desde el Siglo XVI Hasta 1988," Informe científico-técnico, in Spanish, Institute de Geofísica y Astronomía, Academia de Ciencias de Cuba, 1993.

[12] L. Álvarez, M. Rubio, T. Chuy and M. Cotilla, "Estudio de la Sismicidad de la Región del Caribe y Estimación Preliminar de la Peligrosidad Sísmica en Cuba," Informe final del tema 310.01, in Spanish, Institute de Geofísica y Astro- nomía, Academia de Ciencias de Cuba, 1985.

[13] K. Burke, J. Grippi and A. M. C. Sengor, "Neogene Structures in Jamaica and the Tectonic Style of the Northern Caribbean Boundary Zone," *The Journal of Geology*, Vol. 88, No. 4, 1980, pp. 375-386.

[14] M. Cotilla, "Una Caracterización Sismotectónica de Cuba. Tesis en opción al grado de Doctor en Ciencias Geográficas (especialidad geofísica)," in Spanish, Institute de Geofísica y Astronomía, Academia de Ciencias de Cuba, 1993.

[15] C. DeMets, R. G. Gorden, D. F. Arges and S. Stein, "Current Plate Motions," *Geophysical Journal International*, Vol. 101, No. 2, 1990, pp. 425-438.

[16] C. DeMets, P. E. Jansma, G. S. Mattioli, T. Dixon, P. Farina, R. Bilham, E. Calais and P. Mann, "GPS Geodetic Constraints on Caribbean-North American Plate motion," *Geophysical Research Letters*, Vol. 27, No. 3, 2000, pp. 437-440.

[17] J. Deng and L. R. Sykes, "Determination of Euler Pole for Contemporary Relative Motion of Caribbean and North American Plates Using Slip Vectors of Intraplate Earthquakes," *Tectonics*, Vol. 14, 1995, pp. 39-53.

[18] T. H. Dixon, F. Faina, C. DeMets, P. Mann and E. Calais, "Relative Motion between the Caribbean and North American Plates and Related Boundary Deformation from a Decade of GPS Observation," *Journal of Geophysical Research*, Vol. 103, No. B7, 1998, pp. 15157-15182.

[19] P. Mann, F. W. Taylor, R. Lawrence Edwards and K. U. Then-Lung, "Actively Evolving Microplate Formation by Oblique Collision and Sideways Motion along Strike-Slip Faults: An Example from the Northeastern Caribbean Plate Margin," *Tectonophysics*, Vol. 246, No. 1-3, 1995, pp. 1-69.

[20] L. R. Sykes, W. R. McCann and A. I. Kafka, "Motion of the Caribbean Plate during Last 7 Million Years: Implications for Earlier Cenozoic Movements," *Journal of Geophysical Research*, Vol. 87, No. 13, 1982, pp. 10656-10676.

[21] Academias de Ciencias de Cuba y de Hungría, "Levantamiento Geológico de las Provincias Orientales, Escala 1:250,000," in Spanish, Institute de Geología y Paleontología, 1981.

[22] M. Cotilla, P. Bankwitz, H. J. Franzke, L. Álvarez, E. González, J. L. Díaz, G. Grünthal, J. Pilarski and F. Arteaga, "Mapa Sismotectónico de Cuba, Escala 1: 1,000,000," *Comunicaciones Científicas sobre Geofísicay Astronomía*, in Spanish, Vol. 23, 1991, pp. 1-49.

[23] J. Lewis and G. Draper, "Geology and Tectonic Evolution of the Northern Caribbean Region," In: G. Deng and J. Case, Ed., *The Caribbean Region: The Geology of North America*, Geological Society of America, America, 1990, pp. 77-140.

[24] E. Calais and B. Mercier de Lèpinay, "From Transtension to Transpression along the Southern Caribbean Plate Boundary off Cuba: Implications for the Recent Motion of the Caribbean Plate," *Tectonophysics*, Vol. 186, No. 3-4, 1991, pp. 329-350.

[25] P. Mann and K. Burke, "Neotectonics of the Caribbean," *Review of Geophysics and Space Physics*, Vol. 22, No. 4, 1984, pp. 309-392.

[26] J. F. Pacheco and L. R. Sykes, "Seismic Moment Catalog of Large Shallow Earthquakes, 1990 to 1989," *Bulletin of the Seismological Society of America*, Vol. 82, No. 3, 1992, pp. 1306-1349.

[27] J. Prol, G. Ariaza and R. Otero, "Sobre la Confección de los Mapas de Profundidad del Basamento y Espesor de la Corteza Terrestre en el Territorio Cubano," Informe científico-técnico de la Empresa Nacional de Geofísica, in Spanish, Ministerio de la Industria Básica de Cuba, 1993, p. 36.

[28] V. I. Makarov, "Recent Tectonics of Eastern Cuba. Part 2. The Sierra Maestra-Baracoa Orogenic System. General conclusions," *Geotectonics*, Vol. 21, No. 2, 1987, pp. 169-174.

[29] E. C. Gónzalez, M. O. Cotilla, C. C. Cañete, J. L. Díaz, C. Carral and F. Arteaga, "Estudio Morfoestructural de Cuba," *Geografia Fisica e Dinamica Quaternaria*, in Spanish, Vol. 26, No. 1, 2003, pp. 49-70.

[30] M. Cotilla, E. González, H. J. Franzke, J. L. Díaz, J. Oro, F. Arteaga and L. Álvarez, "Mapa Neotectónico de Cuba, Escala 1:1,000,000," *Comunicaciones Científicas Sobre Geofísica y Astronomía*, in Spanish, Vol. 22, 1991A, p. 37.

[31] M. Cotilla and D. Córdoba, "Seismicity and Seismoactive Faults of Cuba," *Russian Geology and Geophysics*, Vol. 48, No. 6, 2007, pp. 505-522.

[32] Gaceta Médica de México, "Cronología Médica Mexicana. Curadores de heridas y boticarios," in Spanish, 31 de Diciembre, 1945.

[33] E. Bacardí, "Crónicas de Santiago de Cuba. Tomos 1-5," Tipografía de Carbonell y Esteva, in Spanish, Barcelona-España, 1925.

[34] J. de la Pezuela, **"**Diccionario Geográfico, Estadístico e Histórico de la Isla de Cuba," Imprenta del Banco Industrialy Mercantil, in Spanish, Madrid, 1866.

[35] J. de la Pezuela, "Diccionario Geográfico, Estadístico e Histórico de la Isla de Cuba," Imprenta del Establecimiento de Mellado, in Spanish, Madrid, 1863.

[36] J. Grases, "Terremotos Destructores del Caribe 1502-1990," UNESCO-RELACIS, in Spanish,Caracas, 1990.

[37] D. Herrera, "Memoria Sobre Los Huracanes en la Isla de Cuba," La Habana, in Spanish, 1847.

[38] E. Monteulieu, "Notas y Apuntes Acerca de Terremotos Ocurridos en Cuba," (Unpublished) Archivo del Instirute de Geofísica y Astronomía, in Spanish, Academia de

Ciencias de Cuba, 1968.

[39] P. Salteraín y Legarra, "Ligera Reseña de los Temblores de Tierra Ocurridos en la Isla de Cuba," *Anales de la Academia de Ciencias Médicas, Físicas y Naturales de La Habana*, in Spanish, Vol. 21, 1884, pp. 203-218.

[40] A. Somohano, "A Catalogue of Earthquakes Felt at Cuba," Thesis of Diploma of Imperial College, London, 1969.

[41] J. Tomblin and G. R. Robson, "A Catalogue of Felt Earthquakes for Jamaica with References to Other Islands in the Greater Antilles, 1524-1971," Mines Geology Division Special Publication, Jamaica, 1977.

[42] S. P. J. Lcitao, "La Ilustración Españolay Americana," *Selgas*, in Spanish, Vol. XV, No. XXXII, 25 de Noviembre 1871, p. 575.

[43] Academia de Ciencias de Cuba, "Nuevo Atlas de Cuba," in Spanish, Edited in Madrid, 1989.

[44] E. Pichardo, "Geografía de la Isla de Cuba," Establecimiento Tipográfico de Don M. Soler, in Spanish, La Habana, 1854.

[45] M. Cotilla and D. Córdoba, "Study of the Cuban Fractures," *Geotectonics*, Vol. 44, No. 2, 2010A, pp. 176-202.

[46] Centro Nacional de Investigaciones Sismológicas, CENAIS, "Informe del Terremoto del 25.05.1992 en Cabo Cruz," in Spanish, Centro Nacional de Investigaciones Sismológicas, 1992.

[47] T. Chuy, "Macrosísmica de Cuba y su Aplicación en Los Estudios de Peligrosidad y Microzonación Sísmica," in Spanish, Fondos de la Fundación "García Siñériz", España, 1999.

[48] L. Morales y Pedroso, "El terremoto de Santiago de Cuba de 3 de Febrero de 1932," *Revista de la Sociedad Cubana de Ingenieros*, in Spanish, Vol. 25, No. 2, 1933, pp. 123-166.

[49] W. Sponheuer, "Methoden zur Herdtiefenstimmung der Makoseismik," Freiberg Forschungs-hefte, C88, in German, Akademie Verlag, Berlin, 1960.

[50] V. Karnik, "Seismicity of the European Area," *Reidel, Dodrecht*, Vol. 1, 1969, pp. 64-82.

[51] N. V. Shebalin, "Methods of Using Engineering-Seismology Data in Seismic Zoning". In: S. F. Medvedev, Ed., *Seismic zoning of the USSR*, Akademik Nauk of USSR, 1968, pp. 101-121.

International Journal of Geosciences, **2010, 14-20**
doi:10.4236/ijg.2010.11002 Published Online May 2010 (http://www.SciRP.org/journal/ijg)

Sedimentation Processes at the Navigation Channel of the Liquefied Natural Gas (LNG) Port, Nile Delta, Egypt

Essam Abd El-Halim Mohamed Deabes
Physical Oceanography Department, Coastal Research Institute (*CoRI*), *Alexandria, Egypt*
E-mail: *Deabes@yahoo.com*
Received March 12, 2010; *revised April* 11, 2010; *accepted May* 5, 2010

Abstract

Liquefied Natural Gas (LNG) port is located at Abu Qir Bay on the northwestern coast of the Nile delta, Egypt. The port was constructed in 2004 to export liquefied natural gas worldwide. The offshore basins of this port including the turning and berthing areas (15-m depth) are connected to the deep water by a 15-m depth dredged channel that extends 4 km offshore. However, the navigation channel and its contiguous basins have experienced problematic shoaling that might affect the navigation activities of gas tankers. Sedimentation processes have been investigated by analyses of waves, currents, bathymetry, grain size of seabed and channel dimensions. Sedimentation rates are estimated using a developed numerical model. Sedimentation rate fluctuates between 0.048×10^6 m^3/month and 0.388×10^6 m^3/month, with an annual sedimentation rate of 1.977×10^6 m^3/yr. The variance in the sedimentation rates between winter and summer resulted in increasing of current speed and direction flowing towards offshore. The sedimentation process is influenced by the temporal variability in the direction and intensity of the predominant waves, currents, orientation of navigation channel, basin breakwaters, seafloor morphology and sediment sources. Due to the geographic location of LNG port it lays within a sediment sink for sediments supplied from different alternating directions by several pathways, flowing towards the N-W, S-W, N-E, and S-E quadrants. Most of these currents components are substantially effective in transporting fine-grained sediment towards the navigation channel axis and contiguous basins. Together with these currents, the predominant NW and SE waves acting to agitate and stirrup sediments in the vicinity of the port, and thereby accelerating sedimentation rates.

Keywords: Sedimentation Rate, Nile Delta, Navigation Channel, Bed Load, Suspended Load and Sediment Transport

1. Introduction

During the last three decades, there have been a large number of harbors built along the Nile delta coast as a result of the increasing development of this valuable region. Unfortunately, most of these harbors are experiencing frequent sedimentation and siltation in their access channels due to the higher littoral drift rate and sedimentation imbalance [1]. Consequently, harbor authorities have to periodically dredge and remove away the accumulated sand in order to improve the navigation shoaling. For example at the Damietta harbor, routinely annual dredging of its channel has being undertaken since 1986, averaging of 1.18×10^6 m^3/yr [2]. Studies dealt with sedimentation of the Damietta channel are also discussed by Deabes [3] and Abd-Allah, *et al*. [4].

The Liquefied Natural Gas (LNG) port was constructed in 2004, to export liquefied natural gas to other countries worldwide. The port is located on the inner continental shelf of the northwestern Nile Delta and at about 13-km southwest of the Rosetta Nile mouth. The turning and berthing basins (15 m depth) are connected to the deep water by means of dredged channel-entrance of 4 km length (**Figure 1**). This navigation channel is oriented in the NW direction (~1350 from the north) and attaining about 15-m depth and 245 m width. The berthing basin is connected with the shore facilities via a ~2.0-km long pier (pilled jetty). This long pier carries the liquefied gas pipeline system up to the berthing basin. The side slopes of the channel are approximately 1:25 (eastern bank) and 1:75 (western bank). The port basins are protected from the N-W waves by a breakwater of ~900 m length which is roughly parallel to the shoreline.

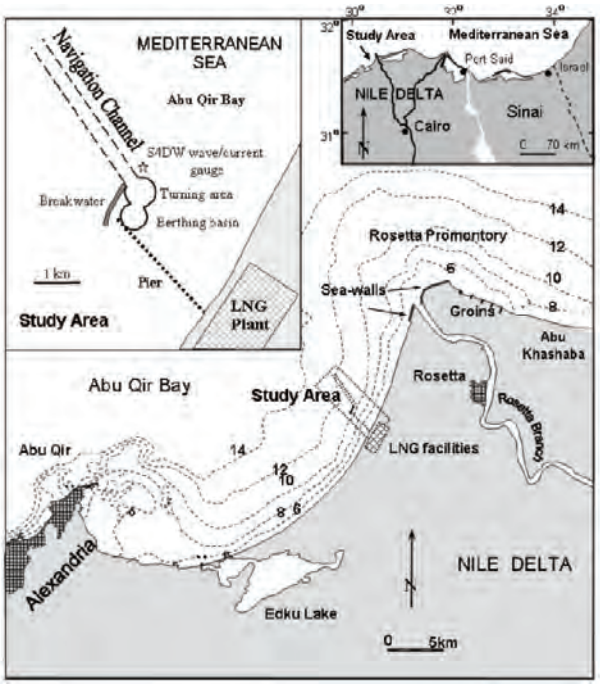

Figure 1. Map of Abu Qir Bay on the Nile delta coast showing location of the Natural Gas (LNG) Port. The inset map shows the navigation channel, the turning and berthing basins of the port. Depth contours in maters.

This breakwater is placed at 11.5 m depth contour. This breakwater also provided shelter for anchored vessels.

The primary objective of this study is to estimate the monthly sedimentation rates in the navigation channel of the LNG port using a developed numerical model. The second objective is to analyze driving forces (waves and currents) that are influenced in the sedimentation process. Generally, there are two approaches commonly used when estimating the sedimentation rates in channels and trenches. The first method involves calculating different change in water depth between two successive bathymetric surveys and the second empirically computes the volume of material that deposited into a navigation channel or a pathway. In this study a mathematical model has been developed to estimate rates of sediment deposited in the navigation channel.

2. Material and Methods

In this study, main factors contributing to the process of sedimentation of the LNG port are assessed, including waves, currents, bathymetry and grain size distribution of seabed sediments. Wave and current data are provided by the coastal Research Institute [5]. Whereas the nearshore bathymetry and mean grain size distribution of the nearshore area hosted the navigation channel and port basins are consulted from Frihy *et al*. [6].

Wave regime is statistically analyzed from wave records measured at Abu Qir Bay (see inset map in **Figure 1** for location). Waves were measured using S4DW gauge installed in 10 m water depth immediately north of the turning area. This wave gauge records both directional wave and current spectrum for 20 minutes every 4 hours. Measurements were recorded over 12 months between October 2004 and September 2005. The raw data obtained from the S4DW gauge was transferred to a PC computer and statistically analyzed to determine wave height, wave period, wave direction and current (speed and direction).

2.1. Mathematical Model Developed

In preceding years, many simplest prediction methods have been proposed to calculate the sedimentation rate of dredged channels. More reliable prediction methods are those used mathematical or numerical model in which the sediment transport rate is computed from current and wave information. Basically, an accurate sedimentation prediction requires diverse information on detailed field survey to determine the boundary conditions, current speed, streamline patterns, wave characteristics, grain size, composition and porosity of bed materials, sediment concentration, particle fall velocities of suspended sediment and effective bed roughness.

Before discussing the mathematical approach developed in this study a cross and longitudinal diagram for the navigation channel with mathematic definition are presented in **Figure 2**. The present model is developed to

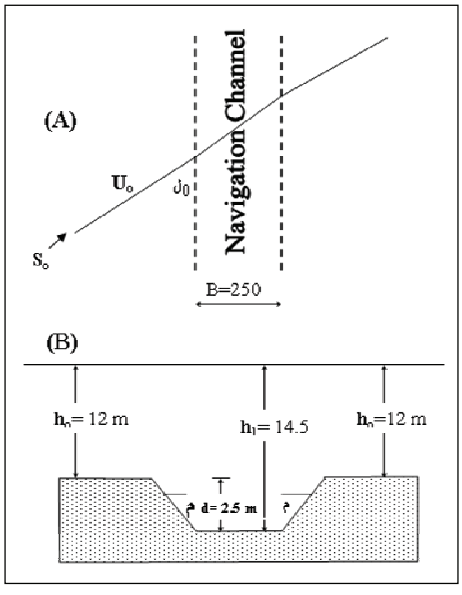

Figure 2. Longitudinal (A) and across-navigation channel sections (B) of LNG port, with mathematic definitions cited in the text.

compute the sediment transport rate (bed-load and suspended-load) from the current and wave characteristics according to the transport law derived by Bailard [7] and Bailard and Inman [8], their formulae are given as follow:

$$q_b = \frac{\rho\ f_w\ e_b}{(\rho_s - \rho)\ g\ \tan\gamma}\left(U^3 - \frac{\tan\beta}{\tan\gamma}\ |U|^3\right) \quad (1)$$

$$q_s = \frac{\rho\ f_w\ e_s}{(\rho_s - \rho)\ g\ W_s}\left(|U^3|\ U - \frac{e_s}{W_s}\ \tan\beta\ |U|^5\right) \quad (2)$$

in which :

q_b = instantaneous bed-load transport rate per unit length (m^2/sec)

q_s = instantaneous suspended-load transport rate per unit length (m^2/sec)

f_w = friction factor

e_b = efficiency factor for bed load transport (= 0.11-0.15)

e_s = efficiency factor for suspended load transport (= 0.016-0.024)

β = local bottom slope (^{o})

γ = dynamic friction angle (^{o})

γ = 0.75 for $\Phi = 0^o$, γ = 0.75 for $\Phi = 90^o$ and

γ = 1.1 for $\Phi = 180^o$

(liner interpolation for intermediate values)

W_s= particle fall velocity (m/sec)

$U = |U^2_w + U^2_c + 2\ U_w\ U_c \cos\Phi|^{0.5}$ (m/sec)

= instantaneous near-bed velocity vector

$U_w = \hat{u}_\delta \sin(\omega t)$ = near-bed orbital velocity (m/sec)

U_c = near-bed current velocity (m/sec)

Φ = angle between current direction and wave propagation direction

$\hat{u}_\delta$ = velocity at the edge of the wave boundary layer $= \omega\ \hat{A}_\delta$ (m/sec)

$\omega = 2\ л / T$ = angular velocity

The friction factor f_w is calculated as follows.

$$f_w = \exp\left[-6 + 5.2\left(\hat{A}_\delta / K_s\right)^{-0.19}\right] \quad (3)$$

in which:

$$\hat{A}_\delta = \frac{H}{2\sinh(kh)}$$

= the peak value of the orbital excursion (m)

H = wave height (m)

k = wave number (m^{-1})

h = water depth (m)

K_s = bed roughness (m)

$K_s = 2\ d_{50}$

d_{50} = is the diameter of grain size

The particle fall velocity is calculated as follows.

$$W_s = \frac{10\ \nu}{d}\left[\left(1 + \frac{0.01(S-1)gd^3}{\nu^2}\right)^{0.5} - 1\right] \quad (4)$$

for $100 < d < 1000$ μm

in which:

$d = d_{50}$ = sieve diameter (m)

S = specific gravity (= 2.65)

ν = kinematic viscosity coefficient (m^2/sec)

$\nu = 1.011 \times 10^{-6}$ m^2/sec at T=20℃

$\nu = [1.14 - 0.031\ (T - 15) + 0.00068\ (T - 15)^2] \times 10^{-6}$

The sedimentation rate per unit length of the navigation channel of LNG port is equal to sum of the bed-load transport which was completely deposited in the channel plus a small portion of suspended-load deposited in the channel (ΔS). According to Sutrench model [9], the sedimentation rate (ΔS) per unit length of channel resulting from the incoming suspended-load sediment transport can be calculated by the following equation:

$$\Delta S = e\ S_0 \sin\alpha_0$$

in which:

e = the trapping efficiency factor

S_0 = incoming suspended load transport

α_0 = the approach angle (angle between the direction of current and channel axis)

The trapping efficiency factor (e) is defined as the relative difference of the incoming suspended load transport and the minimum suspended load transport in the channel. In the present study the trapping efficiency factor (e) for the navigation channel of the LNG port has been determined using the graphs constructed by the application of Sutrench model [9].

3. Results and Discussion

The first requirement in dealing with harbor sedimentation is to understand the processes and hydrodynamic forces dominated, such as waves, water circulation, sediment sources, seabed topography and port orientation.

3.1. Wave Characteristics

Waves and currents are the principal driving forces for the transport of sediments on the most of the coasts and adjacent shelves. The main function of waves is to agitate the sediments and put them in suspension case. They are also responsible for driving sediment along shoreline and/or in the on-offshore directions. So characterization of waves and currents is necessary to understand their role in inducing shoreline changes and sedimentation process in channels and waterways.

Results yielded from statistical analysis of wave data recorded at the LNG port are depicted as monthly and

annual roses in **Figures 3(A)** and **3(B)**. As can be seen, waves mainly approach the port from two quadrants, the N-W (NNW, NW, and WNW) and N-E (NNE, NE, and ENE). The percentage of occurrence of waves blown from the N-W and N-E quadrants, respectively, is 92% and 7% during the examined wave period. Winter storm-waves, Hs > 2 m, occurred 8 times versus ordinary waves (Hs less than 2 m). About 81% of waves have wave height less than 1.0 m. Maximum and average annual significant wave height are 4.51 m and 0.66 m, respectively, (measured at 10-m water depth) with a mean peak spectral wave period of 6.7 second. Overall, the study area is wave dominated environment. Tide is a typical semi-diurnal microtidal regime with a mean tidal range of 50 cm [3].

The monthly distribution of wave direction in **Figure 3(A)** demonstrates that the N-W waves appear in all examined one-year period, while the N-E waves exist only in 5 months (October, November, December, January and April). Only three months (October, December, and May) reveal waves blowing from the S-W quadrant. As expected, the monthly average and maximum wave height in winter period is greater than that in summer period. Among all directions, the N-W and to some extent the N-E waves are of greater importance for sediment transport processes because of their long duration, particularly in winter. These predominant wave components are responsible for driving energy toward the LNG navigation channel resulting in agitation and turbulence of the seabed sediment. The offshore breakwater east of the turning and berthing basins provide natural protection and sheltering from waves arrives from the NW (92%), and totally exposed to the NE component (7%), **Figures 1** and **3**. Therefore, the lack of any significant shelters of the navigation channel means that it is essentially open to all waves approaching from the prevailing N-W and N-E quadrants, leading to stirrup and agitates sediments in the vicinity of the port, and thereby increasing sedimentation.

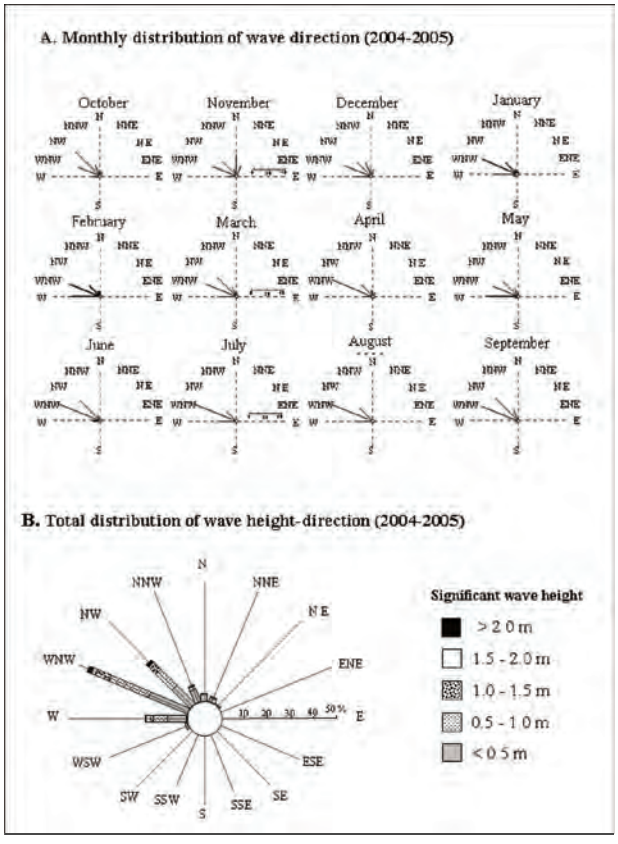

Figure 3. (A) Monthly distribution of waves measured at Abu Qir Bay between October 2004 and September 2005 (12 months). (B) Total distribution of wave height-direction (wave rose) at the same period.

3.2. Current Regime

Current regime was analyzed from records measured immediately east of LNG port using the S4DW wave gauge (see position in **Figure 1**). Results demonstrate that currents in the study area moving towards all directions, being N-W (52%), S-W (20%), N-E (15%) and S-E (13%) quadrants (**Figures 4** and **5**). As the monthly average (9.6 m/sec) and maximum current speeds (32.5 m/sec) in winter are greater than that in summer months (3.2 m/sec and 15.3 m/sec), sedimentation rate in winter is much higher (**Figure 6(C)**). Currents flowing towards the NE to SW (20%) that are responsible for transporting sediment from moving sediment eroded from the Rosetta promontory are essentially effective in the sedimentation process of the navigation channel and the berthing basin. The Rosetta promontory north of the study area has been subjected to some of the most severe shoreline and seabed erosion of all the world's delta coastlines during the 20th century [6,10], see **Figure 1** for location. Under the effect of waves and currents major transport reversal occurs in front of the Rosetta mouth, creating a divergent sediment transport nodal zone where sand moves to both the east and southwest away from the month. Acting with the S-W currents (20%) are the opposing N-E currents (15%) that move sediment from Abu Qir Bay towards the navigation channel as well as the port basins (**Figure 5**). Both the southwest and northeast-directed sediment are the major factors contributed to the sedimentation processes of the LNG port. The other opposing seaward N-W (52%) and landward S-E (13%) currents also affect the port substantially. However, among these two quadrants, the NW (17%) and SE (3.6%) current components have insignificant contribution to the sedimentation processes because they are generally flowing parallel to the main axis of the entrance channel. It has been found that the interpreted current regime in LNG area is closely corresponds to the overall pattern obtained by Frihy *et al.* [6] based on the

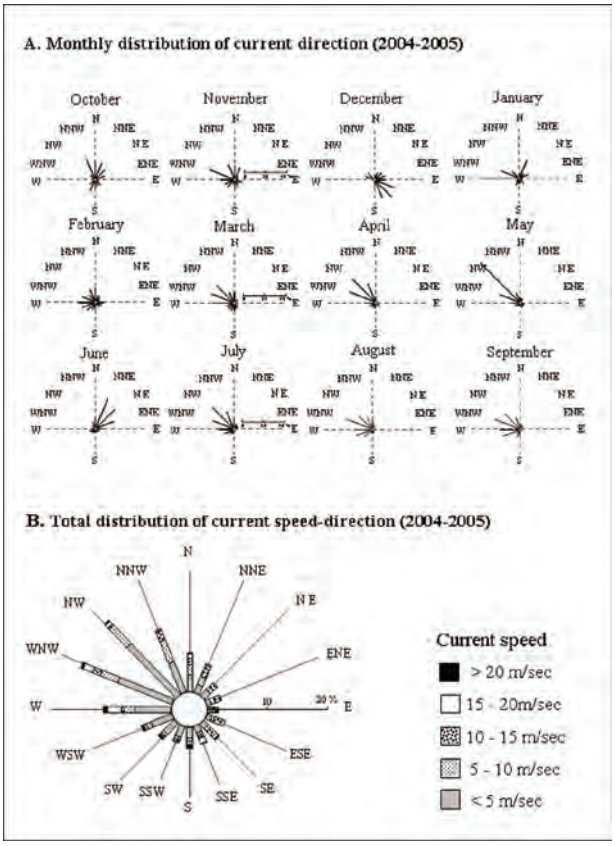

Figure 4. (A) Monthly distribution of current directions at Abu Qir Bay between October 2004 and September 2005 (12 months). (B) Total distribution of current speed direction (current rose) at the same period.

spatial dispersion of mean grain size and magnetic minerals in the seabed sediments.

3.3. Sedimentation Process

Grain size distribution of sediments hosting LNG port has been described by Frihy *et al.* [6]. Accordingly, cross-shelf sediment pattern shows fining trends in two directions. A seaward fining trend starts from the shoreline to a distance of 10 km at 15 m water depth (Mz = 0.004-0.063-mm). This fining pattern indicates sediment transport to the NW and is mainly caused by a shoreward increase of wave energy dissipation induced by shoaling and current-driven sediment transport processes. Unlike this pattern, cross-contour clay and silt belts (0.01 to 0.06 mm) truncate the sand belts at the north sector of the area. This sediment pattern suggests that the fine-grained sand and mud flooring the vicinity of the port area are able to be bypassed to the navigation channel and basins and thereby inducing sedimentation.

The data required to run the developed include time series of waves and currents, grain size of seabed sediment (Mz = 0.09), channel width (250 m), length (4000 m), orientation of channel axis (135° from north) and bathymetric map of (see **Figure 5**). Results obtained from running the developed numerical model are listed in **Table 1**. As can be noticed the sedimentation rate calculated during winter (October 2004-March 2005) is greater than that of summer (April 2005-September 2005). Winter period is generally characterized by higher monthly sedimentation rates (> 0.1×10^6 m^3/month), with a maximum rate of 0.388×10^6 m^3/month occurred in January 2005. Whereas, lower rates (< 0.1×10^6 m^3/month) occurred in summer, with a lowest value 0.048×10^6 m^3/month in July 2005. The annual rate of sedimentation is 1.977×10^6 m^3/yr.

The proportion of bed-load sediments fluctuates between 68.2 and 83.9%, with an average of 78%. Suspended-load varies from 16.1 to 31.8%, with an average 22%. This means that suspended-load sediments contributed to about 22% of the volume of deposited sands, while bed-load sediments represent about 78% of that volume.

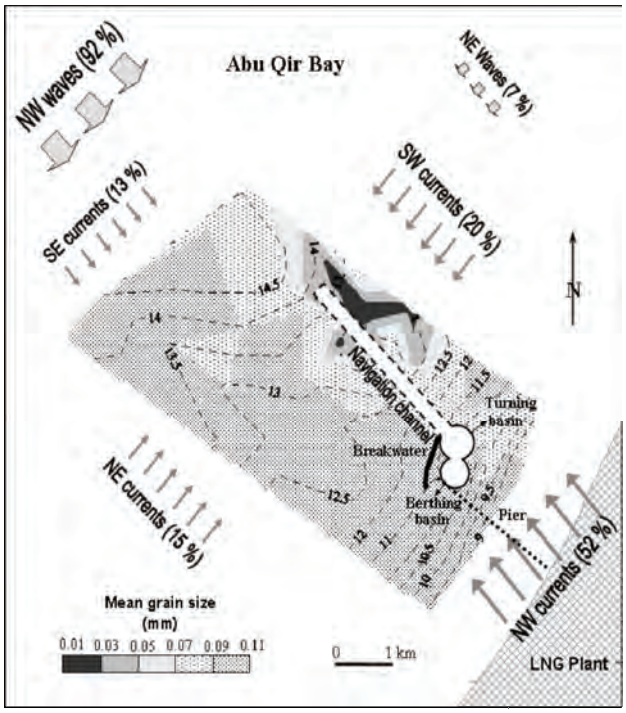

Figure 5. Map of the nearshore area of the study LNG port showing spatial distribution of mean grain size of bottom sediments and bathymetry (modified from Frihy *et al.* [6]). Sediment transport paths involved in the sedimentation processes of the port channel and basins are depicted as arrows. The size of arrows quantitatively represents wave and current proportions. The general transport paths indicate that the port area is interpreted as a sediment sink for several current pathways towards the N-W, S-W, N-E, and S-E quadrants. Depth contours in meters.

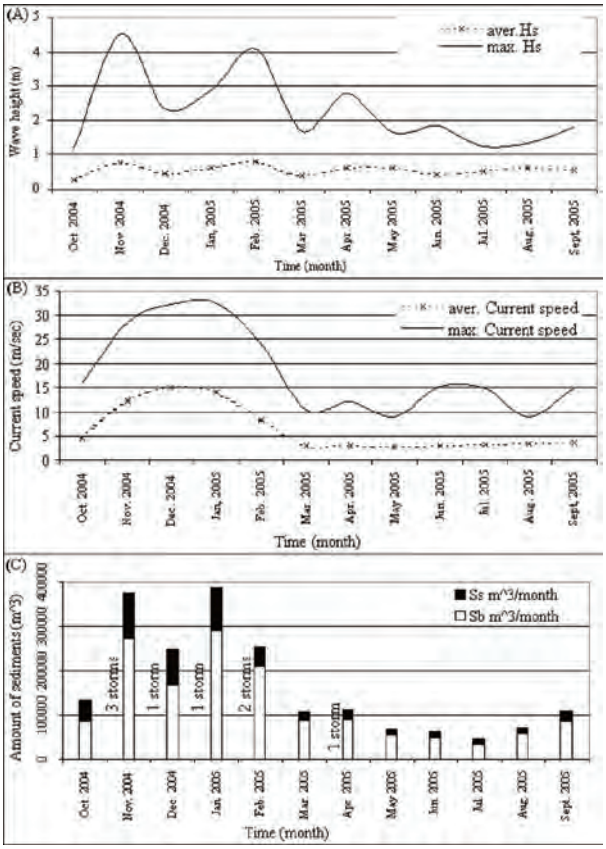

Figure 6. Monthly average and maximum values of significant wave height (A) and current speed (B). (C) Sediments involved in the processes of sedimentation of the navigation cannel and port basins are suspended matters (Ss) and bedload modes (Sb). Results estimated using the model developed in the present study between October 2004 and September 2005.

Table 1. Calculated monthly volume, suspended and bed load sediments acting in the navigation channel of LNG port between october 2004 and september 2005.

Months	Sb (m^3)	Ss (m^3)	total Qs (m^3)	Sb%	Ss%
Oct. 2004	91702.58	33745.54	125448.12	73.10	26.9
Nov. 2004	274124.91	103036.86	377161.77	72.68	27.32
Dec. 2004	169666.30	79275.65	248941.95	68.15	31.85
Jan. 2005	290910.17	97072.49	387982.66	74.98	25.02
Feb. 2005	209939.43	44601.09	254540.52	82.48	17.52
Mar. 2005	89237.03	17067.55	106304.58	83.94	16.06
Apr. 2005	91493.67	20765.84	112259.51	81.50	18.50
May 2005	56443.38	13660.22	70103.60	80.51	19.49
Jun. 2005	49917.33	13782.31	63699.64	78.36	21.64
Jul. 2005	35261.74	12871.43	48133.16	73.26	26.74
Aug. 2005	60384.48	12040.26	72424.74	83.38	16.62
Sept. 2005	85948.23	24332.42	110280.65	77.94	22.06
Total period	1505029.24	472251.66	1977280.9	77.60	22.40

(Sb = bed-load sedimentation rate
Ss = suspended-load sedimentation rate)

4. Summary and Conclusions

The two port basins (turning and berthing areas) and the contiguous navigation channel of LNG port are located at Abu Qir Bay on the northwest margin of the Nile delta. This port is of considerable socioeconomic importance, supporting exporting gas industry that relies on the sheltered port areas to serve as mooring points for the international gas tankers. Presently, the channel entrance and the two basins (15-m water depth) are experiencing considerable sedimentation; therefore they are dredged periodically to insure safety navigation for LNG vessels.

A dataset of waves, current and texture of seabed are interpreted to precisely evaluate sedimentation processes taking place in this port. Waves approach the port blowing from two main dominant quadrants, the N-W and N-E. These waves actively act to agitate and stirrup sediments as bead-load and suspended modes, directly toward the navigation channel and port basins. However, the port basins are protected from wave exposure from the N-W waves by a 900-m breakwater and not from the N-E waves.

Wind and wave-driven currents are responsible to accumulate large portion of sediments (very fine sand and mud) in the port vicinity and subsequently negatively affecting the navigation channel and basins. Both the opposing S-W and N-E current paths produce sand and mud accumulation in the nearshore area hosting the port channel and basins. The principal sources of sediment contributed to the processes of sedimentation of the LNG are the eroded Rosetta promontory and the inner shelf of Abu Qir Bay. These sediment sources supply large quantities of fine-grained sand and mud to the basins and channel via opposing S-W and N-E currents. Other opposing N-W (seaward) and S-E (landward) currents have also significance effect, with exception of the NW and SE components which are flowing parallel to the channel axis. The seaward current moves sediment from the surfzone whereas landward one from offshore sources, both toward the port. This generally implies that the navigation channel and its adjacent basins are apparently acting effectively as a sediment sink for sediments supplied from the four quadrants.

The dataset interpreted in this study are also incorporated into a mathematical procedure for calculating rate of sedimentation in the port facilities. Monthly sedimentation rates yielded from applying the developed model fluctuate between 0.048 × 106 and 0.388 × 106 m^3/month, with an annual rate of 1.977 × 106 m^3/yr. This annual rate is closely comparable to the sediments accumulated in the port as estimated by HR Wallingford (2004) based on bathymetric survey and numerical model. Suspended-load sediment contributed to about one-fifth of the total of sediments, while the bed-load mode is ap-

proximately four-fifth of the sediments that deposited in the navigation channel. In comparison, these estimated proportions are found to be in agreement with results obtained by Komar and Inman [11], Komar [12] and Inman, *et al*. [13].

5. Acknowledgements

The author appreciates the assistance of the staff of the Coastal Research Institute for the field and laboratory activities of this study. Appreciation is also given to Drs. Omran Frihy, Abdel Monaam Badr and Abu Bakr.

6. References

[1] O. E. Frihy and D. Lawrence, "Evaluation of the Modern Nile Delta Promontories: Development of Accretional Features during Shoreline Retreat," *Environmental Geology*, Vol. 46, No. 6, 2004, pp. 914-931.

[2] O. E. Frihy, A. M. Badr and M. S. Hassan, "Sedimentation Processes at the Navigation Channel of the Damietta Harbour on the Northeastern Nile Delta Coast of Egypt," *Journal of Coastal Research*, Vol. 18, No. 3, 2002, pp. 459-469.

[3] E. A. M. Deabes, "The Study of Sea Level Changes and Current at Rosetta and Damietta Outlets and Abu Qir Bay," M. Sc. thesis, Faculty of science, University of Alexandria, 2002.

[4] M. A. Abd-Allah, A. H. El-Gindy and E. A. M. Deabes, "Estimation of Sedimentation Rates in the Navigation Channel of Damietta Harbour, Egypt," *Journal of Arab Academy for Science, technology and Marine Transport*, Vol. 30, No. 59, 2005, pp. 54-61.

[5] CoRI, "Sea Waves and Currents Characteristics at West Side of Loading ARMS, ELNG Port-Idku Site," Technical Reports, Coastal Research Institute, 2004-2006.

[6] O. E. Frihy, M. S. Hassan, E. A. Deabes and A. M. Badr, "Seasonal Wave Changes and the Morphodynamic Response of the Beach-Inner Shelf of Abu Qir Bay, Mediterranean Coast, Egypt," *Marine Geology*, Vol. 247, No. 3-4, 2008, pp. 145-158.

[7] J. A. Bailard, "Total Load Sediment Transport Model for Plane Sloping Beach," *Journal of Geophysical research*, Vol. 86, No. C11, 1981, pp. 10938-10954.

[8] J. A. Bailard and D. L. Inman, "An Energetics Bed Load Model for Plane Sloping Beach," *Journal of Geophysical research*, Vol. 86, No. C3, 1981, pp. 2035-2043.

[9] L. C. Van Rijn, "Sedimentation of Dredged Channels and Trenches," In: Herbich, J. B., Ed., *Handbook of Coastal Ocean Engineering*, Gulf Pub., Co., Houston, TX, 1991, pp. 609-650.

[10] M. A. El Sayed, N. A. Younan, A. M. Fanos and K. H. Baghdady, "Accretion and Erosion Patterns along Rosetta Promontory, Nile Delta coast," *Journal of Coastal Research*, Vol. 21, No. 3, 2005, pp. 412-420.

[11] P. D. Komar and D. L. Inman, "Longshore Sand Transport on Beaches," *Journal of Geophysical Research*, Vol. 75, No. 30, 1969, pp. 5514-5527.

[12] P. D. Komar, "The Relative Significance of Suspension Versus Bed-Load on Beaches," *Journal of Sedimentary petrology*, Vol. 48, 1978, pp. 921-932.

[13] D. L. Inman, J. A. Zampol, T. E. White, D. M. Hanes, B. W. Waldorf and K. A. Kastens, "Field Measurement of Sand Motion in the Surf Zone," *Proceedings of* 17*th International Conference on Coastal Engineeering*, *ASCE*, New York, 1980, pp. 1215-1234.

International Journal of Geosciences, **2010, 21-31**
doi:10.4236/ijg.2010.11003 Published Online May 2010 (http://www.SciRP.org/journal/ijg)

Surface Rupture and Hazard of Wenchuan Ms 8.0 Earthquake, Sichuan, China

Yong Li[1], Runqiu Huang[2], Liang Yan[1], Alexander L. Densmore[3], Rongjun Zhou[4]
[1]*State Key Laboratory of Oil and Gas Reservoir Geology and Exploitation, Chengdu University of Technology, Chengdu, China*
[2]*State Key Laboratory of Geo-hazard Prevention & Geo-environment Protection, Chengdu University of Technology, Chengdu, China*
[3]*Institute of Hazard and Risk Research and Department of Geography, Durham University, Durham, UK*
[4]*Institute of Earthquake Engineering, Seismological Bureau of Sichuan Province, Chengdu, China*
E-mail: *yanliang*1003@163.*com*
Received March 25, 2010; *revised April* 19, 2010; *accepted May* 13, 2010

Abstract

Longmen Shan is located the special joint between the Qinghai-Tibetan Plateau in the west and the Yangtze craton in the east. Consisting of a series of parallel imbricated thrust, it develops, from the west to the east, the Maoxian-Wenchuan, Yingxiu-Beichuan and Pengxian-Guanxian faults. Wenchuan Ms 8.0 earthquake is a thrust with strike-slip type, and surface ruptures are located in Yingxiu-Beichuan fault zone and Pengxian-Guanxian fault zone. Based on the geological background, tectonic setting, the active tectonics of Longmen Shan and surface ruptures of the Wenchuan earthquake, a dynamical model to illustrate possible links between surface processes and upward extrusion of lower crustal flow channel at the eastern margin of the Tibetan plateau have been studied, and the results is the material in lower crust in the Longmen Shan moving as nearly-vertical extrusion and uplift, resulting in the surface rate of tectonic movement differing according to depth rate as well as the occurrence of large shallow Wenchuan earthquake.

Keywords: Wenchuan Earthquake, Longmen Shan, Surface Rupture, Hazard, Sichuan, China

1. Introduction

The Ms 8.0 Wenchuan Earthquake in May 12th, 2008 is one of the most disastrous earthquakes since the foundation of P. R. China, which destroyed not only the epicenter of Sichuan province but also several closed provinces. It was felt in most regions of China, as well as nations outside China. This tragic event provides the opportunity to advance the subject of seismic sciences.

Based on our accumulated activitiy on active tectonics in Longmen Shan area, we have undertaken several new field surveys, including international collaborative efforts after the earthquake. This paper compiles 70 sets of data from accumulated past and new surveys, detailing surface rupture and seismic disasters since our work began in the 1990s [1-15].

This research was supported by National Natural Science Foundation of China grant 40841010 and CGS grant 1212010918010.

2. Geological Structure in Longmen Shan Seismic Belt

Longmen Shan is located the special joint between the Qinghai-Tibetan Plateau in the west and the Yangtze craton in the east, which is a foreland basin and orogeny system with a complex structure and unique structural history. In the depth, it is located in structural transform belt of southwest China and the south part of Helanshan-Longmen Shan. To the northwest, there is thicken crust and thicken mantle area; and to the southeast, there is thin crust and thin mantle area in Sichuan basin. From the Longmen Shan foreland basin to the plateau, the crust is thickening roughly and forms a belt with western-cline belt; the central line of the belt is located the position of Longmen Shan thrust under the surface. Comparing with its surface position, the line moves some distance to the west, which suggests that Longmen Shan thrust dips to the west and does not have a mountain root. It also suggests that Longmen Shan is an Intracontinental

mountain chain and an independent tectonic uploading system.

The isostatic gravity anomaly in Longmen Shan and joint regions show that the crust in this area is still unstable. The figures in Longmen Shan are positive and the figures in Longquan Shan and the area to the east are negative while the figures in the area between them are around zero. Since the Cenozoic, at least 5-10 km strata have eroded in uplift rate of 0.6 mm/a. The survey data in recent years shows that there is an uplift rate in 0.3-0.4 mm/a in Jiuding Shan [1,16].

According to the regional geological setting, this area, from northwest to southeast, consists of Songpan-Ganzi Orogeny (main part), Longmen Shan thrust belt, foreland basin and forebulge; all of these four parts form a complete tectonic system. We would introduce the east margin of Qinghai-Tibetan Plateau as three geological units: Songpan-Ganzi orogenic belt (main part), Longmen Shan thrust belt and foreland basin [1-15].

3. Surface Rupture of the Wenchuan Earthquake

After the earthquake, a number of research institutions have published basic parameters and focal mechanisms. However, those data are different depending on different sources and methods. The USGS recorded that the Mw. is 7.9, the epicenter is located in Yingxiu, Wenchuan (31.099, 103.279), the focal depth is 19 km, the rupture length is 300 km and the duration is 120 seconds, trending 229° and fracture plane dipping 33° with strike-slip. According to the basic parameters and the focal mechanism solution, the Wenchuan earthquake had the following two characteristics: 1) it was a shallow hypocenter earthquake and took place in the brittle-ductility transform belt in 12 km-19 km depth with enormous destructivity; 2) it belongs to thrusting and dextral strike-slip one and from southwest to northeast, it propagated in one direction. The release process of strain was relatively slow and may have led to a greater intensity of aftershocks and longer duration. The intensity of the earthquake had an oval-shaped distribution and its long axis was in a northeast direction. In this direction, the casualties and property loss was much bigger than other directions.

According to the surface rupture survey (**Figure 1**) after the earthquake, the Wenchuan earthquake faults have characteristics of fragile, post-earthquake surface linear image is apparent, cutting a wide range of terrain units. They are located in Yingxiu-Beichuan fault zone (central zone), Pengxian-Guanxian fault zone (front fault) which only a small amount of surface rupture are found and Maoxian-Wenchuan fault zone (back fault) which surface rupture have not yet been found. Those surface rupture extend in northeast direction (in NE 30º-70º, most in NE 50º-60º) and trend to northwest (30º-80º). They distribute along the striking in a few meters to 200 meters range and were also distributed along the Yingxiu-Beichuan fault and Pengxian-Guanxian fault.

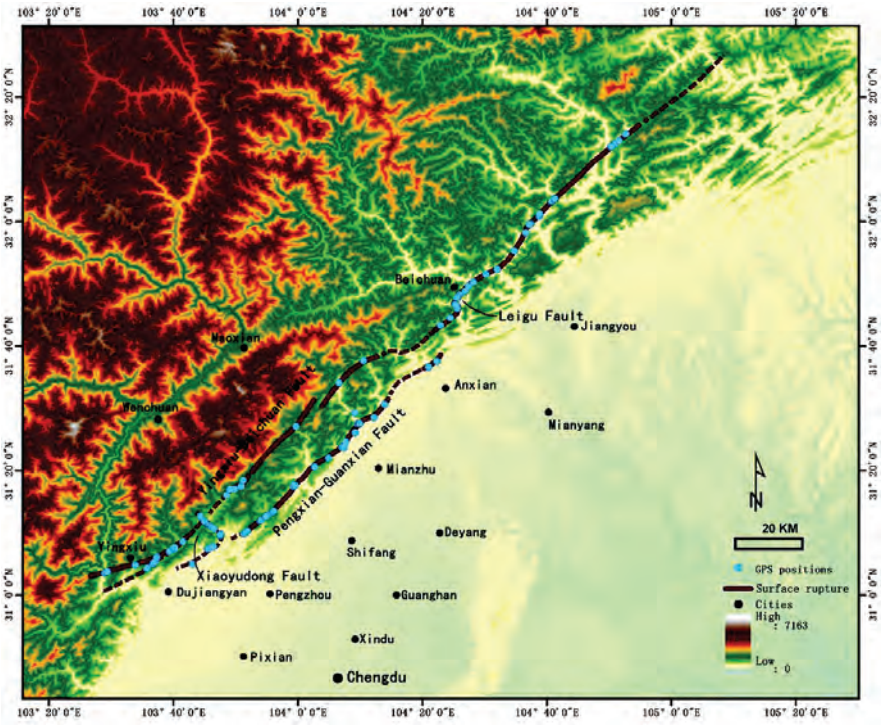

Figure 1. Distribution of surface rupture of Wenchuan Earthquake in Longmen Shan.

3.1. Surface Rupture of Yingxiu-Beichuan Fault

The Yingxiu-Beichuan fault (**Figures 1-3**) is the Wenchuan earthquake's main earthquake fault. The linear characteristics of the earthquake surface rupture belt are apparent. It starts from Yingxiu, Wenchuan in the southwest and then extends to Hongkou, Longmen Shan town (Baishuihe), Donglinsi, Hongbai, Qingping, Chaping, Leigu, Beichuan, Chenjiaba, Guixi, and then ends in Shikanzi, Pingwu, a distance of about 220 km. It was distributed along the strike of Yingxiu-Beichuan fault and disappears in the southwest 10 km of Yingxiu, belonging to the single-side and multi-point type rupture with thrust characteristics. Its plane had a steep dip angle and cut a wide range of terrain units, including mountain bedrocks, river terraces, alluvial fans, highways and bridges with bridge collapse or road displacement. Its vertical offsets were in the range of 1.60-6.20 m and its horizontal offsets were in the range 0.20-6.50, striking NE 30°-50° and trending northwest. The average vertical offset was 3.4 m and horizontal 2.9 m, the biggest offset being 10.3 ± 0.2 m in Maoba, Beichuan (vertical fault) and 6.8 ± 0.2 m in Leigu (horizontal offset). The ratio between thrust and dextral strike-slip components are 1:1, indicating the existence of thrust movement and dextral strike-slip movement, the amount of thrust movement being equal to the dextral strike-slip movement.

Basing this and according to the current surface data obtained from the survey, we calculated vertical and horizontal offsets in four parts of Yingxiu-Beichuan surface rupture. The preliminary analysis results are: 1) the epicenter located in the vicinity of Yingxiu (**Figure 1**) is

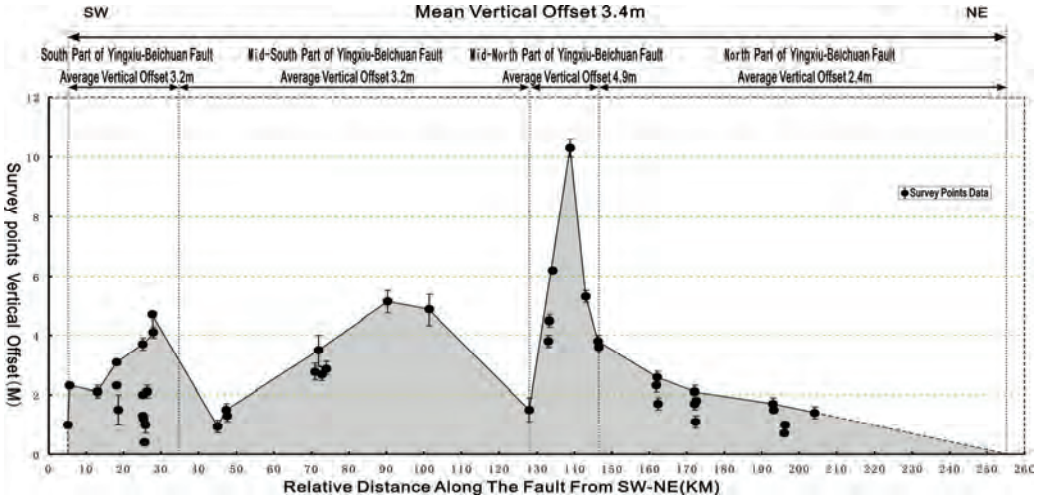

Figure 2. The vertical displacement along the Yingxiu-Beichuan Fault in Wenchuan Earthquake.

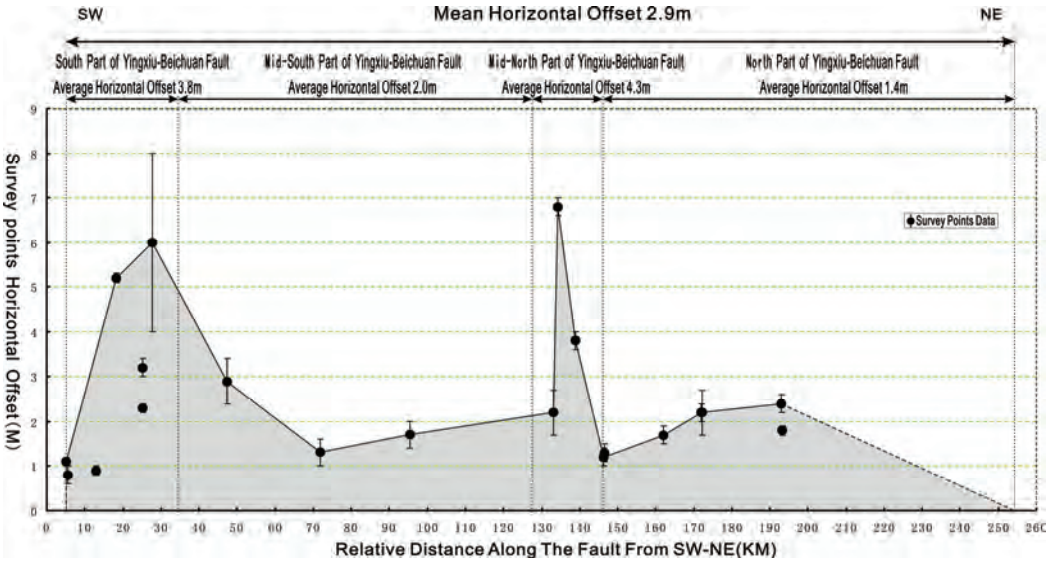

Figure 3. The horizontal displacement along the Yingxiu-Beichuan fault in Wenchuan Earthquake.

not the position where the biggest offset is located; the biggest vertical and horizontal offsets are 10.3 ± 0.2 m (vertical offset) and 6.8 ± 0.2 m (horizontal offset) in Beichuan. According to Wenchuan earthquake focal mechanisms solution, the greatest offset of the main shock is 9 m-10 m. As a result, the surface rupture is smaller than the biggest displacement under ground; the biggest offset are 60%-70% of the biggest offset under ground; 2) by surface offsets, the Yingxiu-Beichuan fault can be divided into two high-value and two low-value zones. The two high-value zones are located in the southern part of Hongkou, Yingxiu and the northern part of the Leigu, Beichuan-Dengjiaba area and the two low-value zones are located in mid-south part of the Baishuihe-Chaping area and Huangjiaba-Shikanzi, Pingwu area. These four sections are divided by Xiaoyudong fault, Leigu fault and Dengjiaba fault; the two high-value areas being caused by the Xiaoyudong and Leigu faults; 3) Chen [17] use the global seismic network data to confirm two largest static sliding displacement areas, which are located at area between epicenter and northeast 100 km to the epicenter and 150 km northeast of the epicenter; the two largest displacement of the slip surface locate in the two high-value areas, indicating that the largest displacement in the surface are the response to the displacement under ground; 4) compared the surface rupture of earthquake with before, the places in Yingxiu, Leigu, Baishuihe and Gaoyuan with historical earthquake rupture are also the places with new rupture[3-8,12,15]. In the places with historical earthquake since Quaternary, there will be new strong earthquake in the future.

3.2. Surface Rupture of Pengxian-Guanxian Fault

The Pengxian-Guanxian fault (**Figures 1** and **4**) experienced surface fractures in this earthquake. The surface rupture started from Xiang'e, Dujiangyan and extended to Cifeng, Pengzhou, Bailu, Jinhua, Hanwang and Sangzao over a total distance of about 40-50 km, characterized by dextral strike-slips shortening with steep dipping. The hanging wall was in the northwest and its foot wall in the southeast. The vertical offset was 0.39-2.70 m and the horizontal offset was 0.20-0.70 m (the average vertical offset was 1.6 meters with an average horizontal offset of 0.6 meter), indicating the existence of thrust displacement and dextral strike-slip displacement and thrust displacement is greater than the dextral strike-slip displacement, showing thrust and shortening characteristics.

Compared with the surface rupture of the Yingxiu-Beichuan, the fault rupture is far less than the Beichuan-Yingxiu fault rupture and it has a relatively short length of the rupture and vertical offset; and on the other hand, the horizontal offset dispalcement is relatively small, the thrust displacement is main.

3.3. Surface Rupture of Xiaoyudong Fault

The fault (**Figures 1**, **5** and **6**) is located between Yingxiu-Beichuan fault and Pengxian-Guanxian fault and is a new fault being discovered after the earthquake, showing that the fault is a transformed fault between the Yingxiu-Beichuan fault and the Pengxian-Guanxian fault. The fault, striking south-north, extends about 15 km through Xiaoyudong Bridge; the stretch of the surface rupture is stable and we have confirmed more than 10 rupture points. The southwest block is a hanging wall and the northeast block is foot wall with an average vertical offset of 1.0 meter and an average horizontal offset of 2.3 meters (vertical offset/horizontal offset ratio is 1:1), showing the vertical offset is equal to the horizontal offset and, from south to north, the thrust displacement is increasing.

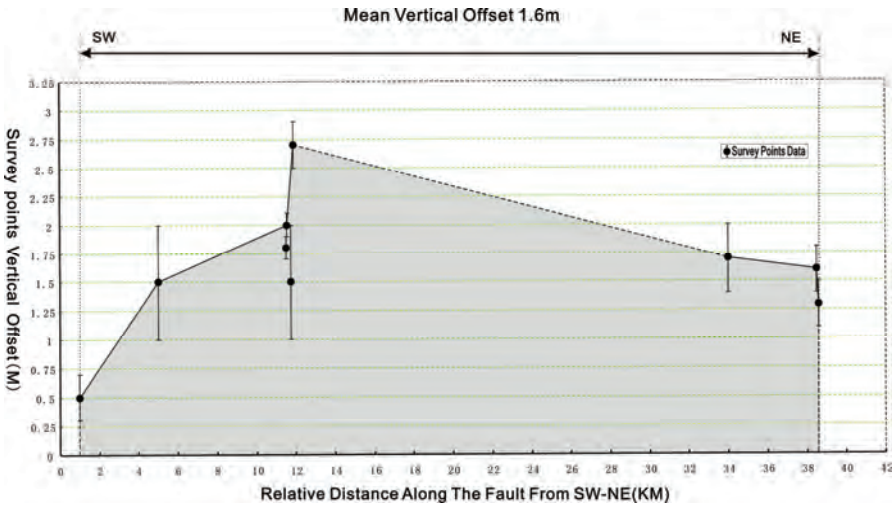

Figure 4. The vertical displacement along the Pengxian-Guanxian fault in Wenchuan Earthquake.

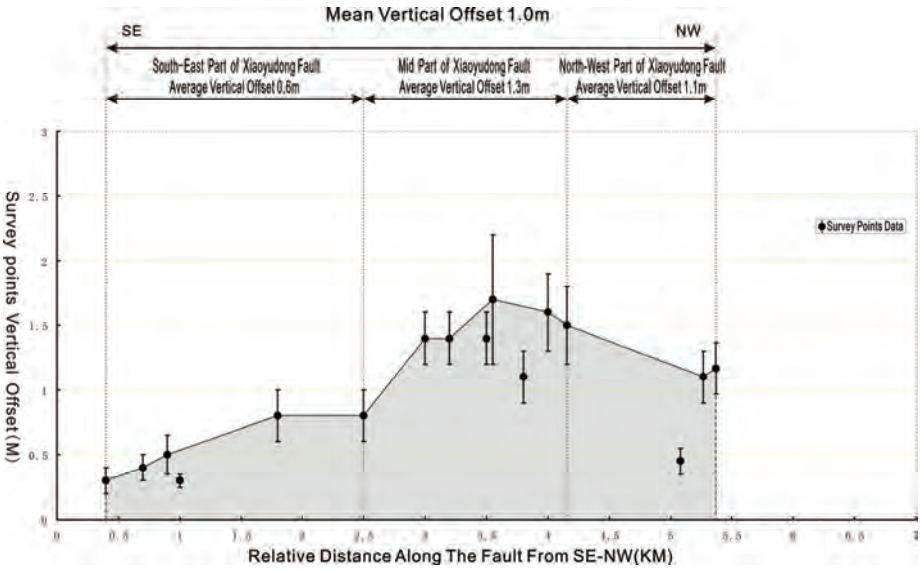

Figure 5. The vertical displacement along the Xiaoyudong fault in Wenchuan Earthquake.

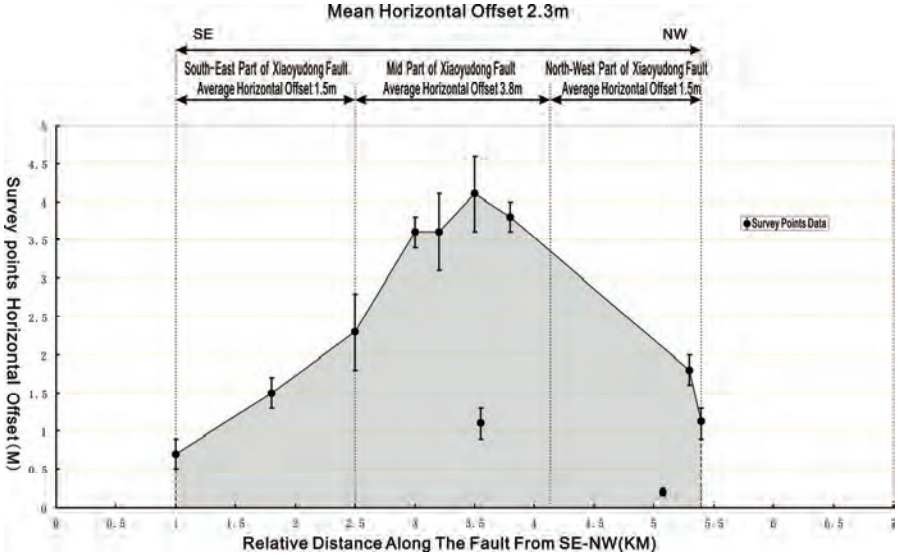

Figure 6. The horizontal displacement along the Xiaoyudong fault in Wenchuan Earthquake.

3.4. Surface Rupture of Leigu Fault

This fault (**Figures 1** and **7**) belongs to Yingxiu-Beichuan fault belt and between two parallel northeast striking faults. The fault's surface rupture is very complex and it is also a new fault discovered after the earthquake, showing that it is a transform fault between those two parallel Yingxiu-Beichuan faults, which has been named Leigu fault by us.

The fault, striking south-north, extends 3-5 km from south to north. The surface rupture pattern is stable and we have confirmed that more than 10 rupture points. Its southwest block is hanging wall and the northeast block is foot wall. The largest vertical offset is 2.2 ± 0.5 m and the largest horizontal offset is 1.9 ± 0.1 m (the average vertical offset is 1.8 m and the average horizontal offset is 1.4 m).

In the surface rupture, there are obvious changes from the north to the south, changing from striking south-north in the north to striking NWW in the south, which shows vertical and sinistral horizontal offset in the north (a channel has been offset vertically 1.9 m and horizontally 1.3 m); and, in the south, the rupture zone shows vertical and dextral offset (a house foundation has been offset vertically 1.5 m and 0.5 m and dextral 1.3 m and 0.3 m).

The vertical offset with horizontal offset ratio is 1:1, showing the thrust displacement is equal to the strike-slip displacement and, from south to north, the thrust changes

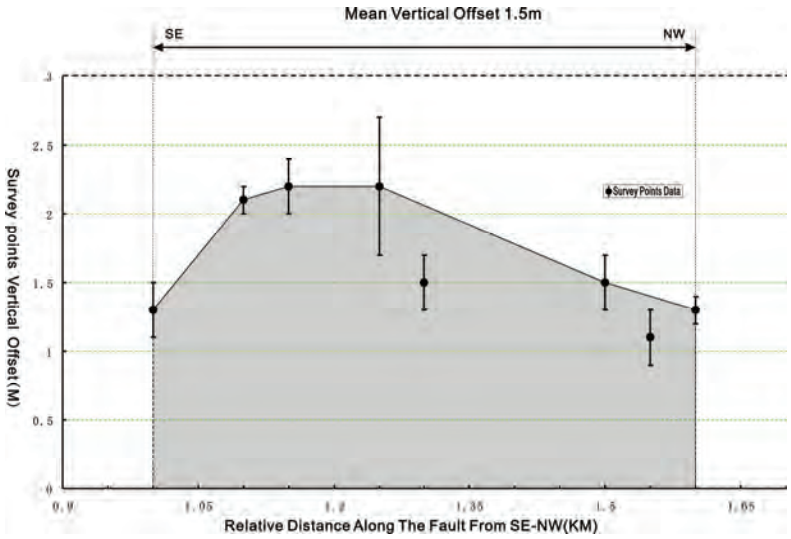

Figure 7. The vertical displacement along the Leigu fault in Wenchuan Earthquake.

bigger. It was noticed that in the north, the fault is sinistral strike-slip and, in the south, it appears to be a dextral strike-slip.

3.5. The landform of Surface Rupture

According to our field observation of the surface rupture, it had various forms, mainly showing as ridge offsets, alluvial fan offsets, terrace offset, slopes offsets, channel offsets, path offsets, highway offsets, cement road overlays, structural fractures, sag ponds, ground cracks, earthquake domes, pressure ridge and other types, of which road scarps are easy to identify.

In Yingxiu region, the surface rupture are showed in structural cracks and road deformation (asymmetrical fold ridge) and graben; in Shengxigou and Gaoyuan, the surface are showed road scarps, road deformation and pressure ridge; in Bajiaomiao, the surface rupture are showed in fault scarps. The width of surface rupture is different along the fault, but on the whole, it is generally less than 20 meters. Strong deformation is distributed in the hanging block of the thrust fault and the foot block has no obvious deformation, or only has deformation in the vicinity of the fault.

3.6. Dip of Surface Rupture

The Yingxiu-Beichuan fault's surface ruptures are generally steep scrapes; the northwest block is hanging wall and southeast block is foot wall, indicating that the fracture plane should trend northwest. But the plane is difficult to be discovered; in Bajiaomiao, Hongkou, the plane was directly exposed at the surface. It tends to northwest with dip angle 80°-86° and its hanging wall is composed of upper Triassic Xujiahe coal-bearing strata and its foot block is loose gravels. The scratches can be distinct in the plane, indicating high-angle thrust characteristics. As a result, in the Yingxiu-Beichuan fault, the northwest tending fault in high-angle should be representative.

However, in Gaoyuan, Hongkou, Yingxiu-Beichuan fault's rupture surface trend to southeast. The plane here is also showed as a very steep scrapes, but the northwest block is foot side and southeast is hanging side, which indicates that the plane should trend to northwest. As a result, we think that Yingxiu-Beichuan fault's surface rupture should be northwest trending high-angle surface, but in some areas, the tendency could be reversed from northwest to southeast.

The Wenchuan earthquake's focal mechanisms solution reveals that the dip angle of plane is only 33°-39° [17]. It is obvious that the surface crack plane is different from one calculated by focal mechanisms solution: the dip angle is gentle when deeper. This characteristic is also similar to an imbricate thrust fault's structural features.

3.7. Surface Rupture and Shortening Rate

Although in the Yingxiu-Beichuan fault there are different structural shortening forms, including road offset and road overlay, the proper measurement position of surface deformation is less. In a cement road in Gaoyuan, we measured the pressure ridge and the thrust overlay, showing a clear structural shortening phenomenon. In the cement road, we measured surface deformation in detail, indicating that the structural shortening rate of this section is 7.61 percent and that the biggest structural shortening rate of the pressure ridge is 28.6 percent.

The Longmen Shan is the most typical klippe zone in China; it has a structural shortening rate of 42-43% [1,3-8]. The result is 7.61%-28.6% in Gaoyuan, showing the clear structural shortening rate in Wenchuan Earthquake.

3.8. Rupture Process of Wenchuan Earthquake

Although the surface rupture in Bajiaomiao is also steep scarp as the main form; its hangling wall is Upper Triassic Xujiahe coal-bearing strata and its foot wall is loose gravel. But the scrape marks have preserved the evidence for the process analysis of Wenchuan earthquake.

The scrapes plane strikes to N60°E, trending to N300°W with a dip angle of 85°. We discovered two scratches in the plane. The first one is nearly vertical, mainly distributing in upper and lower parts of the plane, while the second one is nearly horizontal, mainly locating in the lower part of the plane.

In the plane of the scrapes, we can observe three kinds of cross cutting relationships between nearly vertical and horizontal scratches: a nearly vertical one cutting the nearly horizontal one, a nearly horizontal one cutting the nearly vertical one and a nearly vertical one in the top gradually changing to the nearly horizontal one in the bottom.

In view of the Upper Triassic Xujiahe coal-bearing strata in the hanging block and the loose gravel in the foot block, the scratch preserved in the hangling wall bedrock should be the evidence of foot wall loose gravel in the movement process. As a result, the upper marks preserved in the hangling wall should be the early evidence of the rupture process of the earthquake and the lower marks preserved in the hanging wall should be the late evidence of the rupture process.

For this reason, we speculate that the nearly vertical scratches in the top recorded the thrust movement early, while the scratches in the bottom recorded the strike-slip movement lately. According to these three different kinds of cross cutting relationship of scratches, we think that the late movement is oblique.

According to the focal mechanisms solution, Chen [17] thought that the Wenchuan earthquake can be divided into 7 stages, and that, in the beginning stages, the movement showed thrust and then gradually shifted to strike-slip movement lately. Yuji Yagi [18] has a similar viewpoint on the movement process of the devastating earthquake which includes two phases: the first phase (0-50 seconds) with 6.4 m thrust and the second phase (60-120 seconds) with 4.6 m strike-slip.

As a result, the scratches of the surface rupture reveal the process confirmed by the focal mechanism solution, which is that the thrust movement occurred early and the strike-slip movement occurred lately.

4. Discussion on Kinematic of Active Tectonics in Longmen Shan and Wenchuan Earthquake

Indo-Asia collision is the most important events in Cenozoic, which results in the uplift, deformation and thickening of Qinghai-Tibetan Plateau. The event and its impact to Cenozoic geological structure has been noticed and discussed by geoscientists. Two well-known hypotheses have been presented; one is a crustal thickening model [19] and the other one is a lateral extrusion mode [20].The former emphasizes on north-south crustal shortening and thickening, and the later emphasizes the east-extrusion along main faults. In the eastern margin of the Qinghai-Tibetan Plateau, there are two corresponding pattens which are: Avouac and Tapponnier [20] eastward thrusting mode, and England *et al.*'s dextral strike-slip mode.

However, the active tectonics and Wenchuan earthquake show the Longmen Shan fault is characterize by thrust and dextral strike-slip movement, which does not coincide with England and Molnar's large scale dextral shear movement in the eastern margin of Qinghai-Tibetan Plateau, and which also does not coincide with Avouac and Tapponnier [20] eastward thrusting mode in the eastern margin of the Qinghai-Tibetan Plateau. The performance of Longmen Shan fault zone has its uniqueness, which can not be explained in one single mode.

According to the direction of surface movement showed by GPS measurements [21,22], the northeast corner of Qinghai-Tibetan Plateau consisting of Longmen Shan fault and Kunlun Shan fault has the characteristics of northeastward (Qingling direction) extruding out, which means that when the Songpan-Ganzi block in eastern Qinghai-Tibet moved to the east, because of the blocking of Yangtze platform, it was forced to move to Qinling Mountains in the northeast and resulted in the characters with thrust and dextral strike-slip movement mode in Longmen Shan. The West Qinling fault is thrust with sinistral strike-slip movement and the blocks between Longriba fault and east Kunlun fault is also northeastern extruding out (**Figure 8**).

5. Discussing of Dynamics Mechanism of Active Tectonics in Longmen Shan and Wenchuan Earthquake

According to GPS measurements, India plate is moving to the north in 50 mm a^{-1}, and different blocks in the eastern margin of Qinghai-Tibetan Plateau have significantly different movement rates. The Songpan-Ganzi block in the south has a faster horizontal movement rate than the Songpan-Ganzi block in the north. Active tectonics research [3-8,12,15] shows that the horizontal movement rate in Longmen Shan is small (1-3 mm a^{-1}), so is its uplift rate (0.35-0.40 mm a^{-1}) [1]. Its movement mode is characterized by thrust with dextral strike-slip. But Longmen Shan is the steepest mountain around Qinghai-Tibetan Plateau, in the range of more than 30 kilometers, it uplifts from 700 meters above sea level to more than 5000 meters. The small surface slipping rate

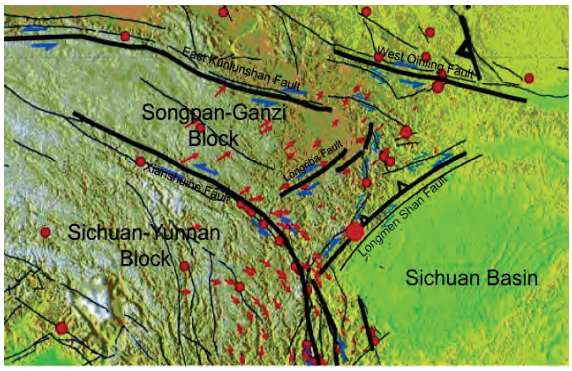

Figure 8. Surface movement, epicenter and tectonic framework in Eastern Qinghai-Tibetan plateau.

does not only coincide with the high and steep mountain, but also does not coincide with the fact of the strong earthquake of Ms 8.0. As a result, in the Songpan-Ganzi block and Longmen Shan in the northeast margin of Qinghai-Tibetan Plateau, the rate of surface movement does not coincide with the deep tectonic movement rate. The deep structural process must be thought about in the seismic hazard assessment.

The Wenchuan earthquake's focal mechanism solution shows that Wenchuan Earthquake's focal depth is 12-19 km, belonging to shallow earthquake. In addition, we count the historical earthquake in Longmen Shan as the longitude [3-8,9-11]. The results show that Longmen Shan tectonic earthquake in lower magnitude was in depth of 5-15 km in advantage and the strong earthquake was in depth of 15-20 km. Obviously, it is clear that the depth of Wenchuan Earthquake coincide with the depth of historical strong earthquake and all of them are shallow earthquakes, which coincide with the depth of 20 km in low-velocity layer and also coincide with the uplift depth of the top of lower crust [9-11].

As a result, in the process of Qinghai-Tibetan Plateau's movement to the east, blocked by the basement of the Sichuan Basin, the lithosphere is not synchronized as a whole flow to the east and the flow velocity is different in different layers. This results in lower crust material in the Longmen Shan moving as nearly-vertical extrusion and uplift [23], resulting in the surface rate of tectonic movement differing according to depth rate as well as the occurrence of large shallow Wenchuan earthquake (**Figure 9**).

6. Geological Hazard Caused by Wenchuan Earthquake

The Wenchuan Earthquake is the most destructive in intensity and the vastest of affected area in China since 1949. The area of the heavily destroyed region is more than 100,000 km^2. It has the most serious casualties after the Cicheng Earthquake (Inner Mongolia, 1290), the Huaxian Earthquake (Shanxi, 1556), the Haiyuan Earthquake (Ningxia, 1920) and the Tangshan Earthquakes (Hebei, 1976).

The hazards caused by the Wenchuan Ms 8.0 Earthquake is known by next main characteristics: 1) seismic waves have propagated with strong ground motion to damage construction; 2) surface rupture zone directly

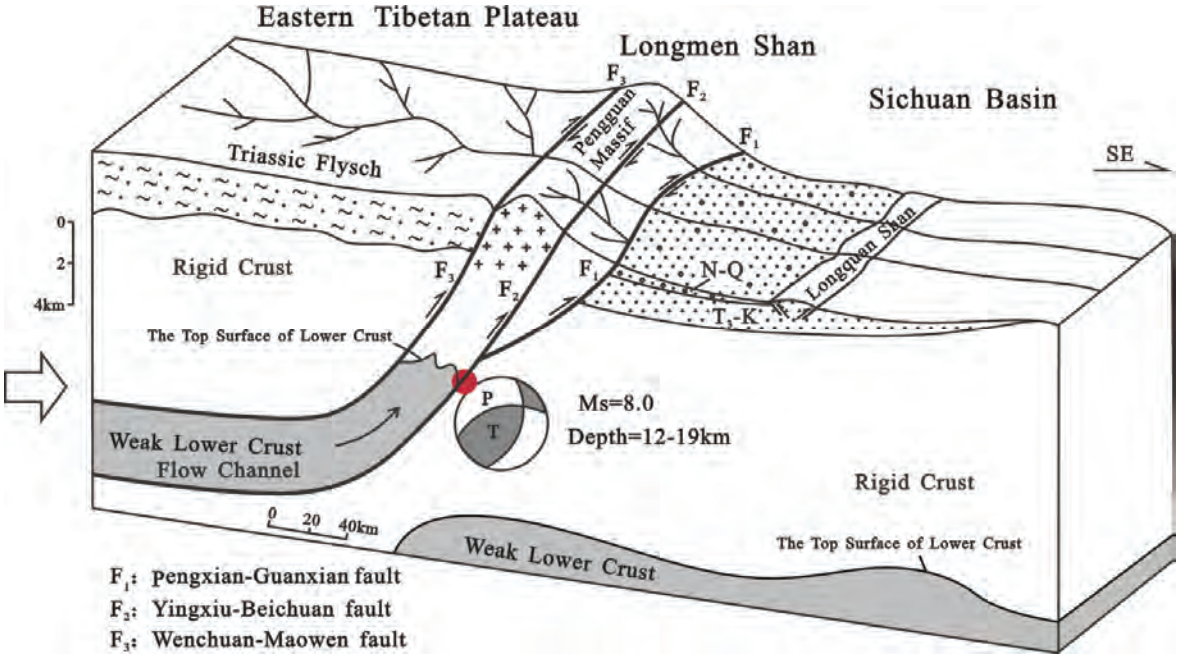

Figure 9. A dynamical model to illustrate possible links between surface processes and upward extrusion of lower crustal flow channel at the eastern margin of the Tibetan plateau.

destroyed and tear construction along Yingxiu- Beichuan fault for 220 km and Pengxian-Guanxian fault for 40-50 km; 3) collapse, landslide and other geological hazards caused by strong vibration of ground motion destroyed buildings. Because the earthquake occurred in the valleys of the Longmen Shan, especially in Yingxiu-Beichuan fault, there have been large-scale collapse, landslides and other geological hazards in Longmen Shan region. Those hazards have buried or destroyed a large amount of buildings, for example, half of the buildings in Chenjiaba, have directly been destroyed by landslides and a large number of barrier lakes have flood buildings and have given potential secondary flood threat to the basin.

According to the earthquake data collected by survey teams of Gansu, Shanxi and Chongqing seismological bureaus, InSAR imaging and seismography records, we studied some important regions with high seismic intensity and have drawn an isoline map of Wenchuan Earthquake and distinct the intensities in this region (**Figure 10**). District Ⅺ is located in Yingxiu-Hongkou, and Leigu-Beichuan, which are distribute along Yingxiu-Beichuan fault zone's hanging wall with a total area of about 680 km^2. Construction in this region almost completely collapsed, especially in Yingxiu town and Beichuan town. Large-scale surface rupture can be followed. A number of large-scale collapses and landslides blocked rivers to form barrier lakes, such as the Qingping and Tangjiashan barrier lakes. District Ⅹ starts from southwest Yingxiu and end in Shikanzi, Nanba in the northeast, including Yingxiu-Beichuan surface rupture in a narrow belt with the long axis N50°E and an area of about 2520 km^2. In this region, most construction collapsed and landslides are common.

To summarize, District Ⅵ and above this of the Wenchuan Earthquake affected the area of about 333000 km^2. The isoline map (**Figure 10**) has the following characteristics: 1) high-seismic intensity lines, especially in district Ⅸ, distributed along the Longmen Shan in N40-50°E direction and the long/short axis ratio are 8:1-10:1. District Ⅺ degrees are distributed in three isolated areas with the typical characteristics of multi-point instant cracks. 2) According to the results of seismic inversion, the earthquake rupture tear from the vicinity of Yingxiu to the northeast with characteristics of a one-direction rupture process. Isoseismal lines also show the direction of disappearing rapidly to the southwest and slowly to the northeast with the characteristics of the

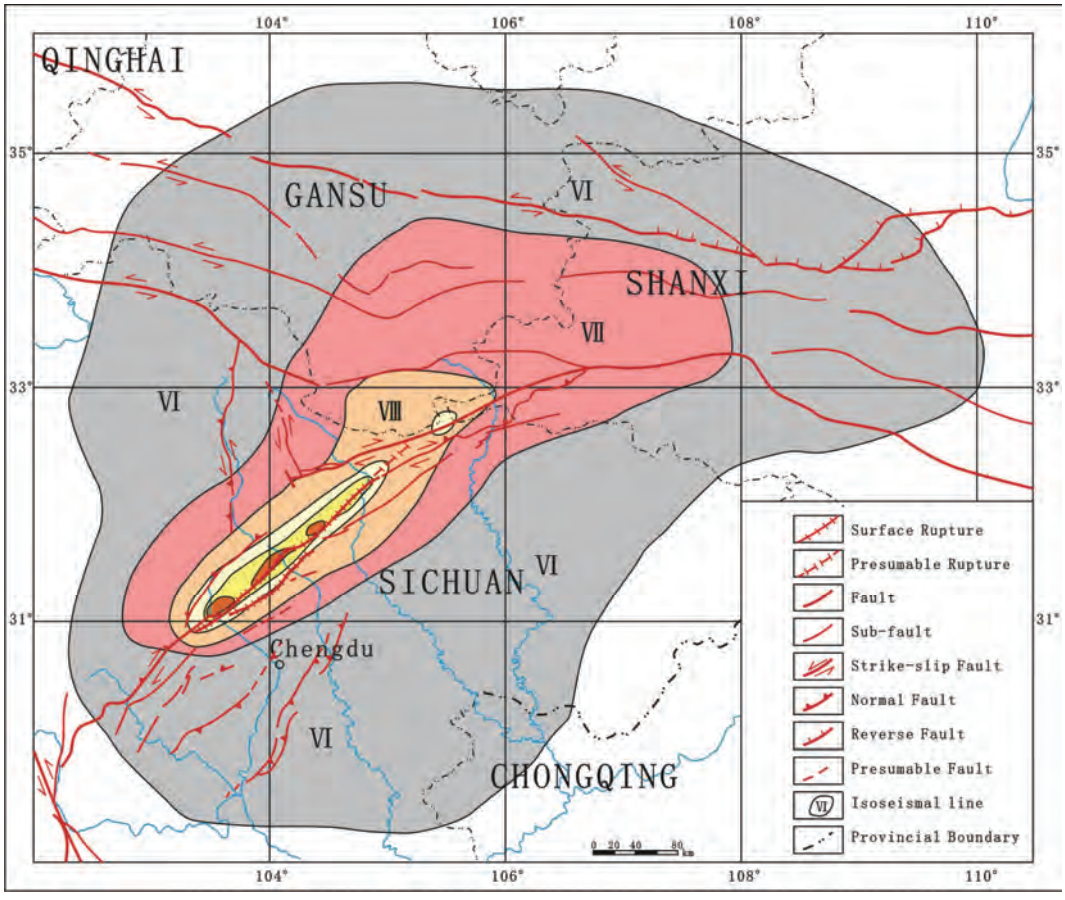

Figure 10. Isoseismal line of Wenchuan M8.0 earthquake on 12 May, 2008.

mode. 3) District Ⅵ disappear to Hongyuan and Ruoergai slower than to the Basin, which may be related to that the Sichuan Basin with relative rigidity Yangtze plate is not easy for seismic wave absorbing as well as the soft soil in Hongyuan and Ruoergai enlarge the damage. 4) District Ⅵ, Ⅶ and Ⅷ in the area of north Sichuan, Gansu and Shanxi are gradually turning to east-west direction and this may be the result of controlling of the regional faults.

7. Preliminary Conclusions

In this paper, based on the Longmen Shan seismic zone's geological background, tectonic setting, stratigraphy and lithology, we have summarized the Longmen Shan surface rupture and progress and explore the tectonic kinematics and dynamics of Wenchuan Earthquake. According to the geological disasters caused by Wenchuan Earthquake, we have made several suggestions for reconstruction in the affected areas.

According to historical records and active tectonics, we believe that the Longmen Shan fault zone is a dangerous earthquake zone and the three main faults have the ability to induce earthquakes > Ms 7. The Yingxiu-Beichuan fault is the most important earthquake-inducing fault; the interval should be at least about 1000 a. It belongs to the low-frequency seismic activity zone, but it has a potential risk to induce a strong earthquake with characteristics of thrust and dextral strike-slip movements.

By comparing the initial analysis of Wenchuan Earthquake and historical earthquakes records, we believe that, the May 12, 2008 Wenchuan Earthquake belongs to thrust and strike-slip type earthquake. According to north-south striking fault (Xiaoyudong, Leigu and Dengjiaba faults) and surface offsets, Yingxiu-Beichuan fault surface rupture zone is divided into two zones of high-value and low-value. According to scratches on the scraps in Hongkou, the earthquake rupture process is divided into two phases: early thrust and lately-inclined strike-slip movement. As a result, in the earthquake ruptured zone, there are two components of thrust and strike-slip, thrust displacement is slightly larger than dextral strike-slip one. This does not coincide with the crustal thickening mode and the lateral extrusion mode, which means that Yingxiu-Beichuan fault is special one and can not be explained by one single model. In view of the surface moving rate of Longmen Shan does not coincide with its moving rate in the depth, we discussed the dynamic geological model between surface process and lower crust flow and think that the vertical pressure and vertical movement of lower crustal materials in Longmen Shan results in the eastern thrust movement, uplift of Longmen Shan tectonic belt and Wenchuan Earthquake as well.

8. Acknowledgements

We are very grateful to the people who provided us supports and help. Finally, we thank the people of the Longmen Shan region for their unending curiosity, hospitality, and generosity.

9. References

[1] Y. Li, Y. F. Zeng and H. S. Yi, "Sedimentary Record and Tectonic Evolution of Longmen Shan Foreland Basin," Chengdu University of Science and Technology Press[A], Chengdu, 1995 (in Chinese).

[2] Y. Li, P. A. Allen, A. L. Densmore and X. Qiang, "Evolution of the Longmen Shan Foreland Basin (western Sichuan, China) during the Late Triassic Indosinian Orogeny," *Basin Research*, Vol. 15, 2003, pp. 117-138.

[3] Y. Li, R. J. Zhou, A. L. Densmore, *et al.*, "Continental Dynamics and Geological Response of the Eastern Margin of Qinghaihai-Tibetan Plateau," Geological Publishing House, Beijing, 2006.

[4] Y. Li, R. J. Zhou, A. L. Densmore, *et al.*, "The Geology of the Eastern Margin of the Qinghai-Tibet Plateau," Geological Publishing House, Beijing, 2006.

[5] Y. Li, R. J. Zhou, A. L. Densmore, *et al.*, "The Geology of the Eastern Margin of the Qinghai-Tibet Plateau," Geological Publishing House, Beijing, 2006.

[6] Y. Li, R. J. Zhou, A. L. Densmore and M. A. Ellis, "Strike-Slip Direction of Longmen Shan Fault and Sediments and Geomorphic Signs," *Minerals and Rocks*, Vol. 26, No. 4, 2006, pp. 26-34.

[7] Y. Li, R. J. Zhou, A. L. Densmore and M. A. Ellis, "Strike-Slip of Eastern Margin in Qinghai-Tibetan Plateau since Cenozoic-Geomorphic Signs of Thrust Movement," *Quaternary Research*, Vol. 26, No. 1, 2006, pp. 40-51.

[8] Y. Li, R. J. Zhou, A. L. Densmore, *et al.*, "Strike-Slip Process in Longmen Shan of Eastern Margin of Qinghai-Tibetan Plateau and Sedimentary Response," *Sedimentary Journal*, Vol. 24, No. 2, 2006, pp. 1-12.

[9] Y. Li, R. J. Zhou, S. L. Dong, *et al.*, "Wenchuan Earthquake Thrust and Ttrike-Tlip and Turface Rupture," *Journal of Chengdu University of Technology* (*natural science*), Vol. 35, No. 4, 2008, pp. 404-413.

[10] Y. Li, R. J. Zhou, A. L. Densmore, *et al.*, "Surface Rupture, Thrusting and Strike—Slipping in the Wenchuan Earthquake," The Gongwana 13 Program and Abstracts, 2008, pp. 114-115.

[11] Y. Li, R. J. Zhou, A. L. Densmore, *et al.*, "Surface and Deformation of the Yingxiu-Beichuan Fault by the Wenchuan Earthquake," *ACTA Geologica Sinica*, Vol. 82, No. 12, 2008, pp. 1688-1706.

[12] R. J. Zhou, Y. Li, A. L. Densmore, M. A. Ellis, Y. L. He, Y. Z. Li and X. G. Li, "Active Tectonics of the Longmen Shan Region on the Eastern Margin of the Tibetan Plateau[J]," *ACTA Geologica Sinica*, Vol. 81, No. 4, 2007, pp. 593-604.

[13] R. J. Zhou, Y. Li, A. L. Densmore, M. A. Ellis, Y. L. He, F. L. Wang and X. G. Li, "Active Tectonics of the Eastern Margin of the Tibet Plateau," *Journal of Mineral Petrol*, Vol. 26, No. 2, 2006, pp. 40-51.

[14] A. L. Densmore, Y. Li, M. A. Ellis, *et al.*, "Active Tectonics and Erosional Unloading of Eastern Margin," *Journal of Mountain Science*, Vol. 2, No. 2, 2005, pp. 146-154.

[15] A. L. Densmore, M. A. Ellis, Y. Li, R. J. Zhou, G. S. Hancock and N. J. Richardson, "Active Tectonics of the Beichuan and Pengguan Faults at the Eastern Margin of the Tibetan Plateau," *Tectonics*, Vol. 26, 2007, p.17.

[16] S. G. Liu, "Longmen Shan Thrust and Evolution of Foreland Basin in West Sichuan," Chengdu University of Technology Press, Chengdu, 1993.

[17] Y. T. Chen, N. S. Xu and Y. Zhang, "Report of Focal Characteristics of Wenchuan Earthquake on May 12th, 2008," 2008. Internet Available: http://www.csi.ac.cn

[18] Y. Yagi and Y. Fukahata, "Importance of Covariance Components in Inversion Analyses of Densely Sampled Observed Data: An Application to Waveform Data Inversion for Seismic Source Processes," *Geophysical Journal International*, Vol. 175, 2008, pp. 215-221.

[19] P. C. England and P. Molnar, "Right-Lateral Shear and Rotation as the Explanation for Strike-Slip Faulting in Eastern Tibet," *Nature*, Vol. 344, 1990, pp. 140-142.

[20] J. P. Avouac and P. Tapponnier, "Kinematic Model of Active Deformation in Central-Asia," *Geophysical Research Letters*, Vol. 20, No. 10, 1993, pp. 895-898.

[21] Z. Chen, B. C. Buchifiel and Y. Liu, "Global Positioning System Measurements from Eastern Tibet and their Implication for India/Eurasia Intercontinental Deformation," J*ournal of geophysical Research*, Vol. 105, No. B7, 2000, pp. 16215-16228.

[22] P. Z. Zhang, Z. K. Sheng, M. Wang, W. J. Gan, R. Brögmann, P. Monlar, Q. Wang, Z. J. Niu, J. Z. Sun, J. C. Wu, H. R. Sun and X. Z. You, "Continuous Deformation of the Tibetan Plateau from Global Positioning System Data," *Geology*, Vol. 32, 2004, pp. 809-812.

[23] Y. Li, G. D. Xu, R. J. Zhou, *et al*., "Isotatic Gravity Anomaly in Longmen Shan and its Constraint in Crustal Uplift of the Eastern Margin of the Qinghai-Tibetan Plateau," *Geological Bulletin of China*, Vol. 24, No. 12, 2005, pp. 1162-1169.

International Journal of Geosciences, **2010, 32-37**
doi:10.4236/ijg.2010.11004 Published Online May 2010 (http://www.SciRP.org/journal/ijg)

The Analysis of Accelerograms for the Earthquake Resistant Design of Structures

Victor Corchete
Higher Polytechnic School, University of Almeria, Almeria, Spain
E-mail: *corchete@ual.es*
Received February 25, 2010; *revised March* 26, 2010; *accepted April* 20, 2010

Abstract

In this paper, the analysis of ground motions (displacements, velocities and accelerations) has been performed focused to the seismic design. The relationships between the peak ground acceleration (PGA), the peak ground velocity (PGV), the peak ground displacement (PGD) and the bracketed duration, with the earthquake magnitude, are presented and their validity and applicability for seismic design is discussed. Finally, the dominant periods of the ground motions (displacement, velocity and acceleration) are obtained from their Fourier Spectrum. Their validity and applicability for the seismic design is discussed also. The results presented in this paper show that the relationships that exist between the important parameters: PGA, PGV, PGD and duration; and the earthquake magnitude, allow the prediction of the values for these parameters, in terms of the magnitude for future strong motions. These predictions can be very useful for seismic design. Particularly, the prediction of the magnitude associated to the critical acceleration, because the earthquakes with magnitude greater than this critical magnitude can produce serious damages in a structure (even its collapsing). The application of the relationships obtained in this paper must be very careful, because these equations are dependent on the source area, location and type of structure. The dominant periods of the ground motions (displacement, velocity and acceleration) that are computed and presented in this paper, are also important parameters for the seismic design, because recent studies have shown that the earthquake shaking is more destructive on structures having a natural period around some of these dominant periods. These parameters must also be handled with caution, because they show dependence with the source area, location and type of structure.

Keywords: Seismic Design, Bracketed Duration, Peak Ground Acceleration (PGA), Peak Ground Velocity (PGV), Peak Ground Displacement (PGD), Dominant Periods

1. Introduction

It is known that earthquakes are responsible of an important part of the casualties, occurred around the world due to natural disasters [1]. In addition, earthquakes produce high economical losses which could be avoided, in most of the cases, with an adequate seismic design [2]. For this reason, it is the principal importance any study performed to mitigate the disasters caused by earthquakes. For it, the seismic design requires the knowledge of some *parameters* that must be included or considered, for the earthquake resistant design of structures. Ones of the most important parameters to be considered are: the peak ground acceleration (PGA), the peak ground velocity (PGV), the peak ground displacement (PGD) and the bracketed duration [3]. These parameters are easy to measure, from the three types of strong-motion record that are usually available: seismogram (ground display-cement), velocigram (ground velocity) and accelerogram (ground acceleration).

The *peak ground acceleration* (PGA) is the maximum value of the ground acceleration (positive or negative) that appears in the accelerogram. The *peak ground velocity* (PGV) is the maximum value of the ground velocity (positive or negative) that appears in the velocigram. The *peak ground displacement* (PGD) is the maximum value of the ground displacement (positive or negative) that appears in the seismogram. The *bracketed duration* is the time duration of the ground shaking, defined as the elapsed time between the first and last acceleration excursions greater than some reference value (usually taken as 0.05 g, where g is the gravity acceleration). **Figure 1**

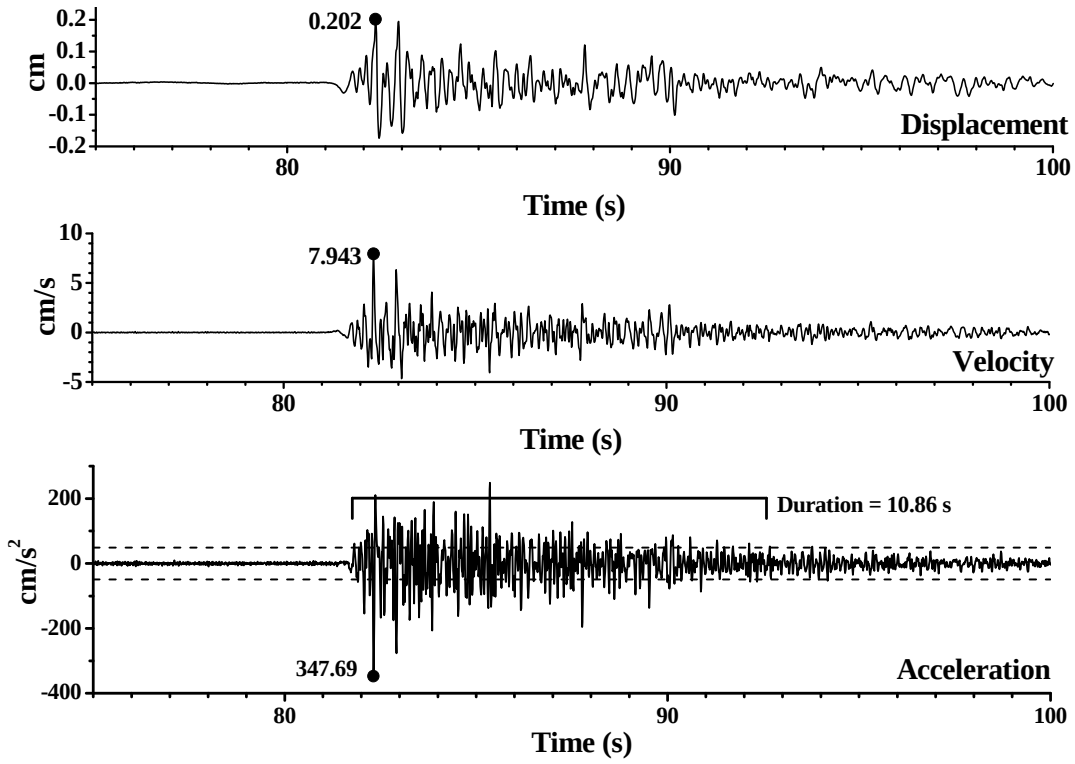

Figure 1. Ground displacement, velocity and acceleration recorded on the vertical component of the EJON station, for the event 3 listed in Table 1. The small circles denote the maximum present in the corresponding trace joint to its numerical value. The dashed lines denote the reference value (0.05 g) selected to determine the bracketed duration. The bracketed duration is marked in the accelerogram joint to its numerical value.

shows the value of these parameters for a ground motion recorded on the vertical component [4].

Recent studies have shown that the *dominant periods* of the Fourier Spectrum of the ground motion (displacement, velocity and acceleration), are also very important parameters to be considered in the seismic design, because the earthquake shaking is more destructive on structures having a *natural period* around some of these dominant periods [5]. Therefore, it is very suitable to consider also the values of these dominant periods, as important parameters for the seismic design.

Thus, it would be very desirable to obtain relationships between the above mentioned parameters (PGA, PGV, PGD and duration) and the earthquake magnitude, to predict the possible values that these important parameters can take for future strong motions. This is the goal of this study, the determination of relationships between PGA, PGV, PGD and duration with the magnitude. The validity and applicability of these formulas also will be discussed. Finally, the dominant periods of the ground motions considered in this study also will be obtained.

2. Methodology and Background

It is known that the *maximum acceleration* A (cm/s^2) of the ground motion produced by an earthquake, is related to the *intensity* of this earthquake, by means of a *linear equation* [3]. On the other hand, also it is known that the *intensity* of an earthquake is also related to the *magnitude* M (mb) of this earthquake, by means of a *linear equation* [6]. Therefore, a *linear relationship* must exist between *maximum acceleration* A (cm/s^2) and *magnitude* M (mb). This relation is given by

$$\mathrm{Log}_{10}(\mathrm{A(cm/s^2)}) = a_1 \mathrm{M(mb)} + b_1 \quad (1)$$

where (a_1, b_1) are constants to be determined. Logically, the existence of the relationship (1) implies that a similar relationship must exist for the *maximum velocity* and the *maximum displacement* [7]. These *linear relationships* are given by

$$\mathrm{Log}_{10}(\mathrm{V(cm/s)}) = a_2 \mathrm{M(mb)} + b_2 \quad (2)$$

$$\mathrm{Log}_{10}(\mathrm{D(cm)}) = a_3 \mathrm{M(mb)} + b_3 \quad (3)$$

where V is the *maximum velocity*, D is the *maximum displacement* and (a_2, b_2, a_3, b_3) are constants to be determined. Respect to the bracketed duration, also exits a relationship between this parameter and the magnitude, but this relation is not linear. Nevertheless, this relationship can be written in linear form by means of the formula [3]

$$\text{Duration(s)} = a_4 \tanh(M(mb) - c) + b_4 \quad (4)$$

where (a_4, b_4, c) are constants to be determined.

Equations (1) to (4) are the relationships that exist between the above mentioned important parameters (PGA, PGV, PGD and duration) and the earthquake magnitude. These linear equations allow the prediction of the values for these parameters, in terms of the magnitude for future strong motions [8]. The application of Equations (1) to (4) must be very careful, because the constants (a_1, b_1, a_2, b_2, a_3, b_3, a_4, b_4, c) of these equations are determined for a *location* (station) and a *source area* (a *small* area in which the epicenters can be grouped), *i.e.*, the values for these constants can be different for different locations and/or different source areas (there are a dependence with the propagation path). Moreover, for the same location and source area, the values of these constants can depend on the type of soil (over which the structure is built), the type of structure (masonry structure, timber structure, iron structure, concrete structure, building, bridge, nuclear power plant, etc.), the foundations of the structure or the type of connection between structure and foundations [1,9]. Thus, Equations (1) to (4) must be handled with caution.

3. Data

In this kind of studies, the primary data are seismograms, velocigrams and accelerograms. Nevertheless, in some cases only the accelerograms are available, then seismograms and velocigrams must be computed from the accelerograms by integration, using the Fast Fourier Transform (FFT) and its properties, applied to the Fourier Spectrum of the corresponding accelerogram [9,10]. In this study, only seismograms have been available, velocigrams and accelerograms have been computed from these seismograms by derivation, using the FFT and its properties, applied to the Fourier Spectrum of the corresponding seismogram [10].

The seismograms used in this study correspond to 22 earthquakes (**Table 1**), which occurred on the neighboring of the Iberian Peninsula. These earthquakes have been registered by the broadband station EJON located on Iberia (latitude 42.4487 ºN, longitude 2.8886 ºE), with a sampling ratio of 100 samples per second (100 sps). The instrumental response (**Figure 2**) has been taken into account to avoid the time lag introduced by the seismograph system and all distortions produced by the instrument [11]. This correction recovers the true amplitude and phase of the ground motion, allowing the analysis of the true ground motion. For this reason, all the traces considered in this study were corrected for instrument response.

The traces used in this study correspond to events grouped in the same *source area*, to ensure that the propagation path be the same for all events, because the constants (a_1, b_1, a_2, b_2, a_3, b_3, a_4, b_4, c), of Equations (1) to (4), are propagation-path dependent as it was mentioned in the previous section of this paper. A *source area* is defined as a location in which the seismic events have occurred with similar epicenter coordinates [12]. The maximum coordinate difference considered to group events has been equal to 0.2 degrees in latitude and longitude.

Table 1. Near events recorded at EJON station (latitude 42.4487 ºN, longitude 2.8886 ºE).

Event (nº)	Date (d-m-y)	Time (h-m-s)	Latitude (ºN)	Longitude (ºE)	Magnitude (mb)
1	27 05 2003	17 11 32.5	36.802	3.610	6.1
2	28 05 2003	11 26 31.6	37.135	3.393	4.5
3	28 05 2003	19 05 22.2	36.932	3.737	4.9
4	31 05 2003	11 44 46.3	37.048	3.780	4.6
5	01 06 2003	02 54 21.0	36.990	3.983	4.6
6	02 06 2003	08 20 24.2	37.017	3.185	4.5
7	03 06 2003	23 17 46.2	37.208	3.710	4.4
8	06 06 2003	03 13 47.0	37.072	3.733	4.4
9	15 06 2003	01 06 10.8	36.893	3.348	4.1
10	17 06 2003	07 52 55.1	37.113	3.838	4.5
11	18 06 2003	19 36 13.1	36.970	3.682	4.5
12	21 06 2003	11 01 27.5	37.038	3.467	4.1
13	05 07 2003	20 03 35.9	37.212	3.470	4.2
14	06 07 2003	02 56 9.2	37.012	3.758	4.4
15	06 07 2003	08 50 20.6	36.998	3.513	4.3
16	14 07 2003	22 52 26.4	36.925	3.308	4.2
17	17 07 2003	21 07 50.3	36.645	3.493	4.4
18	18 07 2003	08 14 53.5	37.202	3.725	4.4
19	07 08 2003	08 23 11.7	37.103	3.722	4.5
20	11 08 2003	20 03 47.2	36.923	3.328	4.6
21	03 09 2003	14 04 49.8	37.155	3.600	4.6
22	12 10 2003	07 08 45.0	37.045	3.418	4.4

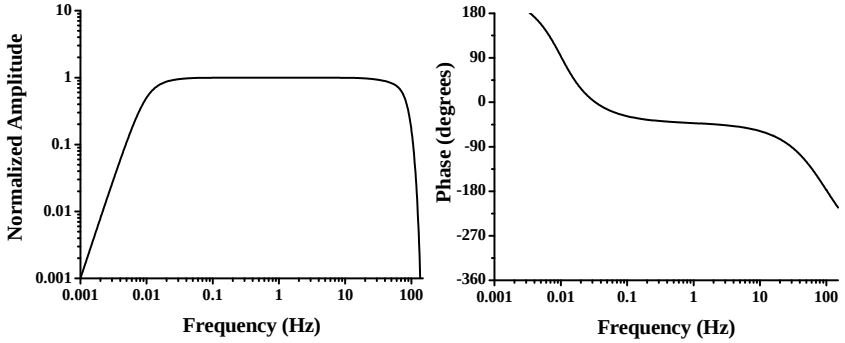

Figure 2. Frequency response of the broadband seismograph (100 sps).

4. Application and Results

The values of the constants (a_1, b_1, a_2, b_2, a_3, b_3, a_4, b_4, c) have been determined for the location and source area considered in this study, from the seismograms corresponding to the events listed **Table 1** recorded at the EJON station (velocigrams and accelerograms has been computed by derivation), by a *linear fit* as it is shown in **Figures 3-6**. These constants could be different for different locations and/or different source areas. Also, these constants could be different for the *same* location and source area, if the type of soil over which the structure is built, the type of structure, the foundations of the structure or the type of connection between structure and foundations; are different [1]. For this reason, Equations (1) to (4), which predict the values of the parameters (PGA, PGV, PGD and duration) with the earthquake magnitude, must be handled with caution, because these predictions could be false when the conditions previously

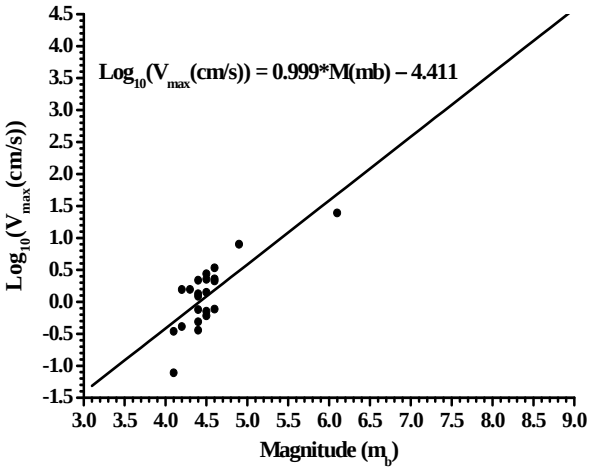

Figure 4. Relationship between PGV and magnitude computed for the velocigrams corresponding to the events listed in Table 1. The continuous line denotes the linear fit performed between PGV and magnitude.

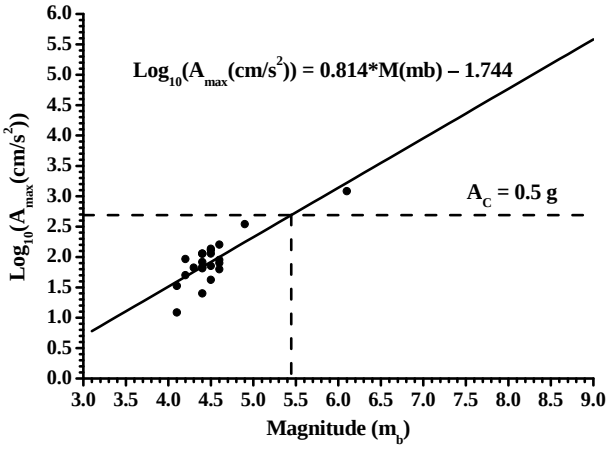

Figure 3. Relationship between PGA and magnitude computed for the accelerograms corresponding to the events listed in Table 1. The continuous line denotes the linear fit performed between PGA and magnitude. The dashed line denotes the value of the critical acceleration assumed in this study as 0.5 g.

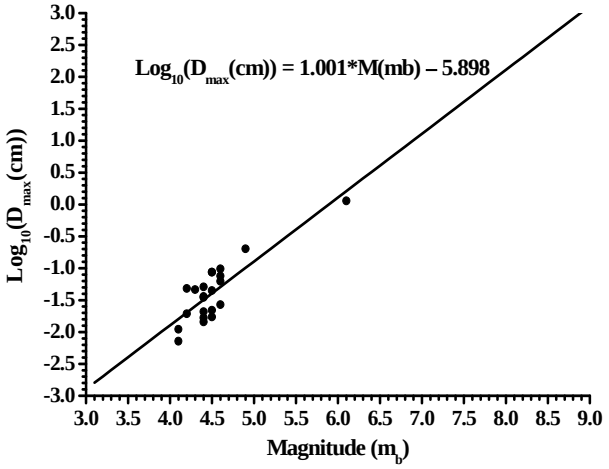

Figure 5. Relationship between PGD and magnitude computed for the seismograms corresponding to the events listed in Table 1. The continuous line denotes the linear fit performed between PGD and magnitude.

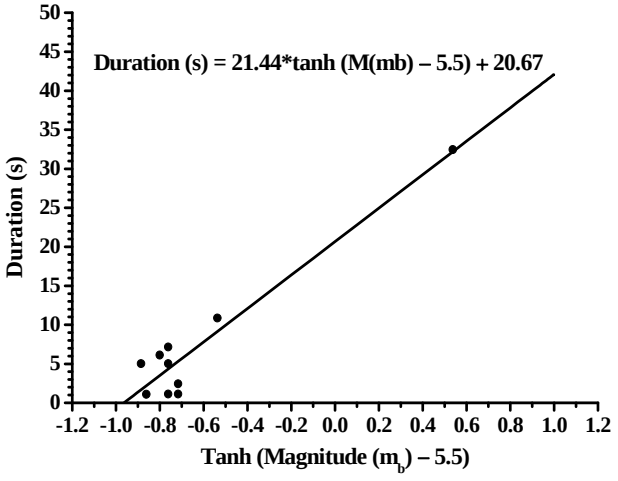

Figure 6. Relationship between bracketed duration and magnitude computed for the accelerograms corresponding to the events listed in Table 1. The continuous line denotes the linear fit performed between duration and magnitude.

mentioned be not satisfied. For different source areas, locations and structures, the values of the constants (a_1, b_1, a_2, b_2, a_3, b_3, a_4, b_4, c) must be recomputed to ensure the validity and applicability of the predictions given by Equations (1) to (4).

The predictions given by Equations (1) to (4) can be very useful for seismic design. Particularly, Equation (1) can be very useful because it allows the knowledge of the *maximum acceleration* that can occur for any earthquake, including earthquakes with high magnitudes which have not occurred up to now. With Equation (1), it can be known in which magnitude the *critical acceleration* is reached (**Figure 3**). The critical acceleration is defined as the *maximum acceleration* that a structure (building, bridge, nuclear power plant, etc.) can bear without damages [1]. For each structure, this critical value of the acceleration exists. The structure can bear serious damages or collapse, if this value of the acceleration is overcame [2]. Thus, an important application of Equation (1) is to know the magnitude associated to the critical acceleration, because earthquakes with magnitude greater than this magnitude can produce serious damages in that structure (even its collapsing).

Finally, the dominant periods of the ground motions (displacement, velocity and acceleration) considered in this study, have been obtained from their Fourier Spectrum, as it is shown in **Figure 7**. These dominant periods are parameters that can be very useful for seismic design, because recent studies have shown that the earthquake shaking is more destructive on structures having a natural period around some of these dominant periods [5]. These parameters also show dependence with the source area, location and type of structure. For it, they must be recomputed for different source area, location and type of structure; to ensure their validity and applicability.

5. Conclusions

Equations (1) to (4) obtained and discussed in this paper, are the relationships that exist between the important parameters: PGA, PGV, PGD and duration; and the earthquake magnitude. These linear equations allow the prediction of the values for these parameters, in terms of the magnitude for future strong motions. The application of Equations (1) to (4) must be very careful, because the constants (a_1, b_1, a_2, b_2, a_3, b_3, a_4, b_4, c) of these equations are dependent on the source area, location and type of structure. The predictions given by Equations (1) to (4) can be very useful for seismic design. Particularly, the prediction given by Equation (1), because it can provide the magnitude associated to the critical acceleration. The knowledge of this critical magnitude is very important in seismic design, because earthquakes with magnitude greater than this magnitude can produce serious damages in a structure (even its collapsing).

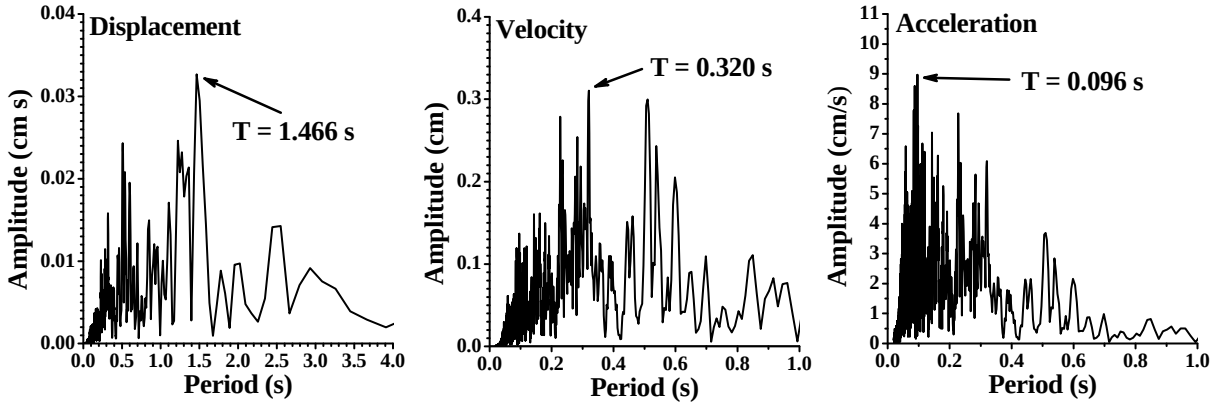

Figure 7. Amplitude Spectrum corresponding to the ground motion (displacement, velocity and acceleration) of the event 1 listed in Table 1, recorded on the vertical component of the EJON station.

The dominant periods of the ground motions (displacement, velocity and acceleration) also have been computed and presented in this paper. These dominant periods are parameters that can be very useful for seismic design, because recent studies have shown that the earthquake shaking is more destructive on structures having a natural period around some of these dominant periods. Nevertheless, these parameters must be handled with caution because they also show dependence with the source area, location and type of structure.

6. Acknowledgements

The author is grateful to Instituto Geográfico Nacional (Madrid, Spain), who has provided the seismic data used in this study.

7. References

[1] S. K. Duggal, "Earthquake Resistant Design of Structures," Oxford University Press, India, 2009.

[2] H. K. Gupta, "Response Spectrum Method in Seismic Analysis and Design of Structures," CRC Press, Boca Raton, Florida, 1992.

[3] K. E. Bullen and A. B. Bolt, "An Introduction to the Theory of Seismology," Cambridge University Press, Cambridge, 1993.

[4] M. O. Erdik and M. N. Toksöz, "Strong Ground Motion Seismology (NATO Science Series C)," Springer, New York, 1987.

[5] K. Adalier and O. Aydingun, "Structural Engineering Aspects of the June 27, 1998 Adana-Ceyhan (Turkey) Earthquake," *Engineering Structures*, Vol. 23, No. 4, 2001, pp. 343-355.

[6] B. F. Howell, "An Introduction to Seismological Research. History and Development," Cambridge University Press, Cambridge, 1990.

[7] H. Doyle, "Seismology," Wiley, New York, 1995.

[8] B. A. Bolt, "Seismic Strong Motion Synthetics," Academic Press, Orlando, 1987.

[9] W. Lee, H. Kanamori, P. Jennings and C. Kisslinger, "International Handbook of Earthquake and Engineering Seismology," Elsevier, New York, 2003.

[10] M. Bath, "Spectral Analysis in Geophysics," Elsevier Scientific Publishing Company, Amsterdam, 1974.

[11] O. Kulhánek, "Anatomy of Seismograms," Elsevier Science Publishers, Amsterdam, 1990.

[12] V. Corchete, M. Chourak and H. M. Hussein, "Shear Wave Velocity Structure of the Sinai Peninsula from Rayleigh Wave Analysis," *Surveys in Geophysics*, Vol. 28, No. 4, 2007, pp. 299-324.

International Journal of Geosciences, **2010, 38-43**
doi:10.4236/ijg.2010.11005 Published Online May 2010 (http://www.SciRP.org/journal/ijg)

The Co-planarity and Symmetry Principle of Earthquake Occurrence

Zhe Yin[1,2]
[1]*Department of Information Management, Beijing University, Beijing, China*
[2]*Mathematics Department, Yanbian University, Yanji, China*
E-mail: *yinzhe@ybu.edu.cn*
Received February 28, 2010; *revised March* 26, 2010; *accepted April* 20, 2010

Abstract

Under the assumption that the earth movement tendency is a sphere, the author does research about the earthquakes occurrence between 2001 and 2010 which over 6 scales of magnitude on occurred time (UTC), magnitude, longitude, latitude and other data, then give out the causal relationship of earthquakes and the co-planarity and symmetry theory of earthquake occurrence. Also, the author does empirical analysis in the paper.

Keywords: Earthquake, Co-planarity, Symmetry

1. Introduction (*Heading* 1)

Research on earthquakes is one of the most important elements about disaster prevention study, because of its devastating and destructive. Especially in recent years, with the rapid development of modern economic activity, destruction to the Earth was continuous. The frequency tends to rise and there are more large earthquakes. Therefore, how to analyze the reason of the earthquake correctly, and predict earthquakes effectively becomes a hot topic in nowadays.

Under the assumption that the earth movement tendency is a sphere and mountains fall to the surface of the earth; estrogens and basin rise to the surface of the Earth. This article gives out the co-planarity and symmetry theory of earthquake occurrence according to research about the earthquakes occurrence between 2001 and 2010 which over 6 scales of magnitude.

2. Questions and Relevant Definitions

The Earth, like a very sensitive being, according to the laws of nature, it has the desire to achieve a balance of features. In this process, it will show a particular trend.

As shown in **Figure 1**, we give some relevant definitions here:

Ecliptic axis: an axis through the center of the Earth which is a vertical line to the ecliptic plane.

Equatorial coordinate system: a celestial coordinate system of the equatorial plane and the axis of rotation.

Ecliptic system of coordinates: a celestial coordinate system of the ecliptic plane and ecliptic axis.

Tangent plane parallel to the equator: the Earth's equatorial plane parallel to the tangent plane (Tangent plane parallel the equator), shown as TPPTE.

Ecliptic line tangent plane: parallel to the ecliptic of the earth tangent plane (Ecliptic line tangent plane), shown as ELTP.

Equatorial vertical plane: after the Earth's surface

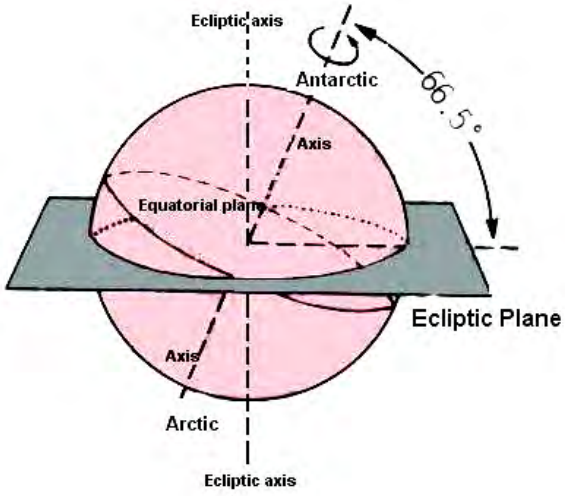

Figure 1. Plane figure.

shock point and the spin axis of the tangent plane (Equatorial vertical plane), shown as EVP.

Longitudinal ecliptic plane: after a shock point and the yellow surface of the Earth axis tangent plane (Ecliptic plane vertical), shown as EPV.

Circular symmetry point: Circular , shown as CSP.

Similar point: Similar Point, shown as SP.

Earthquake effects: measure the Earth's surface; the intensity level of shock is unstable, the stability of the boundary tangent plane level. Plane is the ball away from the more deviation, the more poor results, and the more unstable and more likely point of this earthquake.

3. Basic Assumptions and the Co-Planarity and Symmetry Principle of Earthquake

3.1. Basic Assumptions

1) The Earth became positive sphere with earthquakes which rise or low the ground. That is, because of the ecliptic (23.26 degrees), the Ecliptic Plane TPPTE line tangent planes ELTP have tended to be round;

2) The Earth has tended to balance, and because the earthquake, to re-balance;

3) Crustal thickness tends to vary. Earth's core and mantle movement space tends to a ball space;

4) With the earthquake, the earth rotation axis offset. When there is a earthquake which makes the low rise, the earth rotation axis moves to the seismic vertical, those makes the high low is opposite.

3.2. Co-planarity and Symmetry Principle

After the observation of earthquakes on Earth N (154 earthquakes over 6 scales of magnitude in this article) times, it is occur time H_K, H_{K+1} of adjacent earthquakes M_K, M_{K+1} measure with UTC.

A) The previous earthquake is a cause of the after. The tangent plane balances was destroyed, then tend to a new balance, which Ecliptic line tangent plane generate new state plane all the times.

B) Seismic vertical M_K and seismic vertical M_{K+1} are on the same plane at the time H_K or H_{K+1}. That is parallel to the cut-plane in the equatorial plane or Ecliptic line cut the ecliptic plane, or longitudinal vertical plane or equatorial plane.

C) If the tangent of the plane where seismic vertical M_K and seismic vertical M_{K+1} are tends to round, or fall-rise movement in the earthquake tends to stable, M_K and M_{K+1} tends to symmetry in the circle; otherwise, coplanar circle from the difference of the most unstable point will have an earthquake.

D) After earthquake on M_K occurs, if the most unstable point (poor seismic effect) is still M_K, earthquake M_{K+1} will take place near the same point.

4. Research Basis and Calculation Method

Assumptions (1), (2), (3) are prerequisite of conclusion (A), (B), (C) and (D); symmetry points including the spin axis symmetry, yellow axis symmetry and geocentric axial symmetry. With the existence of the ecliptic obliquity (ecliptic plane and the equatorial plane angle 23.26 degrees) and the Ecliptic plane tangent line, parallel to the equatorial plane tangent tends to a circle, the shape of the earth tends to a sphere becomes possible. This can be concluded with (C) and (D). Assumptions (4) decided the longitudinal movement of the M_{K+1} after M_K. Assumptions (1) and (3) show the possibility that the earthquake and the earthquake potential basis for the order. Be noted that symmetrical points at any time change the fact that, in the premise revolution, a startled different points of the Ecliptic OK UTC timing of your cutting surface is subject to change, and cut parallel to the equatorial plane remain unchanged.

Earthquake time: the time the earthquake is very important, when the earthquake occurred; it generates and identifies Ecliptic line tangent plane, tangent plane parallel to the equator, the ecliptic plane and the equatorial vertical longitudinal cut tangent plane, as well as the corresponding point of the plane of symmetry at the same time.

Symmetrical points on the calculation: Earth autobiographical spherical coordinates on the equatorial plane symmetry coordinates of points on the simple calculation, the same latitude, longitude 180 degrees plus or minus 180 degrees. The following calculation Ecliptic coordinate system on the surface of the ball symmetric point computation of positions is shown in **Figure 2**.

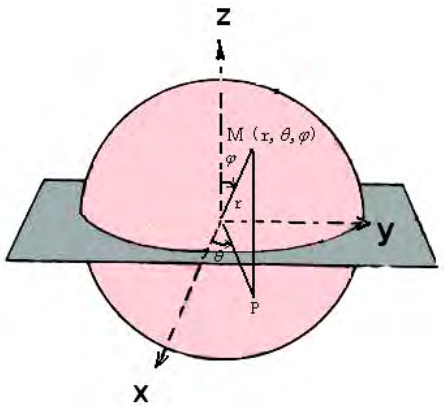

Figure 2. Caculations.

Shock point set M of lat = W, long = J, time (UTC) = a: b, then φ_0 = 90 – W, θ_0 = J + （a + b/60）× 15

Step2:

$$\begin{cases} x = \sin\varphi_0 \cos\theta_0 \\ y = \sin\varphi_0 \sin\theta_0 \\ z = \cos\varphi_0 \end{cases}$$

$$0^\circ \le \theta_0 \le 360^\circ, 0^\circ \le \varphi_0 \le 180^\circ$$

Step3: To the counterclockwise rotation 23°26', then

$$\begin{cases} x' = x\cos 23^\circ 26' + z\sin 23^\circ 26' \\ y' = y \\ z' = x\sin 23^\circ 26' - z\cos 23^\circ 26' \end{cases}$$

M point symmetry point assignment
Step4: Clockwise rotation to 23°26', then

$$\begin{cases} x'' = x'\cos 23^\circ 26' - z'\sin 23^\circ 26' \\ y'' = y' \\ z'' = x'\sin 23^\circ 26' + z'\cos 23^\circ 26' \end{cases}$$

Step5

$$\begin{cases} x'' = \sin\varphi_1 \cos\theta_1 \\ y'' = \sin\varphi_1 \sin\theta_1 \\ z'' = \cos\varphi_1 \end{cases}$$

Step6: symmetry point, lat = $W' = 90 - \varphi_1$, long = θ_1 – (a + b/60) × 15

5. Results

According to the information of 154 earthquakes over 6 scales of magnitude over the world from the USA Earthquake Observation Council, the causal relationship common area, symmetry of them can be concluded as following (**Table 1**) [1]: in the Comments, the next item TPPTE cut parallel to the earthquake in the equatorial plane, ELTP that the next seismic line cutting in the Ecliptic plane, EVP that the next earthquake in the vertical plane perpendicular to the equator, EPV that the next earthquake in the vertical longitudinal ecliptic plane. A total of circular symmetry point, then increasing the CSP, such as TPPTECSP; similar point with the SP said. Two adjacent seismic M_K and M_{K+1}, at present, earthquake moment H_K, when the total surface, then added 1; when the time after the earthquake H_{K+1}, when the total surface, then added 2.

Table 1. Original data.

2001

Date	Time (UTC)	Place	Lat.	Long.	Magnitude	Comments
Jan 13	17:33	Salvador	13.04	-88.66	7.7	ELTPCSP1
Jan 26	03:16	India	23.39	70.23	7.7	TPPTECSP1
Feb 13	14:22	Salvador	13.67	-88.94	6.6	ELTP1
Feb 28	18:54	USA	47.11	-122.6	6.8	EPV2
Jun 23	20:33	Peru	-16.3	-73.55	8.4	ELTPCSP1
Nov 14	09:26	China	36.2	90.9	7.8	ELTP1

2002

Date	Time (UTC)	Place	Lat.	Long.	Magnitude	Comments
Feb 3	07:11	Turkey	38.573	31.271	6.5	TPPTE1
Mar 3	12:08	Afghanistan	36.543	70.424	7.4	SP1
Mar 25	14:56	Afghanistan	36.06	69.32	6.1	TPPTE1
Jun 22	02:58	Iran	35.63	49.05	6.5	TPPTE1
Oct 31	10:32	Italy	41.79	14.87	5.9	ELTPCSP1
Nov 3	22:12	Alaska, USA	63.52	-147.4	7.9	EPV1

2003

Date	Time (UTC)	Place	Lat.	Long.	Magnitude	Comments
Jan 22	02:06	Mexico	18.8	-104.1	7.6	TPPTECSP1
Feb 24	02:03	China	39.61	77.23	6.3	TPPTE1
May 1	00:27	Turkey	39.01	40.46	6.4	TPPTE1

May 21	18:44	Algeria	36.96	3.63	6.8	TPPTE1
Sep 25	19:50	Japan	41.82	143.91	8.3	ELTP2
Nov 17	06:43	USA	51.15	178.65	7.8	
Dec 22	19:15	USA	35.71	-121.1	6.6	ELTP2
Dec 26	01:56	Iran	29.00	58.31	6.6	ELTP1

2004

Date	Time (UTC)	Place	Lat.	Long.	Mag-nitude	Comments
Feb 5	21:05	Indonesia	-3.61	135.53	7.0	ELTP1
Feb 24	02:27	Gibraltar	35.14	-3.99	6.4	TPPTE1
May 28	12:38	Iran	36.29	51.61	6.3	TPPTE1
Sep 5	10:07	Japan	33.07	136.62	7.2	SP1
Sep 5	14:57	Japan	33.14	137.07	7.4	ELTP1
Oct 9	21:26	Nicaragua	12	-86	7.0	ELTPCSP1
Oct 23	08:56	Japan	37.3	138.8	6.6	EVP1
Nov 11	21:26	East Timor	-8.15	124.87	7.5	ELTPCSP1
Nov 15	09:06	Colombia	4.7	-77.51	7.2	ELTP1
Nov 20	08:07	Costa Rica	9.6	-84.17	6.4	TPPTE1
Nov 21	11:31	Islands	15.68	-61.71	6.3	TPPTECSP1
Nov 26	02:25	Indonesia	-3.60	135.40	7.1	EPV1
Nov 28	18:32	Japan	42.94	145.28	7.0	EVP1
Dec 23	14:59	New Zealand	-50.24	160.13	8.1	ELTP1
Dec 26	00:58	Indonesia	3.30	95.87	9.1	ELTP1

2005

Date	Time (UTC)	Place	Lat.	Long.	Magni-tude	Comments
Feb 22	02:25	Iran	30.726	56.817	6.4	TPPTE1
Mar 20	01:53	Japan	33.54	130.12	6.6	EPV1
Mar 28	16:09	Indonesia	2.08	97.11	8.6	ELTPCSP1
Jun 13	22:44	Chile	-19.89	-69.12	7.8	EPV1
Jun 15	02:50	California	41.284	-125.9	7.2	TPPTE1
Aug 16	02:46	Japan	38.259	148.98	7.2	EPV1
Sep 9	07:26	New Guinea	-4.539	153.47	7.6	TPPTE1
Sep 26	01:56	Peru	-5.68	-76.4	7.5	EPVD2
Oct 8	03:50	Pakistan	34.43	73.54	7.6	TPPTE1
Nov 26	00:49	China	29.7	115.7	5.2	TPPTE1
Nov 27	10:22	Iran	26.77	55.86	5.9	EPV1
Dec 5	12:19	Tanzania	-6.212	29.599	6.8	EPV1

2006

Date	Time (UTC)	Place	Lat.	Long.	Mag-nitude	Comments
Jan 8	11:34	Greece	36.250	23.498	6.7	EPV1
Feb 22	22:19	Mozam-bique	-21.32	33.58	7.0	EPV1
Apr 20	23:25	Russia	61.075	167.08	7.6	EPV1
May 3	15:26	Tonga	-20.13	-174.1	8.0	EVP1
May 16	10:39	New Zea-land	-31.55	-179.2	7.4	ELTP2
May 27	22:54	Indonesia	7.977	110.31	6.3	EPV1
Jul 17	08:19	Indonesia	-9.334	107.26	7.7	EPV1
Aug 20	03:41	Scotia Sea	-61.02	-34.37	7.0	EPV1
Sep 10	14:56	Mexico	26.339	-86.56	5.9	TPPTE1
Oct 15	17:07	USA	19.801	-156.0	6.7	EPV1
Nov 15	11:14	Russia	46.616	153.22	8.3	ELTP1
Dec 26	12:26	Taiwan	21.818	120.53	7.1	ELTP2

2007

Date	Time (UTC)	Place	Lat.	Long.	Mag-nitude	Comments
Jan 13	04:23	Russia	46.288	154.44	8.1	ELTP1
Jan 21	11:27	Molucca Sea	1.207	126.29	7.5	EPV1
Feb 12	11:27	Portugal	36.09	10.26	6.0	ELTP2
Mar 6	05:49	Indonesia	-0.490	100.52	6.4	ELTP2
Mar 25	00:40	Vanuatu	-20.59	169.41	7.1	EPV1
Mar 25	00:42	Japan	37.537	136.43	6.7	EPV1
Apr 1	20:39	Islands	-8.474	156.95	8.1	ELTP1
May 16	08:56	Laos	20.470	100.70	6.3	ELTP1
Jun 2	21:34	China	23.013	101.05	6.1	ELTPCSP1
Jun 13	19:29	Guatemala	13.628	-90.73	6.7	ELTPCSP1
Jul 16	01:13	Japan	37.574	138.44	6.6	ELTP2
Jul 18	17:30	Tanzania	-2.586	36.281	5.9	ELTP1
Aug 1	17:08	Vanuatu	-15.67	167.60	7.2	EPV2
Aug 2	02:37	Russia	47.259	141.75	6.2	EPV1
Aug 8	17:04	Indonesia	-5.968	107.65	7.5	ELTPCSP2
Aug 15	23:40	Peru	-13.32	-76.50	8.0	ELTPCSP1
Sep 12	11:10	Indonesia	-4.517	101.38	8.5	ELTP1
Sep 28	13:38	USA	21.980	142.68	7.5	EPV1
Sep 30	05:23	New Zealand	-49.39	163.84	7.4	SP1
Oct 15	12:29	New Zealand	-44.68	167.21	6.8	EPV1
Oct 24	21:02	Indonesia	-3.909	101.06	6.8	ELTP2
Oct 31	03:04	USA	37.432	-121.7	5.6	ELTP1
Oct 31	03:30	USA	18.854	145.31	7.2	ELTP2
Nov 14	15:40	Chile	-22.18	-69.84	7.7	ELTPCSP1
Nov 25	16:02	Indonesia	-8.294	118.36	6.5	EPVD1
Nov 29	19:00	France	14.951	-61.24	7.4	EPV1
Dec 9	07:28	Fiji	-26.15	-177.4	7.8	EVP1
Dec 19	09:30	Alaska, USA	51.495	-179.4	7.1	ELTP1

2008

Date	Time (UTC)	Place	Lat.	Long.	Mag-nitude	Comments
Jan 5	11:01	Canada	51.299	-130.7	6.6	ELTPCSP1
Feb 3	07:34	Congo	-2.314	28.896	5.9	EVP1
Feb 14	10:09	Greece	36.646	21.833	6.9	ELTP2
Feb 20	08:08	Indonesia	2.751	95.966	7.4	EPV1
Feb 21	15:26	(Norway)	77.41	14.48	6.1	ELTP1
Feb 21	14:16	USA	41.076	114.77	6.0	TPPTE1
Apr 18	09:37	USA	38.450	87.890	5.2	ELTP1
May 7	16:45	Japan	36.141	141.54	6.9	ELTP2
May 12	06:28	China	31.099	103.27	7.9	ELTP2
May 24	19:20	Colombia	4.447	-73.67	5.9	EPV2
May 29	15:46	Iceland	63.992	-21.01	6.3	ELTP2
Jun 8	12:25	Greece	38.029	21.464	6.4	TPPTE1
Jun 13	23:43	Japan	39.122	140.67	6.9	ELTP2
Jul 15	03:26	Greece	35.983	27.785	6.4	ELTP1
Jul 19	02:39	Japan	37.627	142.11	7.0	SP1
Jul 23	15:26	Japan	39.807	141.46	6.8	ELTP2
Jul 29	18:42	California	33.955	-117.7	5.5	ELTP2
Aug 21	12:24	China	25.066	97.737	6.0	EPV2
Aug 25	13:21	China	30.893	83.614	6.7	ELTP2
Aug 30	08:30	China	26.277	101.91	6.0	EPVD2
Sep 8	18:52	Vanuatu	-13.51	166.96	6.9	ELTP1
Sep 10	11:00	Iran	26.823	55.825	6.1	ELTP1
Sep 11	00:20	Japan	41.979	143.62	6.8	EPV1
Sep 29	15:19	New Zealand	-29.87	-177.6	7.0	
Oct 5	15:52	Kyrgyzstan	39.515	73.768	6.6	ELTP2
Oct 6	08:30	China	29.759	90.302	6.3	ELTP1
Oct 11	09:06	Russia	43.271	46.262	5.8	ELTP2
Oct 16	19:41	Mexico	14.443	-92.42	6.7	ELTP2
Oct 19	05:10	Tonga	-21.85	-173.8	6.9	ELTP2
Oct 28	23:09	Pakistan	30.653	67.323	6.4	ELTP1
Nov 16	17:02	Indonesia	1.290	122.10	7.3	EPV1
Nov 24	09:02	Okhotsk	54.194	154.31	7.3	EPV2

2009

Date	Time (UTC)	Place	Lat.	Long.	Mag-nitude	Comments
Jan 3	19:43	Indonesia	-0.510	132.78	7.6	ELTPCSP1
Jan 8	19:21	Costa Rica	10.197	-84.15	6.1	ELTPCSP2
Jan 15	17:49	Russia	46.862	155.15	7.4	EPV1
Feb 11	17:34	Indonesia	3.902	126.40	7.2	ELTP1
Mar 19	18:17	Tonga	-23.05	-174.6	7.6	ELTPCSP2
Apr 6	01:32	Italy	42.334	13.334	6.3	ELTPCSP2
Apr 7	04:23	Islands	46.088	151.49	6.9	ELTPCSP1
Apr 16	21:27	Afghanistan	34.197	70.065	5.4	ELTPCSP1
May 28	08:24	Honduras	16.730	-86.20	7.3	TPPTECSP1
Jul 9	11:49	China	25.619	101.08	5.7	EPV2
Jul 15	09:22	New Zealand	-45.75	166.58	7.8	EPV1
Aug 9	10:55	Japan	33.144	138.04	7.1	ELTP1
Aug 10	19:55	Andaman	14.013	92.923	7.5	EPV2
Sep 2	07:55	Indonesia	-78.09	107.25	7.0	TPPTE1
Sep 12	20:06	Venezuela	10.70	-67.92	6.3	ELTP1
Sep 29	17:48	Samoa	15.509	-172.0	8.1	ELTP1
Sep 30	10:16	Indonesia	-0.725	99.856	7.6	ELTP2
	22:03		-13.05	166.18	7.6	SP1
Oct 7	22:18	Vanuatu	-12.55	166.32	7.8	SP1
	23:13		-13.14	166.29	7.3	ELTP1
Dec 19	13:02	Taiwan	23.763	121.68	6.4	ELTP2

2010

Date	Time (UTC)	Place	Lat.	Long.	Mag-nitude	Comments
Jan 3	22:36	Solomon	-8.912	157.30	7.2	ELTP2
Jan 10	00:27	California	40.645	-124.7	6.5	EPV1
Jan 12	21:53	Haiti	18.451	-72.44	7.0	ELTPCSP1
Feb 26	20:31	Japan	23.472	123.71	7.0	ELTPCSP1
Feb 27	03:34	Chile	-35.84	-72.71	8.8	SP1
Feb 27	15:45	Argentina			6.1	ELTPCSP1
Mar 4	0:18	Taiwan			6.4	EPV1
Mar 5	23:29	Sumatra			6.5	ELTP1
Mar 8	4:32	Turkey			6.0	ELTP1
Mar 11	11:39	Chile	-34.25	-71.88	6.9	ELTPCSP1
Mar 14	9:57	Indonesia			6.4	EPV1
Mar 14	8:08	Japan			6.6	ELTPCSP1
Mar 16	2:21	Chile			6.7	EPV1
Apr 4	22:40	Mexico	2.128	115.3	7.2	ELTP1

6. Analysis

According to the information of 154 earthquakes over 6 scales of magnitude over the world from the USA Earthquake Observation Council, the causal relationship common area, symmetry of them we can get the following results, as shown in **Table 2**:

Table 2. Results.

Type	Equatorial level Line plane	Which Symmetry	Ecliptic Line plane	Among Symmetry	Vertical Flat	Similar point	Other Not coplanar	Total
Quantity	22	(Four)	77	(23)	45	7	3	154
Percentage of total	14%	(3%)	50%	(15%)	29%	5%	2%	100%

7. Conclusions

This study allowed existence of the errors, but those errors do not interfere the co-planarity and the symmetry principle. Errors may come from the inaccuracy of observation time, perhaps the errors accelerate the process of the Earth becoming to sphere. In the next step of our research, we plan to study on earthquake prediction and the relationship between earthquake and economic development.

8. References

[1] Http://earthquake.usgs.gov/recenteqsww/quakes/quakes_all.html

International Journal of Geosciences, **2010, 44-50**
doi:10.4236/ijg.2010.11006 Published Online May 2010 (http://www.SciRP.org/journal/ijg)

Effects of Polypropylene Fibers on the Shear Strength of Sandy Soil

Mousa F. Attom, Adil K. Al-Tamimi
Civil Engineering Department, College of Engineering, American University of Sharjah, Sharjah, UAE
E-mail: *mattom@aus.edu*
Received March 1, 2010; *revised March* 27, 2010; *accepted April* 20, 2010

Abstract

This paper presents the effect of two types of polypropylene fibers on shear strength parameters of sandy soil. To achieve the goals of this research, a sandy soil was obtained from a depth of 40 cm from the natural ground surface around American University of Sharjah. Two types of polypropylene fibers; one highly flexible with flat profile and the other with relatively high stiffness and crimpled profile were used in this study with four different aspect ratios (L/D) for each type. The initial physical properties of the sand such as specific gravity, angle of internal friction and shear strength were obtained in accordance with American Standard for Testing and Materials (ASTM). The sandy soils were mixed with the two types of fibers at different percentages by dry weight of the sand and four different aspect ratios. The test results of the study showed that the shear strength of the sand increased with increasing the flexible flat profile fibers content. Also it was noticed that by increasing the aspect ratio of the flexible flat profile the angle of internal friction and the shear strength increased. The crimpled profile fiber increased the shear strength of the sand under high normal load and has small or no effect on shear strength of the sand at low aspect ratio under low normal load.

Keywords: Sand, Fibers, Angle of Internal Friction, Shear Strength, Aspect Ratio

1. Introduction

Due to the increasing cost of high quality materials needed for different geotechnical projects, engineers try to improve the physical properties of local soils throughout different methods and techniques. The word improvement means to increase the shear strength, reducing settlements, resists harsh environment conditions such as thawing and freezing, and decreases or eliminates all problems associated with weak soils. Soil stabilization could be applied to both sandy and clayey soil through mechanical and chemical methods. There are many common methods-mechanical or chemical-found in the literatures that were used to improve the physical properties of the soils. [1] showed that the increase of the compaction energy effort will increase the shear strength properties of the clayey soils. [2] used gypsum as an additive for stabilization of clay against swelling. He concluded that the gypsum can be used as a stabilizing agent for expansive clay against swelling effectively. Al-Rawas *et al.* [3] indicated that the addition of lime and cement will reduce both the swell potential and swelling pressure of expansive clayey soils. [4] used natural resources such as volcanic ash, ground natural lime, cement and their combination to stabilize soil for construction application. [5] studied the effect of silica fume on fine grain soils exposed to freeze and thaw. He found that the addition silica fume can be successfully used to reduce the effect of freezing and thawing cycles on strength and permeability of fine grained soils. In addition to these methods, other methods also exist such as wet-dry cycles and thermal methods [6,7].

Recently, engineers started to use different types of fiber in soil stabilizations. These fibers are found in the market as short, discrete materials with different aspect ratio and they can be mixed randomly with the soil, as cement, lime, or other additives at different percentages. The main reason of using randomly oriented fibers is to maintain strength isotropy and the lack of potential weak planes that may develop parallel to oriented reinforcement [8,9]. Fatani *et al.* [10] studied the effect of both aligned and randomly oriented metallic fibers on silty sand. It was found that mixing fibers with silty sand soil will increase the peak strength and residual strength 100% and 300% respectively over the untreated soil. Ziegler *et al.* [11] studied the effect of short polymeric

fibers on crack behavior of clay subjected to drying and wetting conditions. He concluded that the addition of fibers to the clay soil is very effective in reducing the amount of desiccation cracking and increasing the tensile strength. [12] in his study indicated that the residual shear strength angle of sand will increase by mixing sand with discrete fiber. Esna-ashari [13] used cord waste fiber to reinforce the sandy soil. They found that the inclusion of tire cord fiber can change significantly the brittle behavior of sandy soil to more ductile and also increased both the peak strength and angle of internal friction of sand. Gray and Ohashi [14] and Park and Tan [15] used randomly oriented discrete fibers in their research to reinforce sand. Freitag [16] mixed the fiber with clayey soil and showed that addition of fiber will increase the strength and ductility than plain clayey soil. The addition of nylon fiber by Kumar and Tabor [17] resulted in significant increase in the residual strength of silty clay soil. The test by Cai *et al*. [18] reported that there is a significant improvement on the engineering properties of the fiber-lime treated soil. Due to the encouraging findings of using discrete fiber with both sandy and clayey soils, the fibers are used in different construction applications such as retaining structures, embankments, subgrade and landfill liners and covers. The main objective of this study is to investigate the effect of two types of fibers on some physical properties of sandy soil. The parameters investigated in this study include shear strength properties and angle of internal friction at different fiber percentages and aspect ratios.

2. Polypropylene Fiber Type A & B

Two types of fibers are used in the research; both fibers are extruded from a natural Polypropylene homo polymer. The two fibers were given symbols A and B in the discussion. Type A is formed into a flat profile with high flexibility where type B formed into a crimped profile with high relative stiffness in order to anchor it with the matrix. The combination between the large number of fibers per kg, its shape and anchoring capability with the matrix, would provide a toughness and ductility to the material. Both types have high resistance to acid/alkali attack and are therefore suitable for use in wet underground conditions. **Table 1** shows the physical properties of the two types of fibers used in this research.

3. Experimental Program

A sandy soil was selected from around American University at Sharjah and brought to soil testing laboratory. The soils were extracted from 40 cm in depth from original ground surface. The initial physical properties of the sandy soil such as gradation ASTM D-422, specific gravity ASTM D-854, and maximum dry density and optimum water content ASTM D-1557 were determined in accordance with American Standard for Testing and Materials (ASTM) standard procedures. **Table 2** shows the initial physical properties of the sandy soil used in the study. The sandy soil was mixed with the two types of fibers at different percentages by dry weight of the sand and different aspect ratios. The percentages of the fibers are 1%, 2%, 3%, 4%, and dry weight of the sand. The aspect ratio index of the fibers, which is dimensionless, was used in the analysis instead of the length. At each percentage, four different aspect ratios (L/D) of the fibers were used with constant diameter and variable length. Because of the difference in diameter between type A and type B fiber four different aspect ratios were used for each type. The aspect ratios used for type A are 38.5, 77, 115.5 and 154 while the aspect ratio for type B are 10.4, 20.8, 31.2 and 41.7.

Table 1. Properties of the two types of fibers used in this study.

Characteristics	*Fiber*	*Fiber*
	Type A	*Type B*
Fiber Cross section mm²	0.234	0.75
Fiber length	50 mm	40 mm
Diameter	0.13 mm	0.48 mm
Tensile strength at yield (N/mm²)	1004	250

Table 2. Physical prosperities of the sand used in this study.

Physical Properties	
Shear Strength	
Angle of Internal friction (*deg*)	19
Cohesion (kPa)	0
Compaction	
Maximum dry unit weight (kN/m^3)	17.9
Minimum dry unit weight (kN/m^3)	14.3
Optimum moisture content (%)	12.8
Grain size distribution	
Clay ($<$ 2 μm)	6
Silt (2 μm-75 μm)	18
Sand (75 μm-2mm)	76
*Effective size D*10 (mm)	0.007
*D*30 (mm)	0.12
*D*60 (mm)	0.33
Specific gravity of solid, G_s	
G_s	2.66

Enough number of samples was prepared at 95% relative compaction and optimum moisture content with different fiber content. Predetermined amount of soil was obtained and mixed with the two types of fibers separately and compacted in the direct shear mold to obtain the 95% relative compaction. Direct shear test ASTM D-3080 was conducted on all sample under three normal loads. (28 kPa, 55 kPa, 110 kPa). The remolded specimens were sheared under a constant strain rate and deformations were recorded throughout the experiment. To obtain the shear strength and the angle of internal friction of the sand-fiber mixture at each percentage three identical specimens were prepared and tested under three different normal loads.

4. Results and Discussion

4.1. The Effect of Fibers on the Shear Strength, Angle of Internal Friction and Stress-Strain Relationships of the Sand

Figures 1 and **2** depicts the shear strength behavior and stress-strain relationships of sandy soil mixed with the type A and type B fiber respectively at different percentages and under normal load equal to 28 kPa. **Figure 1** concluded that the increase in the percentages of type A fiber will result in increasing the shear strength. **Figure 2** showed the increase of type B fiber has a small or no effect on shear strength up to 3%. The increase in the percentage of type B fiber more than 3% will result in decreasing the shear strength. The summary of the effect of adding both fiber A and fiber B on shear strength of sand under three normal loads was shown in **Figure 3**. This figure was obtained from the stress-strain relation from the direct shear test under different normal loads equal to 28 kPa, 55 kPa and 110 kPa and for sand mixed

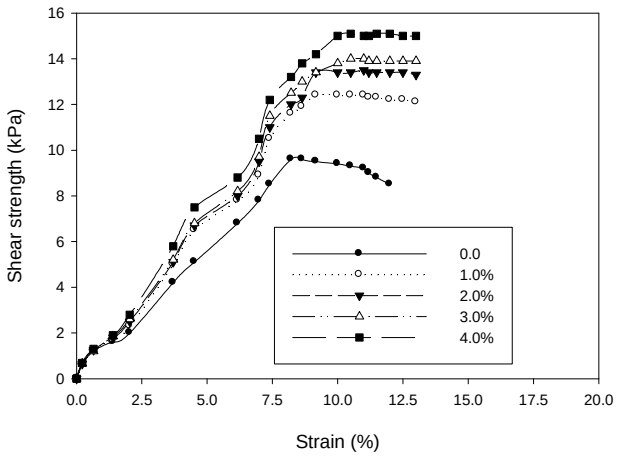

Figure 1. The effect of type A fiber on shear strength of sand under normal load equal to 28 kPa.

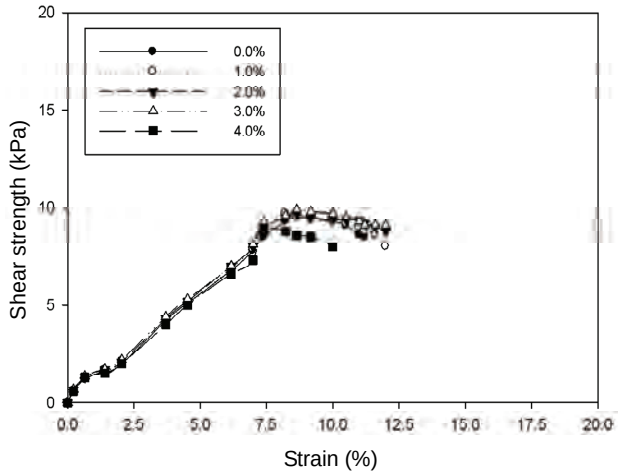

Figure 2. The effect of type B fiber on shear strength of sand under normal load equal to 28 kPa.

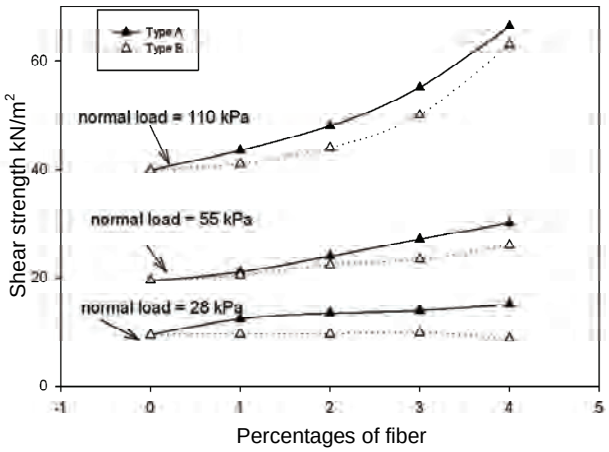

Figure 3. The effect of the fibers on the shear strength of the sand under three different normal loads.

with type A and type B respectively. This figure concludes that the addition of type A fiber will increase the shear strength of the sand under the three normal loads. The increase in the percentages of nylon fiber from 0.0% to 4% resulted in increasing the shear strength from 9.5 kPa to 15.1 kPa respectively, under normal load equal to 28 kPa. The addition of type A fiber up to 4% increased the shear strength of the sand up to 59%. As the normal load increased the addition of type A resulted in increasing the shear strength. For example the shear strength of the sand increased from 39.9 kPa to 66.4 kPa when the type A fiber increased from 0.0% to 4.0% under normal load equal to 110 kPa. The percentages in shear strength increased is about 66.4% under normal load equal to 110 kPa compares to 59% increased under normal load 28 kPa.

Different findings was noticed when the sand was mixed with type B fiber. As shown in **Figure 4** the addition of Type B fiber up to 3% by dry weight of the sand

has small or no effect on the shear strength at small normal load (28 kPa). The addition of further fiber will result in decreasing the shear strength at 28 kPa normal load. The shear strength decreased from 9.5 kPa at 0.0% fiber content to 8.8 kPa at 4% fiber content. However, addition of type B fiber resulted in increasing shear strength of sand at higher normal load. As shown in **Figure 3** and at 55 kPa and 110 kPa normal loads the increase in the percentages in the type B fiber resulted in increasing the shear strength of the sand. The shear strength of sand under normal load equal to 55 kPa increased from 19.5 kPa and 26 kPa when the percentages of B fiber increased from 0.0% to 4%. The same behavior was noticed at higher normal loads. The shear strength increased under normal load 110 kPa from 39.9 kPa at 0.0% fiber content to 63 kPa when the fiber content reached 4%.

Another conclusion can be drawn from the stress strain relationship. It was noticed there was no peak behavior of sand due to addition of these two fibers. All specimen with both fiber reached fail without exercising peak strength.

The effect of adding both types of fibers on the angle of internal friction of the sand is shown in **Table 3**. It is clear in this table that the addition of type A fiber will increase the angle of internal friction of the sand under any loading level. The angle of internal friction increased as much as 49% when the Type A fiber increased by 4%. Under normal load equal to 28 kPa. As the normal load increased the angle of internal friction increased to reach 64% under 110 kPa normal load and 4% fiber content. The effect of type B fiber is also shown in **Table 3**. The addition of type B fiber has no effect on the angle of internal friction under small loading condition. As the normal load increased the addition of type B fiber will result in increasing the angle of internal friction. The angle of internal friction increased as much as 57% under 110 kPa normal load and 4% fiber content. It can be concluded that the type B fiber has a very small on no effect on the angle of internal friction under small normal load and it has a significant effect on the angle of internal friction at large value of normal loading.

As it was mentioned earlier, the stress-strain relation curves were obtained from a direct shear test under 28 kPa normal loads. **Figure 1** shows the effect of type A fiber on the stress stain relation of sand. It is clear from this curve that as the percentages of type A fiber increased the strain failure increased too. The failure strain due to addition type A fiber increased from 8.6% to 10.0% and 11.5% when the fiber percentages increased from 0.0% to 2% and 4% respectively. This finding may conclude that the addition of type A fiber will increase the ductility of the sandy soil which is defined as the strain at failure of the soil specimen. The increase of the ductility of the soils with increasing the fiber contents is attributed to the effect of fibers inclusions in the sandy soil that improved the properties of the soil. **Figure 2** shows the effect of type B fiber on the stress-strain relation of the sand. It was noticed that adding the type B fiber up to 3% has insignificant effect on ductility of the sand while adding the type B fiber more than 3% will result in decreasing the ductility of the sand. All the samples were failed about the same strain of 9.0% when mixed up to 3% of type B fiber. The samples mixed with 4% type B fiber failed at 7.5% strain. The effects of increasing the percentages of type A fiber and type B fiber on the failure strain are shown in **Figure 4**.

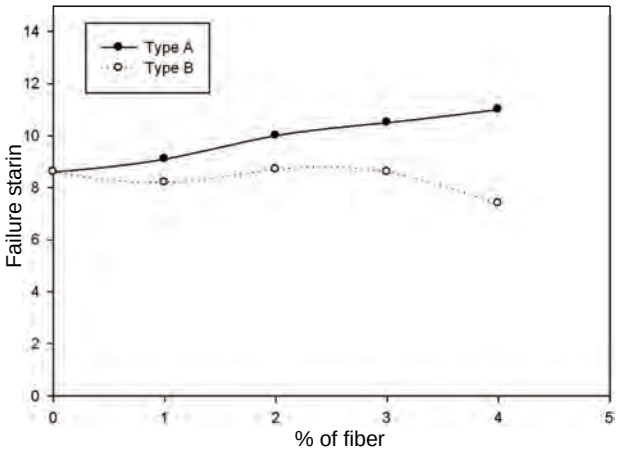

Figure 4. The effect of fibers on the failure starin of the sand under normal load = 28 kPa.

Table 3. The percentages increase in the angle of internal friction due to addition of fibers.

Load 28 kPa	*Fiber A*		*Fiber B*	
% of fiber	*φ*	*% increase*	*φ*	*% increase*
0	19	0	19	0
1	24	25.6	19	0.5
2	26	35	19	0.5
3	27	40	19	2
4	28	49	18	–8
Load 55 kPa	*Fiber A*		*Fiber B*	
% of fiber	*φ*	*% increase*	*φ*	*% increase*
0	19	0	19	0
1	21	1035	20	7
2	24	24	22	17
3	26	38	23	21
4	29	52	25	33
Load 110 kPa	*Fiber A*		*Fiber B*	
% of fiber	*φ*	*% increase*	*φ*	*% increase*
0	19	0	19	0
1	22	13.7	20	7
2	24	24	22	15
3	27	40	24	28
4	31	64	30	57

4.2. The Effect of the Length of the Fiber on the Shear Strength of Sand

The effects of length of both type A and type B fibers on shear strength of sand were studied in this research. The aspect ratio which is defined as the length over diameter ratio (L/D) was used herein instead of length alone as an indication for fiber length. Since the two types of fibers have different diameters, four aspect ratios were used for each type. The four aspect ratio for type A are L/D = 38.5, 77, 115.5, 154 and for type B are L/D = 10.4, 20.8, 31.2, 41.6 respectively. The four aspect ratios were studied under three different loads 28 kPa, 55 kPa and 115 kPa. **Figures 5** and **6** show the effect of aspect ratio on shear strength under two normal loads 28 kPa and 110 kPa respectively at 4% type A fiber content by dry weight of the sand. It is clear from these two figures that the increase of aspect ratio resulted in increasing the shear strength. In **Figure 5**, the shear strength of sand increased from 11.4 kPa to 14.5 kPa when the aspect ratio increased from 38.5 to 154 under normal load 28 kPa. At the same time as shown in **Figure 6**, the shear strength increased from 45.1 kPa to 66.1 kPa when the aspect ratio increased from 38.5 to 154 under normal load equal to 110 kPa. The percentage in shear strength due to increase in aspect ratio from 38.5 to 154 varies between 27% and 47% under the three normal loads.

It was also noticed that increased in the aspect ratio of type A fiber resulted in increasing the ductility of the sand. This observation is clear in **Figures 5** and **6**. The sand in all samples at different aspect ratio and under different normal loads fails at higher strain than if there is no fiber. **Figures 7** and **8** show the effect of type B fiber on shear strength of sand under two normal loads 28 kPa and 110 kPa at 4% fiber content by dry weight of the sand.

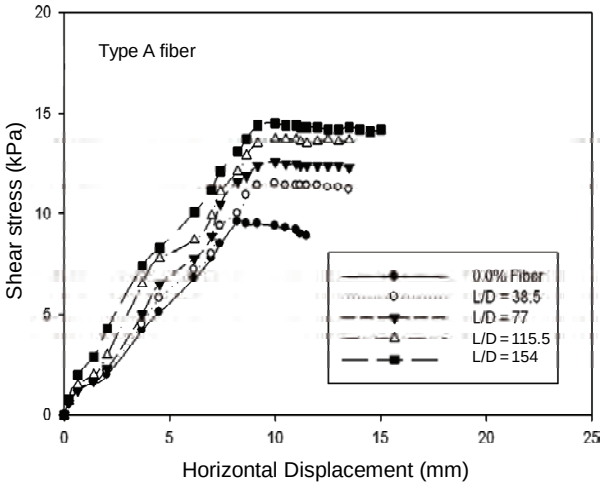

Figure 5. The effect of the aspect ratio on the shear strength of the sand at normal load 28 kPa at 4%.

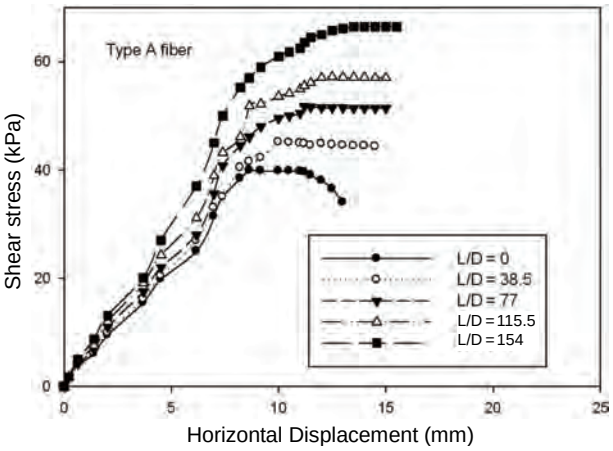

Figure 6. The effect of the aspect ratio on the shear strear strength of the sand at normal load 110 kPa at 4% type A fiber.

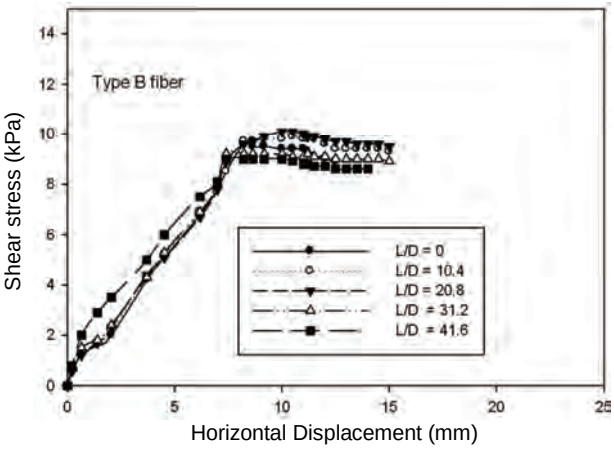

Figure 7. The effect of the aspect ratio on the shear strength of the sand at normal load 28 kPa at 4% type B fiber.

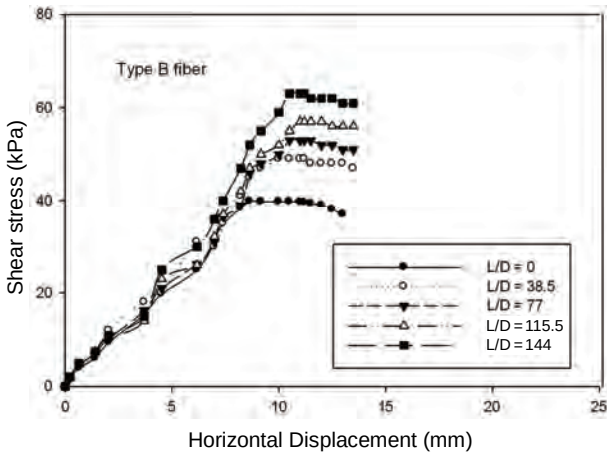

Figure 8. The effect of the aspect ration on the shear strength of the sand at normal load 110 kPa at 4% type B fiber.

It is clear from **Figure 7** that the type B has a small or no effect on shear strength if the aspect ratio is less than 20.8 (L = 1.0 cm). Increasing the aspect ratio of more than 20.8 will result in decreasing the shear strength. The shear strength decreased from 9.6 kPa to 9.2 kPa and 8.6 kPa when the aspect ratio increased from 10.4 to 31.2 and 41.6 respectively. The reduction in shear strength was noticed in all samples tested under at small normal load equal to 28 kPa. This behavior can be attributed to the plastic-like-surface which makes the sand particles moves and slip over that surface easier resulted in decreasing the shear strength.

The effect of aspect ratio of type B fiber on shear strength under high normal load is shown in **Figure 8**. This figure indicated the increase in the aspect ratio will increase the shear strength under normal load 110 kPa. The shear strength increased from 49 kPa to 63 kPa when the aspect ratio increased from 10.4 to 41.6. This can be explained as the following. As the normal load increased, the contact surface between sand and the crimpled surface of the fiber increased. This increase in the contact surface makes the sand particles harder to move and thus increasing the shear strength of the sand.

4.3. The Effect of Aspect Ratio on Angle of Internal Friction

The effect of aspect ratio both fibers on the angle of internal friction angle of internal of the sand was studied on **Figures 9** and **10**. **Figure 9** shows that the increase in the aspect ratio results in increasing the angle of internal friction of the sand. This increase was noticed under all different loads. The angle of internal friction increased from 19^o to 31^o when the aspect ratio increased from 0.0 to 154 under normal load equal to 110 kPa. The increase in the angle of internal friction will result in increasing

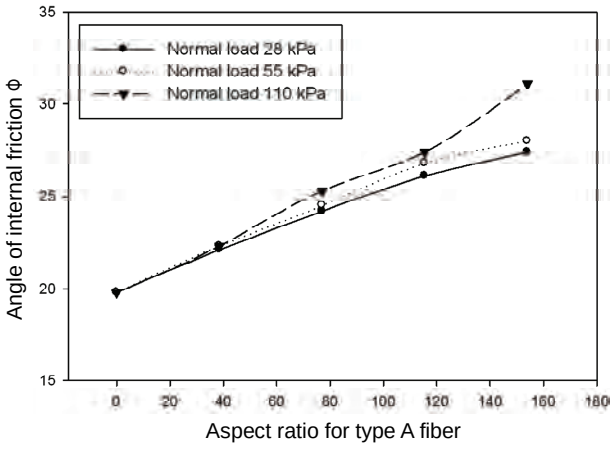

Figure 9. The effect of aspect ratio of type A fiber on the angle of internal friction under three different normal loads.

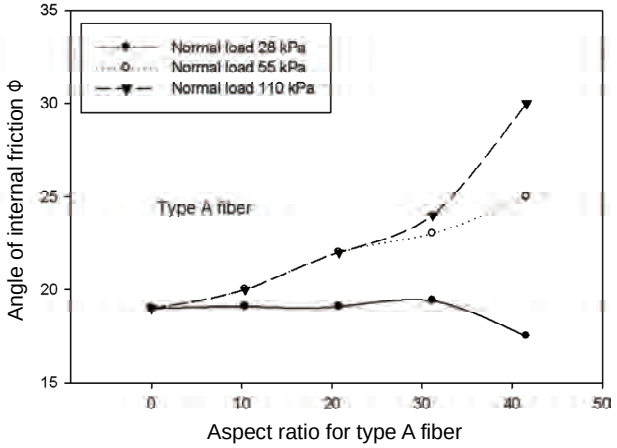

Figure 10. The effect of aspect ratio of type B fiber on the angle of internal friction under three different normal loads.

the shear strength of the sand. **Figure 10** studied the behavior of sand due to the addition of type B fiber under three normal loads. As it is shown in this figure the aspect ratio has no effect on the angle of internal friction of the sand under a normal load of 28 kPa. The angle of internal friction remains about 19^o at 10.4, 20.8 and 31.6 aspect ratios. As the aspect ratio increase more than 31.6 it was noticed that the shear strength decreased. On the other hand and as the normal load increased, it was noticed that the angle ofinternal friction increased. The increase become larger at higher normal load and the angle of internal friction increased from 10 to 30 at normal load equal to 119 kPa and aspect ratio equal to 41.6.

5. Practical Consideration

The results of the study have shown that addition of polypropylene fibers to sandy soil have improved significantly the physical engineering properties. These fibers may be used practically to increase the shear strength of sand especially under high loads. The result from this research concludes that the two types of polypropylene fibers could be promising materials and can be mixed with sandy soils in different construction projects to increase sand shear strength with the exception to use type B fiber at high normal stresses.

6. Conclusions

This research presents the results of using two polypropylene fibers at different percentages and different aspect ratio to improve the some physical properties of sandy soil. Based on the test results of this study, the following conclusions may be drawn out:

1) The shear strength of sand increased by increasing

the percentage flat profile fiber with high flexibility (type A fiber). The increase of in the percentage of the crimped profile fiber with high relative stiffness (type B fiber) increased the shear strength at high normal stress.

2) The increase of the percentages of the both type of fiber will result in increasing the angle of internal friction of sand.

3) The ductility of sand increased by adding the two types of fibers.

4) The increase in the aspect ratio resulted in increasing the both the shear strength of the sand and angle of internal friction. Butter results can be obtained at high.

5) The sand showed no peak strength at the four percentages of fibers.

7. References

[1] M. F. Attom, "The Effect of Compactive Energy Level on Some Soil Properties," *Applied Clay Science*, Vol. 12, No. 1-2, 1997, pp. 61-72.

[2] I. Yilmaz and B. Civelekoglu, "Gypsum: An Additive for Stabilization of Swelling Clay Soils," *Applied Clay Science*, Vol. 44, No. 1-2, 2009, pp. 166-172.

[3] A. A. Al-Rawas, A. W. Hago and H. Al-Sarmi, "Effect of Lime, Cement, and Sarooj (Artificial Pozzolan) on the Swelling Potential of an Expansive Soil from Oman," *Building and Environment Journal*, Vol. 40, No. 5, 2005, pp. 681-687.

[4] K. M. A. Hossain, M. Lachemi and S. Easa, "Stabilized Soils for Construction Applications Incorporating Natural Resources of Papua New Guinea," *Resouces Conservation and Recycling Journal*, Vol. 51, No. 4, 2007, pp. 711-731.

[5] E. Kalakn, "Effects of Silica Fume on the Geotechnical Properties of Fine-Grained Soils Exposed to Freeze and Thaw," *Cold Regions Science and Technology*, Vol. 58, No. 3, 2009, pp. 130-135.

[6] J. D. Nelson and D. J. Miller, "Expansive Soils: Problems and Practice in Foundation and Pavement Engineering," John Wiley and Sons Inc., New York, 1992.

[7] M. M. Abu-Zreig, N. M. Al-Akhras and M. F. Attom, "Influence of Heat Treatment on the Behavior of Clayey Soils," *Applied Clay Science*, Vol. 20, No. 3, 2001, pp. 129-135.

[8] K. L. Lee, B. D. Adams and J. M. Vagneron, "Reinforced Earth Retaining Walls," *Journal of Soil Mechanics and Foundation Division, ASCE*, Vol. 99, No. 10, 1973, pp. 745-764.

[9] S. W. Park, R. L. Lytton and J. W. Button, "Forensic Investigation of Pavement Distortions Using Soil Suction," *Journal of Transportation Engineering*, Vol. 125, No. 1, 1999, pp. 60-66.

[10] M. N. Fatani, G. H. Bauer and N. Al-Joulani, "Reinforcing Soil with Aligned and Randomly Oriented Metallic Fibers," *Geotechnical Testing Journal*, Vol. 14, No. 1, 1991, pp. 78-87.

[11] S. Ziegler, D. Leshchinsky, H. I. Ling and E. B. Perry, "Effect of Short Polymeric Fibers on Crack Development in Clays," *Japanese Geotechnical Society*, Vol. 38, No. 1, 1998, pp. 247-253.

[12] T. Yetimoglu and O. Salbas, "A Study on Bearing Capacity of Randomely Distributed Fiber-Reinforced Sand Fills Overlying Soft Clay," *Geotextiles and Geomembranes Journal*, Vol. 23, No. 2, 2003, pp. 174-183.

[13] M. Esna-ashari and M. Asadi, "A Study on Shear Strength and Deformation of Sand Soil Reinforced with Tire Cord Waste," *Proceeding the Fourth Asian Regional Conference on Geosynthetics*, Shanghai, China, 2008, pp. 355-359.

[14] D. H. Gray and H. Ohashi, "Mechanics of Fiber Reinforcement in Sand," *Journal of Geotechnical Engineering, ASCE*, Vol. 1109, No. 3, 1983, pp. 335-353.

[15] T. Park and S. A. Tan, "Enhanced Performance of Reinforced Soil Walls by the Inclusion of Short Fiber," *Geotextile and Geomembrene Journal*, Vol. 23, No. 4, 2005, pp. 348-361.

[16] D. R. Freitag, "Soil Randomly Reinforced with Fibers," *Journal of Geotechnical Engineering, ASCE*, Vol. 112, No. 8, 1986, pp. 823-826.

[17] S. Kumar and E. Tabor, "Strength Characteristics of Silty Clay Reinforced with Randomly Oriented Nylon Fiber," *Electronic Journal of Geotechnical Engineering*, Vol. 127, No. 9, 2003, pp. 774-782.

[18] Y. Cai, B. Shi, C. W. W. Ng and C. Tang, "Effect of Polypropylene Fiber and Lime Admixture on Engineering Properties of Clayey Soil," *Engineering Geology Journal*, Vol. 87, No. 3-4, 2006, pp. 230-240.

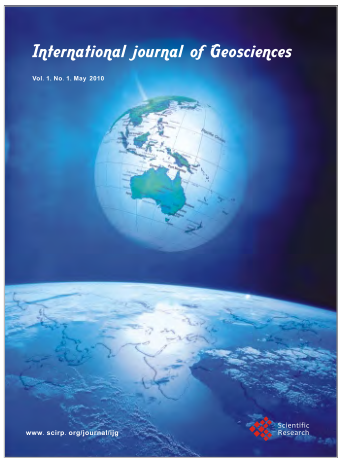

Call for Papers

International Journal of Geosciences

http://www.scirp.org/journal/ijg/

International Journal of Geosciences(IJG) is an international refereed journal dedicated to the latest advancement of geosciences. The goal of this journal is to keep a record of the state-of-the-art research and to promote study, research and improvement within its various specialties.

Editor-in-Chief

Prof. Shuanggen Jin University of Texas, USA

Editorial Board

Subject Coverage

All manuscripts submitted to IJG must be previously unpublished and may not be considered for publication elsewhere at any time during IJG's review period. Additionally, accepted ones will immediately appear online followed by printed in hard copy. Topics to be covered by this journal include, but are not limited to:

- Atmosphere
- Biosphere
- Cartography
- Environmental Science
- Geodesy and Surveying
- Geography
- Geoinformatics (GIS)
- Geostatistics
- Hydrosphere
- Lithosphere or Geosphere
- NASA Earth Science Enterprise
- Pedosphere

We are also interested in: 1) Short Reports - 2 to5 pages where the paper is intended to present either an original idea with theoretical treatment or preliminary data and results; 2) Book Reviews - Comments and critiques of recently published books in Geosciences.

Notes for Intending Authors

Submitted papers should not have been previously published nor be currently under consideration for publication elsewhere. Paper submission will be handled electronically through the website. All papers are refereed through a peer review process. For more details about the submissions, please access the website.

Website and E-Mail

http://www.scirp.org/journal/ijg **Email: ljg@scirp.org**

International Journal of Geosciences, **2010, 1-50**
Published Online May 2010 in SciRes (http://www.SciRP.org/journal/ijg/)

TABLE OF CONTENTS

Volume 1 Number 1 **May 2010**

The Bayamo Earthquake (Cuba) of the 18 October 1551

M. O. Cotilla-Rodríguez, D. Córdoba-Barba..... 1

Sedimentation Processes at the Navigation Channel of the Liquefied Natural Gas (LNG) Port, Nile Delta, Egypt

E. A. M. Deabes..... 14

Surface Rupture and Hazard of Wenchuan Ms 8.0 Earthquake, Sichuan, China

Y. Li, R. Q. Huang, L. Yan, A. L. Densmore, R. J. Zhou..... 21

The Analysis of Accelerograms for the Earthquake Resistant Design of Structures

V. Corchete..... 32

The Co-planarity and Symmetry Principle of Earthquake Occurrence

Z. Yin..... 38

Effects of Polypropylene Fibers on the Shear Strength of Sandy Soil

M. F. Attom, A. K. Al-Tamimi..... 44